INVESTIGATING GOLD MINERALIZATION POTENTIALS IN PART OF THE KIBI-WINNEBA BELT OF GHANA USING AIRBORNE MAGNETIC AND RADIOMETRIC DATA

By

CHRISTOPHER AKULGA, BSc Applied Physics (Hons)

A Thesis Submitted to the Department of Physics,

Kwame Nkrumah University of Science and Technology

in partial fulfillment of the requirements for the degree

of

MASTER OF PHILOSOPHY (GEOPHYSICS)

College of Science

Supervisor: Dr. K. Preko

JUNE, 2013

Certification

I hereby certify that this thesis work is my own work as part of the requirements for the award of a Master of philosophy degree, and that it contains no material previously published by another person or material which has been accepted for the award of any other degree by the university, except where due acknowledgement has been made in the text.

……………………	……………	……………….
Student name & ID	Signature	Date

Certified by:

……………………	……………	……………….
Supervisor(s) Name	Signature	Date

Certified by:

……………………	……………	……………….
Head of Dept. Name	Signature	Date

Abstract

Gold is an important resource located within the subsurface, and its mineralization is controlled by geology, structures and hydrothermal alteration within rock formations. The search for gold is therefore the search for structures within hydrothermally altered zones in the subsurface. For this reason two geophysical surveys namely airborne magnetic and radiometric, proven to be excellent in mapping structures, geology and hydrothermally altered zones were employed in the Birimian formation in the Eastern region of Ghana. The airborne magnetic and radiometric data obtained were processed into grids with Geosoft. Data enhancement filters such as reduction to the pole, vertical integral, analytical signal, first and second vertical derivatives and continuation filters were applied to the total magnetic intensity grid to enhance anomalies. The radiometric data were also gridded to produce the concentration maps of K, Th, and U. Additionally, ratio maps of the three elements and their ternary images were produced. The images obtained from the enhanced magnetic data and the radiometric data showed that the study area is structurally complex with a few of the structures corresponding to D1 deformation and most structures corresponding to D2 deformation. The structures are dominate in the mafic volcanic, metavolcanic and the Tarkwaian formation. The metasediments and the Buem formation had very few structures. The results also showed a number of hydrothermal alterations within the mafic volcanic, Tarkwaian, and metavolcanic formation. From the results obtained, a composite map of the study area consisting of the geology, structures and hydrothermally altered zones were produced with ARC GIS. From the composite map eight zones were delineated as having potentials of considerable gold mineralization.

Table of Content

List of Tables

List of figures

List of Symbols and Acronyms

ICRU International Commission of Radiation Units and Measurements

FS Filling Service Canada

GSD Geological Survey Department of Ghana

RGC Reunion Gold Corporation Australia

SGC Sovereign Gold Company Limited Australia

MCG Minerals Commission Ghana

BIF Bonded Iron Formation

K Magnetic susceptibility

B Total magnetic field

Z Vertical component of total magnetic field

H Horizontal component of total magnetic field

I Angle of inclination

D Angle of declination

J Induce magnetization

H Magnetizing field strength

μ Permeability of a medium

nT Nanotesla

No Number of radioactive nuclei present at time t=0

Nt Number of radioactive nuclei remaining after time t(s)

λ Decay constant

$T_{1/2}$ Half life

U Uranium

Th Thorium

K Potassium

Acknowledgments

I thank the Lord Almighty God for making it possible for me to undertake this project successfully. Throughout this project, the Lord has shown His mercies upon me and has provided me with good health that enabled me to complete this project successfully, thank you Lord. Secondly I would like to say a very big thank you to my supervisor, Dr. K. Preko and my co-supervisor, Mr. D. D. Wemegah for providing me with the data and taking time to shape and fine-tune this project, God bless you all abundantly for the immeasurable contributions you offered to the success of this project.

To the head of Department (Physics) Professor S.K Danour and the entire staff of the physics department KNUST, I say thank so much and may God bless you for the time and patience you had for me during this project. To my colleague Graham, I say thank you so much for providing me with Arc GIS, Geosoft and giving me tutorial on these software, God bless you. To my other colleagues Anachina and co., I say God bless you all for the various ways you contributed to the realization of this project, it has been a wonderful time having you around.

Last but not the least, I would like to say thank you so much to my wife, my sisters and to all my relatives for the many supports that you have offered for the successful completion of this project, God bless you abundantly.

CHAPTER ONE: INTRODUCTION

1.1 Background of Studies

In Ghana, gold mining forms a major economic activity and has contributed significantly to the socio-economic development of the country since the early days of mining to recent times. Most of the gold in Ghana occurs in structures (faults, veins, fold, shear zones and fractures) within the Early Proterozoic metamorphosed Birimian greenstones; and early Proterozoic metamorphosed Tarkwaian formation. The early Proterozoic formations are dominated by broad basins of sediments along the margins of comparatively narrow, NE trending greenstone belts, which contain a great variety of volcanic units, sediments and intrusions (MCG, 2010). The early Proterozoic formation bears much similarity with most Archean greenstone deposits, particularly in terms of its high gold potential.

Airborne magnetic and radiometric methods are geophysical tools that are capable of delineating the subsurface geology in terms of its lithology, structures (fractures, shear zones, folds, veins and faults) and hydrothermally altered zones. These parameters are essential in the identification of areas with possible gold mineralization. The search for gold is therefore the search for hydrothermally altered zones, structures (faults, folds, fractures, veins and shear zones) and lithology that is known to favour the mineralization of gold.

Airborne magnetic survey involves flying a light aircraft with a magnetometer mounted on it to investigate the subsurface geology on the basis of anomalies in the Earth's magnetic field resulting from the magnetic properties of the underlying rocks. Although most rock-forming minerals are effectively non-magnetic, certain rock types contain sufficient magnetic minerals such as magnetite and pyrrhotite to produce significant magnetic anomalies. Even though gold is non-magnetic, the magnetic method has proven to be a valuable tool in the search for gold, because gold is closely associated with pyrite which is also nonmagnetic, but pyrite can metamorphosed into pyrrhotite at the upper green schist-lower amphibolite grades, and pyrrhotite can be metamorphosed into magnetite (Keary et al, 2002). Minerals that contain pyrrhotite and magnetite are clearly delineated by airborne magnetic surveys. In addition, magnetic surveys can determine the presence of younger intrusive rocks, and cross-cutting structures that are typically associated with shear hosted Archaean orogenic gold deposits as well as differentiate between Banded Iron Formation (BIF), metasediments, metavolcanics and other rock types, when it comes to geological mapping.

Airborne radiometric survey involves flying a light aircraft with a gamma ray spectrometer mounted on it to measure gamma rays that originate from radioactive elements within 30 cm to 40 cm of the top soil. Notwithstanding the shallow depth from which the radiations are emitted, the radioactive element content of the bedrock is reflected in the composition of the superficial radioactive elements. The gamma rays measured are characteristic of the radioactive elements from which they are emitted in the subsurface. Even though there are many naturally occurring radioactive isotopes or elements, majority of them are rare or possess very weak radioactivity, therefore the radioactive elements of principal interest in radiometric survey are uranium (238U), thorium (232Th) and potassium (40K). The distribution of these radioelements relates to the differences of lithology of common rocks and alteration processes. The concentration of these radioactive elements is therefore used in geological mapping, as different rock types can be recognized from their distinctive radioactive signatures (Moxham, 1963). K/Th and U/Th ratios are important indicators of alteration zones (Airo, 2002); these alteration zones are favourable zones for the mineralization of gold and should be looked for in exploration.

1.2 Project Area

The study area is located within five districts in the Eastern Region of Ghana as shown by red ink in figure 1.1. The districts are the Atiwa District located at the northern part of the study area, the west Akim and Suhum / Kraboa districts located at the southern part of the study area, the East Akim District located on the eastern part of the study area, and the Kwaebibirem District located on the western part of the study area. Using the Universal Transverse Mercator (UTM) geographic coordinate system, the study area is geographically located between UTM zone 755000 m to 773000 m in the eastern and 671000 m to 698000 m on the northern as shown in figure 1.2.

1.2.1 Accessibility

The study area can be accessed by road through the Accra - Kumasi highway to the town of Anyinam. From the town of Anyinam, a second class tarred road heads south to Bomaa, a village south of Kwabeng town. From Bomaa a number of untarred roads and foot paths link most of the towns in the study area. Alternatively, the area can be access through the Accra - Kumasi highway, which goes through Suhum to Apedwa Nkwanta and a left turn via 15 km tarred road through Amanforo, Odumase and Potroase to Kibi. Access to the area by road can also be made through Nsutam on the Accra - Kumasi highway through Asiakwa, Sagyimase and to Kibi. In general road accessibility to some of the towns in the study area is fairly good.

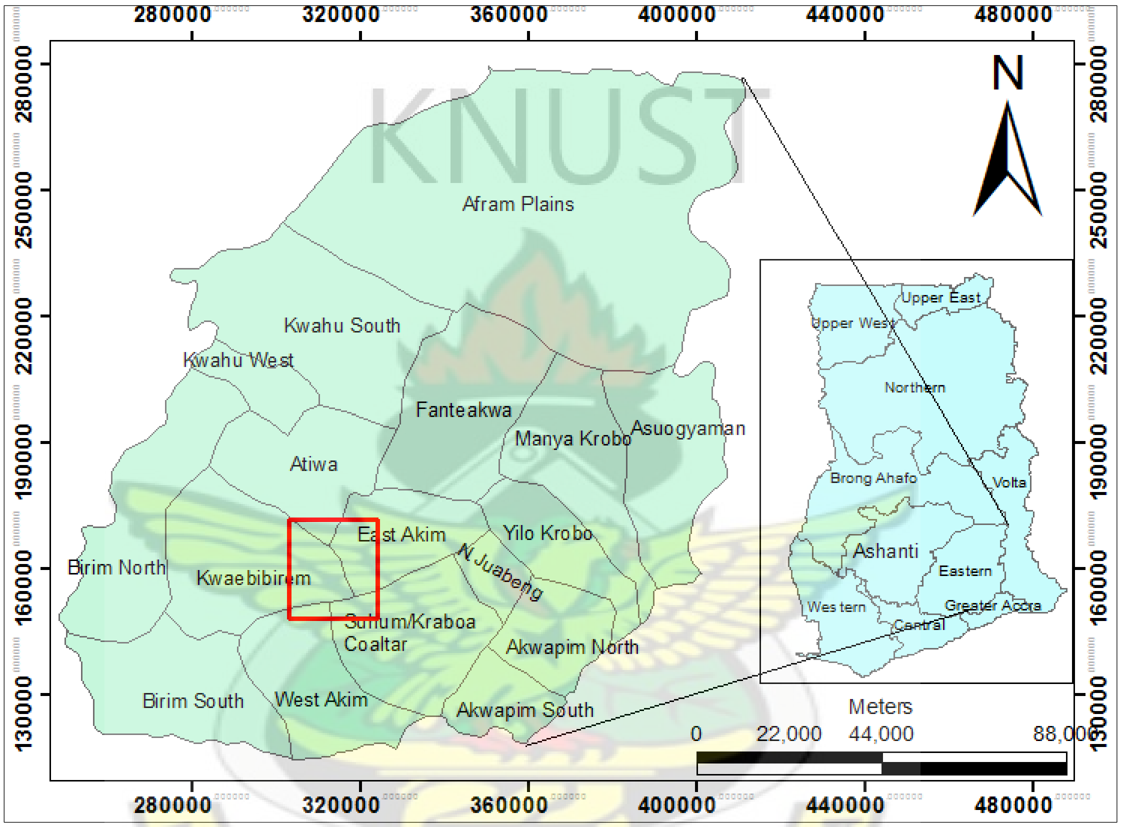

Figure 1.1 a map of Eastern region with the study area highlighted in red. (modified after GSD, 1988).

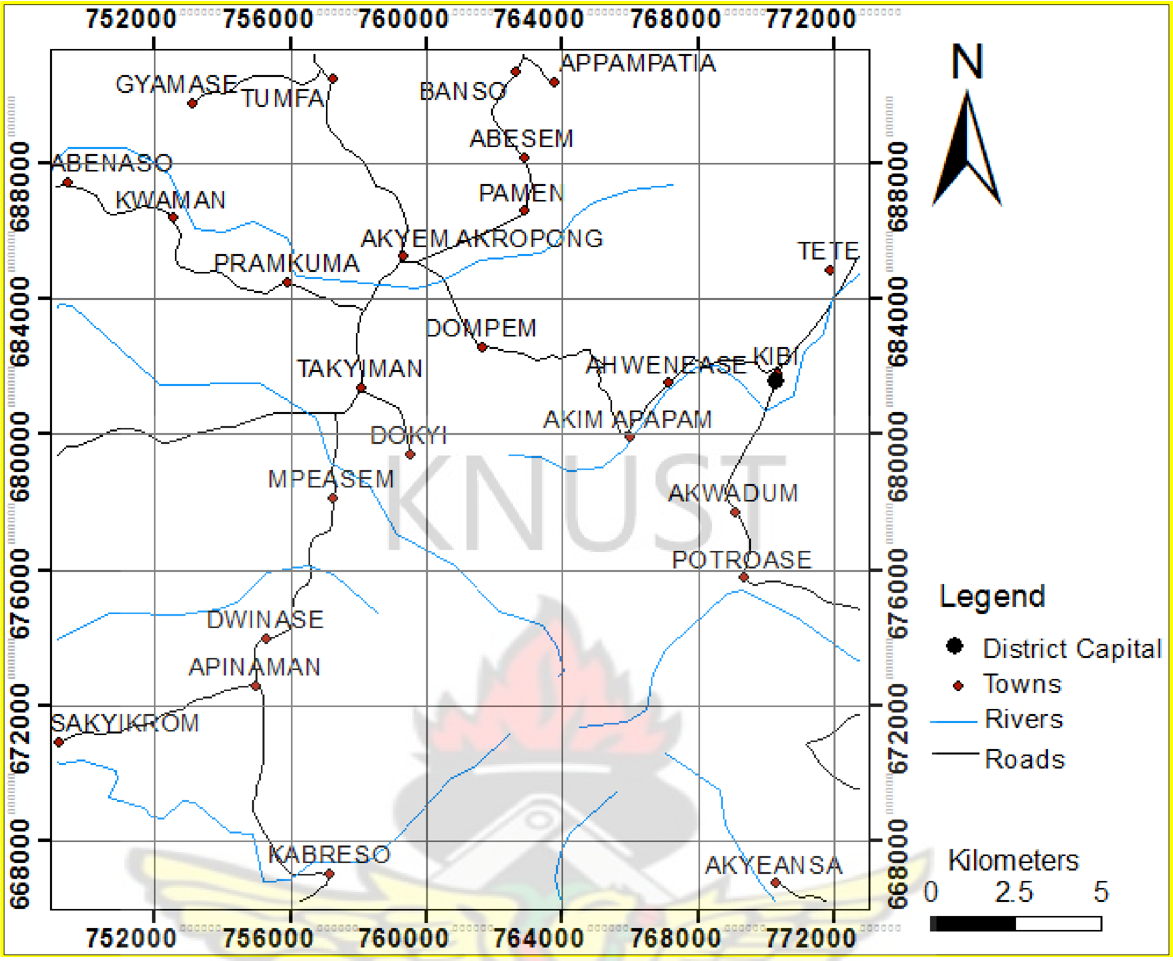

Figure 1.2 a map of the study area. (Modified after GSD, 1988).

1.2.2 Climate

The study area has two raining seasons, the first raining season is from the month of March to July and the second raining season is from September to November. The annual rainfall figure is in the range of 1500 mm - 2000 mm, occasionally some areas record 2000+ mm of rainfall. The months of April, July, September and October record more than four raining days in a month. The two raining seasons make the dry season unnoticeable in the district. Temperatures in the districts are in the range of 31°C – 37°C and 23°C - 26°C for day and night respectively with high relative humidity values in the range of 65% - 80% (Simon et al., 2010). The area also has an average wind speed of about 6 km/h in the south west direction.

1.2.3 Vegetation

The main vegetation of the area is basically moist deciduous forest which is characterized by thick canopy tall trees with a layer of shorter trees and evergreen shrubs in the undergrowth. The area is dominated by tropical hard wood species such as Odum, Wawa, Ofram, Asamfra, mahogany, teak, bamboo and Okyenkyen. Tree crops such as cocoa, oil palm, coffee, mango and citrus are also found to be striving well in the area.

1.2.4 Socioeconomic Activities

The economy of the districts in the study area hinges on Agriculture, Industry, Trade and Services. Agriculture is the dominant economic activity of the area with about 60 % of the labour population engaged in it (Atiwa District Assembly, 2012).

The Birimian series forest ochrosol soil couple with the moist deciduous forest vegetation enables the cultivation of crops and the rearing of livestock. Crops such as, plantain, cassava, maize, yam, cocoyam, oil palm cocoa and vegetables are cultivated in the districts.

1.3 Objectives

The main aim of this project is to investigate gold mineralization potentials in parts of the Kibi-Winneba belt of Ghana using airborne magnetic and radiometric data.

In order to achieve this main objective, the under listed specific objectives have to be achieved:

1. Mapping the lithology and geological setting of the area.
2. Mapping geological structures within the study area, that are capable of hosting gold mineralization.
3. Mapping areas that are hydrothermally altered and have the potentials for gold mineralization.

1.4 Research Problem Definition

The study area is one of the regions that have the paleoproterozoic granite greenstone belts. These belts are known to host commercial quantities of gold in structures such as faults and folds, and in hydrothermally altered zones. However, identifying these structures and hydrothermal altered zones within the greenstone belt is very challenging if the appropriate geophysical method is not used. It is for this reason that airborne magnetic and radiometric methods have been used in the study area to map the geology, structures and hydrothermal altered zones. The mapped zones would then be used in the analysis and interpretations of areas with the potentials of gold mineralization in the study area.

1.5 Literature Review

The search for gold is on the ascendancy worldwide due to its economic importance, explorers have used different tools in their search for this precious mineral, and over the years one of such tools that have proven to be an excellent recognizance tool for mapping geological structures all over the world is airborne radiometric and magnetic survey.

Airborne magnetic surveys allow us to map magnetic anomalies constrained by field structural and geological observations (Boyce and Morris, 2002). The surveyed data serve as a tool for deriving both lithological and structural information from which geological interpretations can be carried out on a surveyed area (Betts et al., 2007).

In 1952, Ostle from United Kingdom Geological Survey, and Hale from the then Gold Coast Geological Survey were able to delineate radiometric anomalies in laterites within the Accra North above the Dahomeyan formation, in addition they were able to delineate radiometric anomalies in the Bongo granite, and moreover they delineated radiometric anomalies of the Bobikuma in laterite above the older Basin granite (Kesse, 1985). All these radiometric anomalies were delineated after carrying out radiometric surveys in the areas.

The Hunting Surveys Limited of the United Kingdom in 1960 explored for minerals in two different blocks in Ghana using airborne magnetic and radiometric method. The blocks were named block ‘A’ and block ‘B’. Block ‘A’ had a land coverage of 12430 km^2 (Kesse, 1985) and ran from the west coast of Takoradi via Tarkwa and Prestea, to Dunkwa and Obuasi up to Konongo. Block B had land coverage of about 4662 km^2 in the southeastern part of Ghana and ran through the Buem and Togo formation. In both blocks, the magnetic data obtained were successful in delineating contact zones between magnetic and non-magnetic formations, fractures, intrusions and dykes within the two blocks. In addition, the magnetic data was able to delineate the well-known reefs in the mineralization zones close to the intersection of shear zones and fault zones.

Magnetic data was part of the geophysical data that mapped the lithology and geological structures with possible mineralization in West Wits Line, Free State, Klerksdorp and Evander in the Republic of South Africa, this then led to the discovery of the West Wits Line Goldfield, the Free State Goldfield, the Klerksdorp Goldfield and the Evander Goldfield that produced 80 per cent of the gold from the Republic of South Africa (Roux, 1967).

El-awady et al. (1984) used aeromagnetic data to study the complex crystalline basement structural pattern, shallower structures and local structures in four sedimentary formations at Faiyum in the western desert of Egypt. Additionally, the aeromagnetic data revealed the distribution of magnetic minerals in the bedrock without any influence by the non-magnetic regolith that overlay the bed rock.

Billings (1998) and Wilford et al. (1997) found out that gamma ray spectroscopy was a better alternative to aerial photography and satellite images in terms of soil and regolith mapping; since soil properties are determined from satellite images and aerial photograph which depend on vegetation and landform. Land forms and vegetation are affected by anthropogenic factors such as bush burning thereby obscuring the aerial photographs and satellite images. These anthropogenic factors however, do not affect gamma rays. Moreover, many of the factors that control the distribution of soil and regolith also control the distribution of radioactive elements.

Airborne magnetic surveys conducted in 2007 at the Bulman leases in Australia identified many areas that needed further investigation for fault system that relates to carbonate hosted Mississippi valley type Pb-Zn mineralization, it also suggested that the known Pb-Zn mineralization in the Bulman is under laid by sill (Sawyer and Gunn, 2008). In addition, the interpreted airborne magnetic survey revealed a system of north-south and east-west fault that correlates with mineralization and Pb-Zn anomalies from soil geochemistry. Anomalies from potassium coincided with east-west offset in the Bulman fault and a north-south trending Pb geochemical soil anomaly. The anomalous potassium was indicative of potassic alteration associated with an increase in hydrothermal activities. With airborne magnetic and radiometric data, Reunion Gold Cooperation were successful in mapping the lithology and geological structures, possible hydrothermal alteration zones and potential mineralization zones in the Lely gold project in Surinam (RGC., 2008).

The Filing Services of Canada (FS) successfully, evaluated the potentials of the western extension of the Main vein and Contact zone gold-silver-tellurium vein system using radiometric and magnetic data to map the lithology, geological structures, and hydrothermal alteration zones of the area (FS., 2011). Airborne magnetic and radiometric survey has provided a very detailed structural image for identifying potential conduits for gold bearing fluids at the Rocky River-Uralla Goldfield. This led to the identification of large amount of gold deposits and the successful establishment of potential sites for the primary source of gold deposits in the Rocky River-Uralla (SGC., 2012)

Interpretation of airborne geophysical data integrated with field structural and lithological observation was successfully employed in the creation of the litho-structural framework in a poorly exposed Paleoproterozoic granite-greenstone terrain of Burkina Faso in the

West African Craton. The geophysical data portray sufficient details of the lithological units and structural features present. The results suggested that, the granitoid domains are formed by numerous small to medium-sized plutons. The existence of several generations of magmatic episodes has a significant impact on the development of a regional tectonic model. The magnetic data provided a better definition of the actual pluton shapes and several highly magnetic late-orogenic plutons were reliably identified (Metelka, 2011). Interpretations of airborne magnetic and radiometric data in the Konongo District of Ghana, led to the mapping of gold mineralization indicators, such as geology, structures and zones that are hydrothermally altered within the area. It was proven that airborne magnetic and radiometric methods are potent and could be applied in deeply weathered terrains or regolith to pick exploration targets for blind ore deposits. The interpreted high-resolution magnetic dataset also provided both an overview of the regional structure as well as further insight into structural controls of the greenstone-hosted-gold deposits in Konongo (Boadi et al., 2013).

It is the successful delineation of gold bearing structures in Ghana and the world at large with the use of radiometric and magnetic tools as reviewed in literature that has necessitated the enhancement of such data with Geosoft data enhancement techniques, in order that the lithology and geological structures, possible hydrothermal alteration zones and possible potential mineralization zone could be mapped in the study area. This would go a long way to shed light on the gold mineralization potentials of the study area.

1.6 Scope of Work

This project involves processing airborne radiometric and magnetic data with Geosoft.

The project seeks to map out the lithological, geological, structural and the hydrothermally altered zones using the enhanced radiometric and magnetic data. Possible sites for gold mineralization are then inferred from the geological and structural maps. This project however, does not seek to model the shape of the mineralized zones and does not also quantify the amount of mineralization in the subsurface.

1.7 Structure of Thesis

The Thesis work has six (6) chapters with each chapter addressing a main heading. Chapter one introduces the field of research and the geophysical tool that are employed in the research, it also deal with the location, and socioeconomic activities of the research area. The objectives, importance and the problems the research seeks to address are also mentioned. This chapter additionally, contains the literature that has been reviewed and the scope of the work and the structure of the entire thesis work. Chapter two gives a general overview of the national and local geological setting of the study area. This chapter also deals with the major types of gold deposits found in Ghana and guidelines for the exploration of gold. Chapter three outlines the theoretical background of radiometric and magnetic methods. Chapter four deals with the materials and the procedure used in collecting data, it also outline the data processing tools that were used to enhance anomalies for data interpretation. Chapter five presents the results obtained and discusses the results presented in the various maps obtained from the radiometric and magnetic data. It also contains integrated geological maps that are deduced from the findings of both radiometric and magnetic datasets, with potential zones of gold mineralization. Chapter six presents conclusions and recommendations.

CHAPTER TWO: GEOLOGICAL SETTINGS

2.1 Regional Geology of Ghana

Ghana lies within the West African craton that was formed as a result of the Eburnean orogeny which got stabilized during the early proterozoic era (2.2 Ga) with isoclinal folding and intrusion of pre-, syn-, and post-tectonic granite preserves (Eisenlohr and Hirdes, 1992). Similarly this orogeny also formed the Zaire craton and affected vast parts of West Africa and South America.

The West African craton has extensive preservation of metamorphosed volcanic and sedimentary rock units that are exposed in Ghana, Burkina Faso, Niger and Cote d' Ivoire. The craton is bounded by the late Proterozoic mobile belt (Pan African mobile belt) (Kesse, 1985; Wright et al., 1985; Leube et al., 1990).

The West African craton has many geological formations, and in Ghana some of these formations that are pronounced include the paleoproterozoic aged Birimian systems, the Tarkwaian systems, the Voltain formation, the Dahomeyan formation, the Togo formation and the Buem formation. Figure 2.1 below is the map of Ghana with the different geological formations that are within the country and the study area marked with black ink. All of these geological formations present in Ghana have undergone some form of metamorphism and it is only the metamorphosed Birimian systems and the Tarkwaian systems that are known to host commercial quantities of gold mineralization in Ghana.

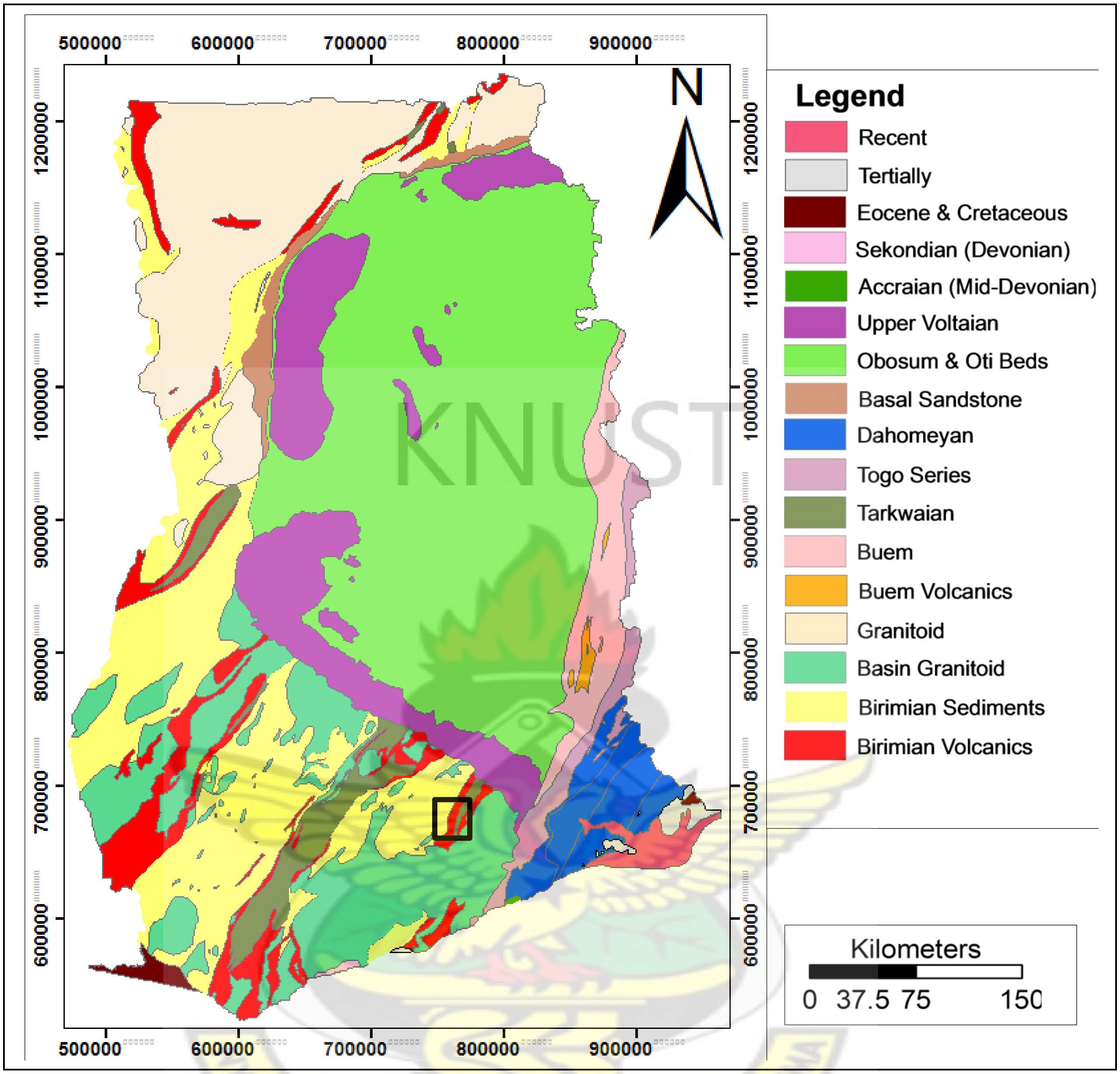

Figure 2.1 Geological Map of Ghana with study area marked with black ink (modified after GSD, 1988).

2.1.1 Metamorphosed Birimian Formations

The paleoproterozoic aged Birimian super groups are located within the western and northern parts of the country and constitute about 45% of the country's landmass. The Birimian super group is divided into two main groups. These are the metavolcanic and metasediments (Leube et al., 1990). The metavolcanic consist of mainly mafic volcanics with pyroclastics, hypabyssal intrusives, phyllites and greywackes. The metasediments are characterized by a predominance of immature or volcaniclastic sediments, including argillites, tuffs and greywackes (Junner, 1940).

Six main Birimian belts known as paleoproterozoic granite-greenstone belts and their intervening metasedimentary basins are identified in Ghana (Abbott and Koimtsidis, 2010). The granite-greenstone belts include the Kibi-Winneba belt, the Ashanti belt, the Sefwi-Bibiani belt, the Bui belt, the Bole-Nangodi belt and the Lawra belt. With the exception of the Lawra belt that trends north-south, the remaining five granite-greenstone belts trend NE-SW. Their intervening metasedimentary basins include the Cape Coast basin, Kumasi basin, and the Sunyani basin.

2.1.2 Metamorphosed Tarkwaian System

The Tarkwaian systems consist of distinctive sequence of clastic sediments that include polymictic conglomerate with bedded quartzite, sandstone and phyllite. They unconformably overlie the Birimian formation with an average thickness of about 1800-3000 m (Junner, 1940) within the Ashanti, Bui, Lawra, and the Nangodi belt. They are believed to have been formed from alluvial fan deposits that are linked to braided stream channel (Hirdes and Nunoo, 1994). The Tarkwaian series are subdivided into Huni

Series, Tarkwa phyllite Series, Banket Series and Kawere Series based on their thickness, facies and the direction of the cross bedding. The Huni Series is composed of sandstones, grits and quartzites with phyllites, with an average thickness of about 1370 m. The Tarkwa phyllite series has a thickness of about 120 - 400 m and is composed of Huni sandstone transitional beds and green and greenish-grey chloritic and sericitic phyllites and schists. The Banket series are Tarkwa phyllite transitional beds and sandstones, quartzites, grits, breccias and auriferous conglomerates with a thickness in the range of 120 - 160 m. The Kawere series are quartzites, grits, phyllites and conglomerates with a thickness of 250 - 700 m.

2.2 Geology of the Study Area

Geologically, the study area is located within the NE-SW trending Kibi - Winnneba paleoproterozoic metamorphosed granite greenstone belt in which four different geological formations can be identified. These are the Birimian volcanics, the Birimian sediments, the Tarkwain formation, and the granitoids as shown in figure 2.2.

About half of the study area is occupied by the Birimian sediments which consist of phyllites, schist, and tuff and greywacke formation (GSD, 1988).

On the eastern flanks of the Birimian sediments are the Birimian volcanic that are intruded by a north east trending Tarkwaian series that have divided the Birimian volcanic formation into almost two parallel volcanic units. The Birimian volcanic in this area are mainly metamorphosed lava, pyroclastic rock, hypabyssal basic intrusive (felsic volcanic rock units), phyllite and greywacke (GSD, 1988).

The Tarkwaian series unconformably overlay the Birimian formation and are made of basically quartzite, phyllite, grit, conglomerate and schist, including basic intrusive (felsic volcanic rock units). The main rock formation in the southeastern corner of the study area is the basin granitoid which consists basically of undifferentiated granitoids (GSD, 1988). Regionally, the belt has a number of north eastern trending faults, a large batholith in the southern part of the Atiwa range, high potassium basin and belt granitoid intrusions, and dolerite dyke intrusions. The faults in the eastern flank of the range are found to be reverse faulting, with a number of the northeastern trending faults having many cross cutting features in most of the valleys of the range which appears to be associated with alluvial gold deposit.

The geology of the belt gives room for two kinds of gold deposits, namely primary or lode (Orogenic) deposit, and alluvial or eluvial deposit.

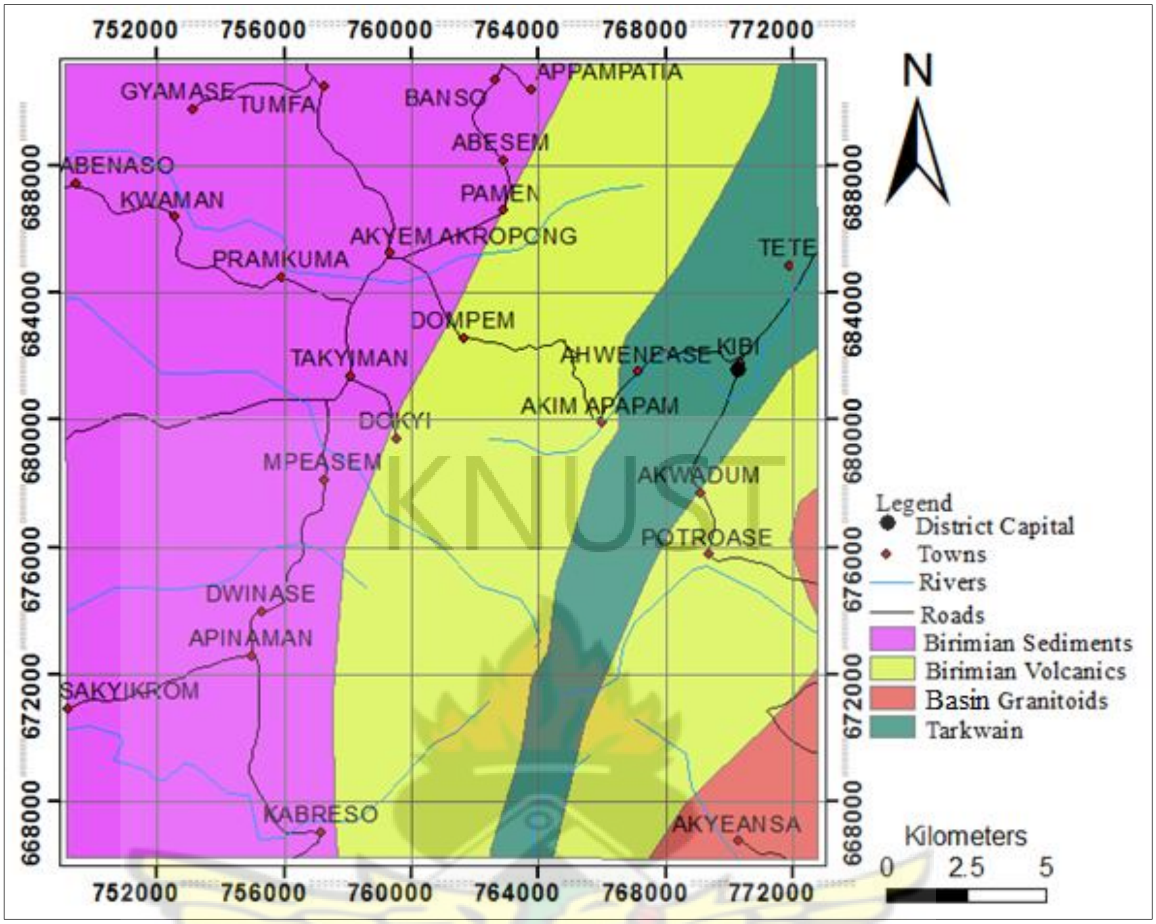

Figure 2.2 Geological map of the study area (modified after GSD, 1988).

2.3 Types of Gold Deposits in Ghana

The gold deposits in Ghana are formed by activities of the Eburnean orogeny and are primarily confined to the greenstone belt especially along the margins of the greenstone belts and the adjacent basin sediments (MCG, 2010). The dominant gold deposits in Ghana are the greenstone hosted deposit and the Tarkwaian deposit.

2.3.1 Greenstone-Hosted Deposits

The Greenstone-hosted deposit is a type of orogenic gold deposit that is observed in most parts of southern Ghana especially in Obuasi, Prestea, Ahafo, Akyem and Chirano in the Ashanti region (MCG, 2010). This kind of deposit is characterized by complicated high grade quartz-carbonate vein system that has combined laminated veins in steep to very steep dipping reverse shear zone, with adjacent competent and lower strain rocks having arrays of shallow-dip extensional veins, an indicative feature of greenstone formation during crustal shortening (Sibson et al., 1988; Robert et al., 1991). In addition they are characterized by vertical zoning as shown in figure 2.3 below.

Mostly they are in regional compressional to transpressional structures that are located within boundaries of contrasting lithologies and in clusters in bends (Goldfarb et al., 1998; Robert et al., 2005). They occur in supracrustal rocks with a greenstone belt from mafic-ultramafic, volcanic to upper clastic sedimentary stratigraphic level. The formations of these deposits are influenced by structural and lithologic factors such as faults, shears, and Fe rich tholeritic basalt respectively (Robert, 2004b).

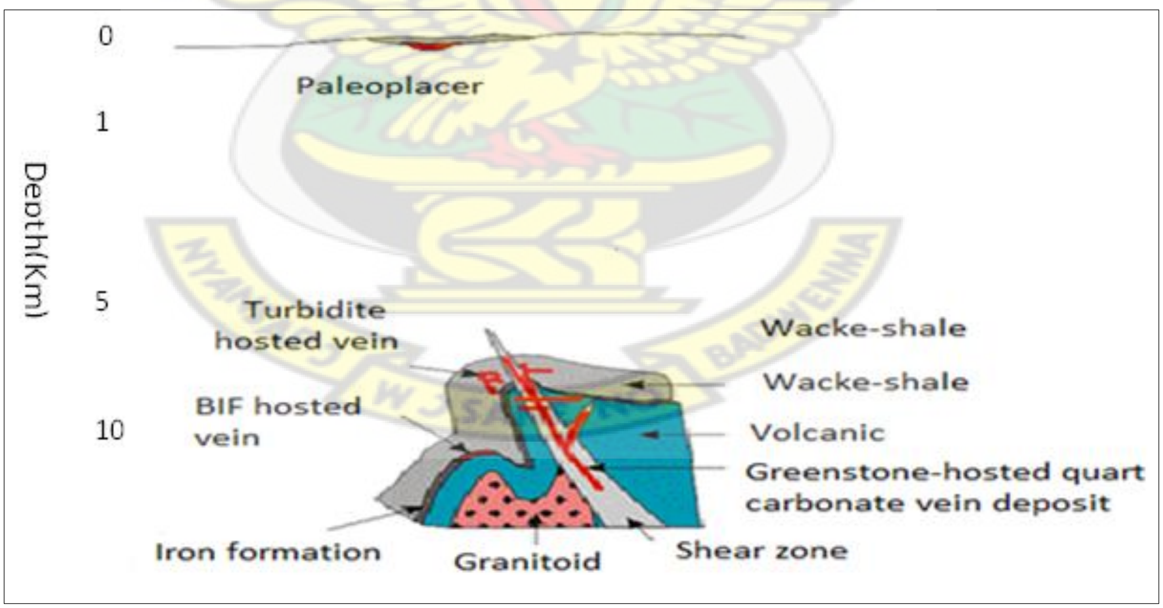

Figure 2.3 Orogenic deposits (Modified after Robert, 2004b).

Greenstone-hosted deposits are also associated with extensive disseminated sulphides.

The broad disseminated sulphide zones are generally highly silicified and form part of the alteration envelopes of the mineralized systems. They are also associated with low salinity, and CO_2-H_2O hydrothermal fluid. The ore body may be quartz-dominated single vein, an en echelon vein swarm or a network of veins that are in the range of 0.5 - 50 m wide and 100 m - 2 km long. The vein in the ore body may be 1 cm - 10 m thick and 20 - 1000 m long. The veins can be as long as 1000+ m along strike direction with a width of about 10+ m. Example are the Obuasi and Bibiani deposit and in some case the vein may also be narrow example are the Prestea and Konongo deposits, the vein can also extend to a depth of about 500+ m. An individual vein system can pinch out rapidly but a separate one can be discovered along strike, down dip or anywhere within the confines of the boarder's favourable structural zone.

The ore bodies are surrounded by carbonate-sericite-pyrite alteration haloes with varied development host rock composition. The ore also have Ag, As, Te, Bi, Mo, B, ± W in significant quantities. In the greenschist stage ore, pyrite is the dominant sulfide mineral while in the amphibolites and clastic sediment hosted ore at greenschist stage, pyrrhotite, loellingite and arsenopyrite are the dominant sulfide minerals respectively.

2.3.2 Tarkwaian Paleoplacer Deposit

The Tarkwaian deposit in Ghana bear similar characteristics with the Banded Iron Formation (BIF) deposits of the orogenic type of gold deposit. The BIF deposits are distinctive units of sedimentary rock that are formed during the Precambrian era, as a result of sulfide replacement of Fe-rich layers in magnetite or silicate BIF close to quartz vein and veinlet of variable development. They occur in volcanic or sediment dominated greenstone belt located near regional volcanic-sedimentary transition in the absence of large mafic volcanic rock and near the edge of large clastic sedimentary basins. In greenschist grade, magnetite BIF dominates with intermediate to felsic porphyry stocks, and dykes, while in amphibolites grade, silicate BIF dominates (Kerswill, 1996). BIF deposits are strata bound and plunge parallel to their host fold hinge; structurally they are linked with hinges of folds, anticlines or synclines and between faults and shear zones.

In Ghana the Tarkwaian deposits consist of conglomerates beneath and above the Banket series of the Tarkwaian formation, they appear to have originated from a series of alluvial fans on a piedmont surface. The conglomerates host high amount of gold and their intervening cross bedded quartzite also contain some amount of gold. At the eastern part of the Tarkwa syncline, the conglomerates are thiner (about 1 m) than the western part and consist of well-rounded coarse quartz pebbles, cobbles and boulders with high grade gold that has a fineness of more than 950 confined to the matrix of the conglomerates. Also in the Tarkwaian formation are the quartz vein deposits which trend NNE and are associated with extensive silicification, pyrite and pyrrhotite mineralization. They also contain small amount of sulphides with carbonate, sericite, tourmaline and ilmenite.

2.4 Prospecting for Gold

To be certain that the subsurface under investigation holds commercial quantities of gold mineralization, a thorough geophysical and geochemical assessment of the site needs to be carried out before drilling, this involves mapping the geology, structures and hydrothermally alteration zone. These are key factors that would determine potential sites of gold mineralization. A good knowledge of the geophysical techniques coupled with a good understanding of the geology of greenfield and brownfield environments are crucial to the discovery of deposits (Sillitoe and Thompson, 2006). Knowledge of the different types of gold deposits and the conditions that favours their geological settings both regionally and locally, and the depth of formation is also vital in locating potential sites of gold deposits. The detection of geological features such as hydrothermal alteration and mineralization together with their dispersion characteristics at surficial environment are very indicative of gold deposits and should be looked out for. Notwithstanding the above mentioned the unusual and unique characteristics of certain deposits must be catered so that they are not skipped unrecognized. (Sillitoe, 2000b).

The use of data processing tools such as 2D and 3D GIS are also very helpful in modeling the structure of deposits in the subsurface. 3D is generally good for modeling near mines whereas 2D is good for modeling in regional exploration. In both cases the most important parameter that would inform a decision as to drill or not is the indication of mineralization or elements of mineralization. Finally, prospecting is a team work and all the team members need to cooperate and collaborate with one another.

CHAPTER THREE: THEORETICAL BACKGROUND

3.1 Airborne Magnetic Method

Airborne magnetic method makes uses a magnetometer mounted on an aircraft to carry out magnetic surveys. It is fast, cheaper and allows surveys to be carried out in areas that are inaccessible by road. The magnetic method is a potential field (passive) geophysical method that is used to investigate the subsurface geological structures of the Earth. In airborne magnetic survey, it is the magnetic field intensity of the Earth that is measured. Changes in the magnetic field intensities of the Earth are due to the variations of the magnetic susceptibilities of the various rock units beneath the subsurface. The magnetic method used in the investigation of the subsurface therefore operates on the assumption that a target is limited in space and has a contrasting magnetic susceptibility from its surrounding geology that leads to the natural variation of the Earth's magnetic field between the target and the surrounding geology (Keary et al., 2002).

3.1.1 Magnetic Susceptibility (*K*)

Magnetic susceptibility measures the ability of a material or a mineral to be magnetised in the presence of an applied magnetic field. The susceptibility (k) of a mineral or a rock is the ratio between the induced magnetic field (I) and the Earth magnetic field (H) or the inducing field.

Mathematically it is expressed as $k = I/H$ (1)

The magnetic susceptibility of most rock forming minerals is low, and the magnetism in rocks is as a result of the presence of magnetic minerals (Keary et al., 2002). A high-susceptibility body will produce a stronger induced field than a low-susceptibility one.

The amplitude of the measured parameter (magnetic susceptibility) reflects the presence of magnetic or non-magnetic bodies and the shape of the measured parameter traduces the shape and the geometry of the body in depth.

3.1.2 Measure of Magnetic Mineral Content of the Rock.

Magnetic minerals can be classified into two important groups as shown in figure 3.1. These are the titanomagnetite series and the titanohematite series. The third series in figure 3.1 is the pseudobrookites which are not common and besides that, they are paramagnetic at room temperature, hence they are not important in the magnetism of rocks (Lowrie, 2007).

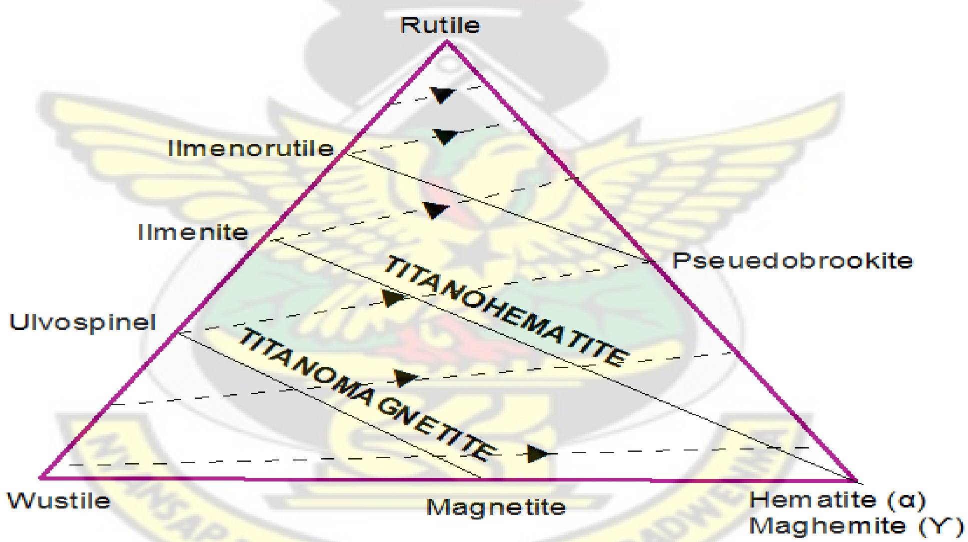

Figure 3.1 Ternary compositional diagram of the iron-titanium oxide solid solution magnetic minerals (McElhinny, 1973).

The titanomagnetite series has the general formular $Fe_{3-x}Ti_xO_4$ where x is the relative proportion of titanium in the compound and their members range from magnetite (Fe_3O_4) which has the highest susceptibility value among the magnetic minerals, to ulvospinel (Fe_2TiO_4) which is paramagnetic at room temperature and antiferromagnetic at very low temperature. The titanohematite series has a general formular $Fe_{2-x}Ti_xO_3$ with their members ranging from hematite (Fe_2O_3) to ilmenite ($FeTiO_3$). Other minerals in the sulfide group such as pyrrhotite (Fe_7S_8) are magnetic minerals (ferrimagnetic).

Table 3.1 Common Minerals and their magnetic Susceptibility values (Bullock and Isles, (1994); *Fallon and Backo, (1994); Lowrie, 1997)*

MINERAL	SUSCEPTIBILITY
Quartz	-0.01
Rock Salt	-0.01
Calcite	-0.001-0.01
Sphalerite	0.4
Pyrite	0.05-5
Hematite	0.5-35
Illmenite	300-3500
Magnetite	1200-19200

Table 3.1 above shows some common magnetic minerals and their susceptibility values. The presence of different types of magnetic minerals in various compositions in rock formation results in different rock formation having different magnetic susceptibility values as seen in table 3.2 below.

Table 3.2 Common Rocks with their magnetic susceptibility values (Bullock and Isles, (1994); *Fallon and Backo, (1994); Lowrie 1997)*

ROCK	SUSCEPTIBILITY x10^3 (SI)
Limestone	0-3
Sandstone	0-20
Shale	0.01-15
Schist	0.3-3
Gneiss	0.1-25
Slate	0-35
Granite	0-50
Gabbro	1-90
Basalt	0.2-175
Peridodite	90-200

Besides the presence of a magnetic mineral in a rock unit that would result in a magnetic anomaly, other features such as dykes, faults, folds or truncated sills and lava flow, massive basic intrusions, and metamorphic basement rocks also give rise to magnetic anomalies (Keary et al, 2002).

3.1.3 Rock Magnetization

The magnetization in rocks is either due to remanent or induced magnetization or both. Remanent magnetization could be Thermoremanent Magnetization (TRM), Detrital Remanent Magnetization (DRM), Chemical Remanent Magnetization (CRM) or Viscous

Remanent Magnetization (VRM).

- Thermoremanent Magnetization (TRM): is acquired when an igneous rock cools and solidifies through the curie temperature of its magnetic minerals.
- Detrital Remanent Magnetization (DRM): is acquired when magnetic particles of sediments realign within the Earth's field during sedimentation.
- Chemical Remanent Magnetization (CRM) is developed later in a rock as the magnetic mineral recrystallizes during diagenesis or metamorphism.
- Viscous Remanent Magnetization (VRM) is acquired slowly in rocks that are place in an ambient magnetic field and the magnetic domains orientate in the direction of the ambient field.
- Induced Magnetization is induced on a magnetic body when the body is placed in a magnetic field.

In a rock the resultant magnetization is a vector summation of induced and the remanent magnetization. The magnitude of the resultant *(J)* determines the amplitude of the anomaly and the orientation of the resultant *(J)* influences the shape of the anomaly.

3.1.4 Principle of Magnetic Method

The principle of the magnetic method is based on the fact that when a magnetic mineral or a ferrous material is placed within the Earth's magnetic field, it develops an induced magnetic field *(J)* that is superimposed on the Earth's field at that location, hence creating a magnetic anomaly at that point. The magnitude of the anomaly detected depends on the amount of magnetic material present and its distance from the sensing equipment.

The Earth's magnetic field B in an undisturbed state is proportional to the magnetizing force H and is given by

$$B = \mu_\circ H \tag{2}$$

Where $\mu_\circ$ is the permeability of vacuum. It is similar to the permeability of air and water (Keary et al, 2002).

When a magnetic material is placed in a magnetic field, the total field developed at that point is proportional to the sum of the magnetizing field strength H and the field J produced by the magnetization of the material.

Mathematically,

$$B = \mu_\circ (H + J) \tag{3}$$

But the induced magnetization J is proportional to the strength of the magnetizing force H of the inducing field

$$J = kH \tag{4}$$

where the constant of proportionality (k), is the magnetic susceptibility of the material. When equation (4) is put into equation (3) we obtain equation (5). Equation (5) is further manipulated to obtained equation (6) which is an equation for the total magnetic field intensity of the Earth at a place that has got a magnetic mineral (Keary et al., 2002).

$$B = \mu_\circ (H + kH) \tag{5}$$

$$B = \mu_\circ H(1 + k)$$

$$B = \mu_\circ \mu_R H$$

$$B = \mu H \tag{6}$$

Where μ is the permeability of the medium

The total Earth's geomagnetic field is a vector addition of the horizontal and the vertical component (Keary et al., 2002) as shown in figure 3.2.

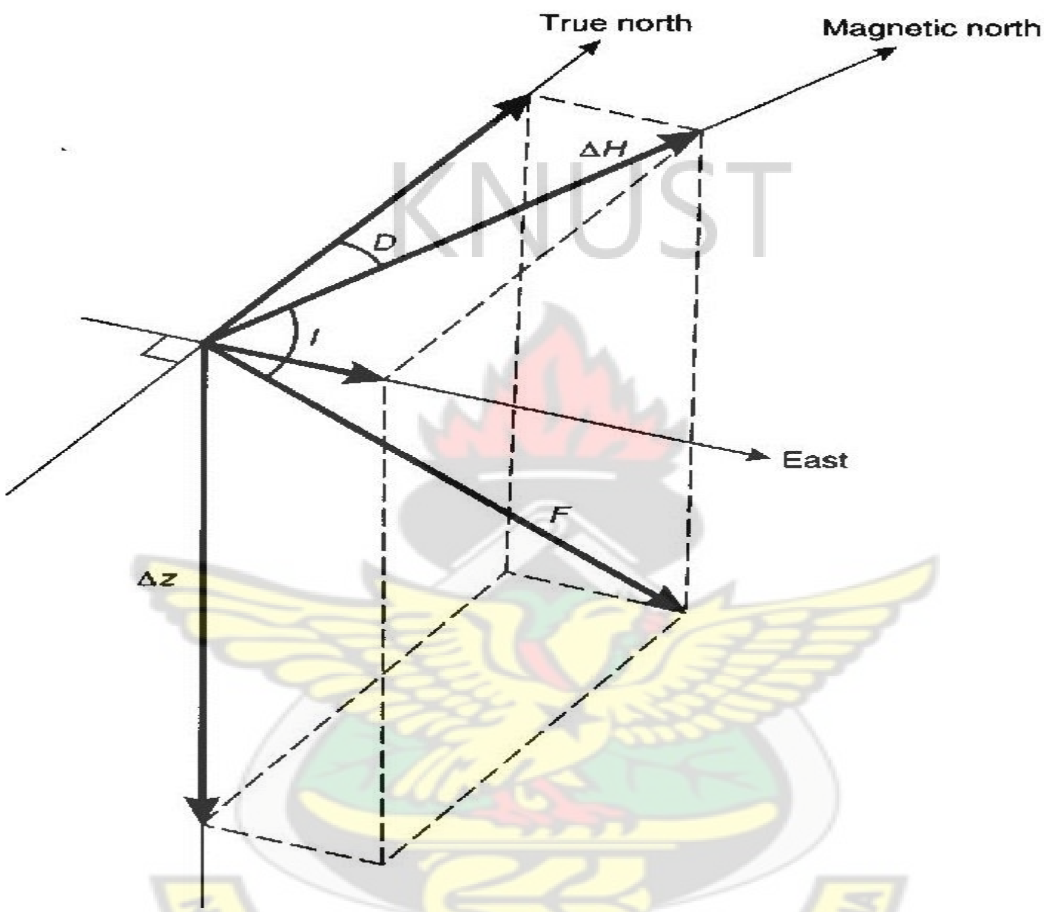

Figure 3.2 Geomagnetic elements

$$B^2 = H^2 + Z^2 \tag{7}$$

The magnetic anomaly caused by rocks in the subsurface are superimposed on the geomagnetic field of the Earth. This changes the geomagnetic elements so that B then change by ΔB, H by ΔH and Z $by\ \Delta Z$ so that equation (7) above now becomes

$$(B+\Delta B)^2 = (H+\Delta H)^2 + (Z+\Delta Z)^2 \tag{8}$$

If ΔH is at an angle α to H, it is only that part of ΔH in the direction of H given as $\Delta H'$ that would contribute to the anomaly. Therefore equation (8) then becomes (Keary et al., 2002).

$$(B+\Delta B)^2 = (H+\Delta H')^2 + (Z+\Delta Z)^2 \tag{9}$$

and $\Delta H'$ is given by

$$\Delta H' = \Delta H Cos \propto \tag{10}$$

Expanding (9) and neglecting higher orders of Δ^2 we have

$$\Delta B = \Delta Z \frac{Z}{B} + \Delta H' \frac{H}{B} \tag{11}$$

But from the diagram of the magnetic elements above we have

$$\frac{Z}{B} = SinI \tag{12}$$

$$\frac{H}{B} = CosI \tag{13}$$

Where I is the angle of inclination of the geomagnetic field.

Substituting equation (12), (13) and (10) into equation (11), the field of the anomaly is then given by (Keary et al., 2002).

$$\Delta B = \Delta Z Sin I + \Delta H Cos I Cos \propto \tag{14}$$

However, if a small isolated magnetic pole of strength m at a depth z with a radial distance r and horizontal distance x from an observer as shown below in figure 3.3, due to a magnetic mineral, then the magnetic anomaly caused by such a body beneath the subsurface of the Earth can be expressed as shown below.

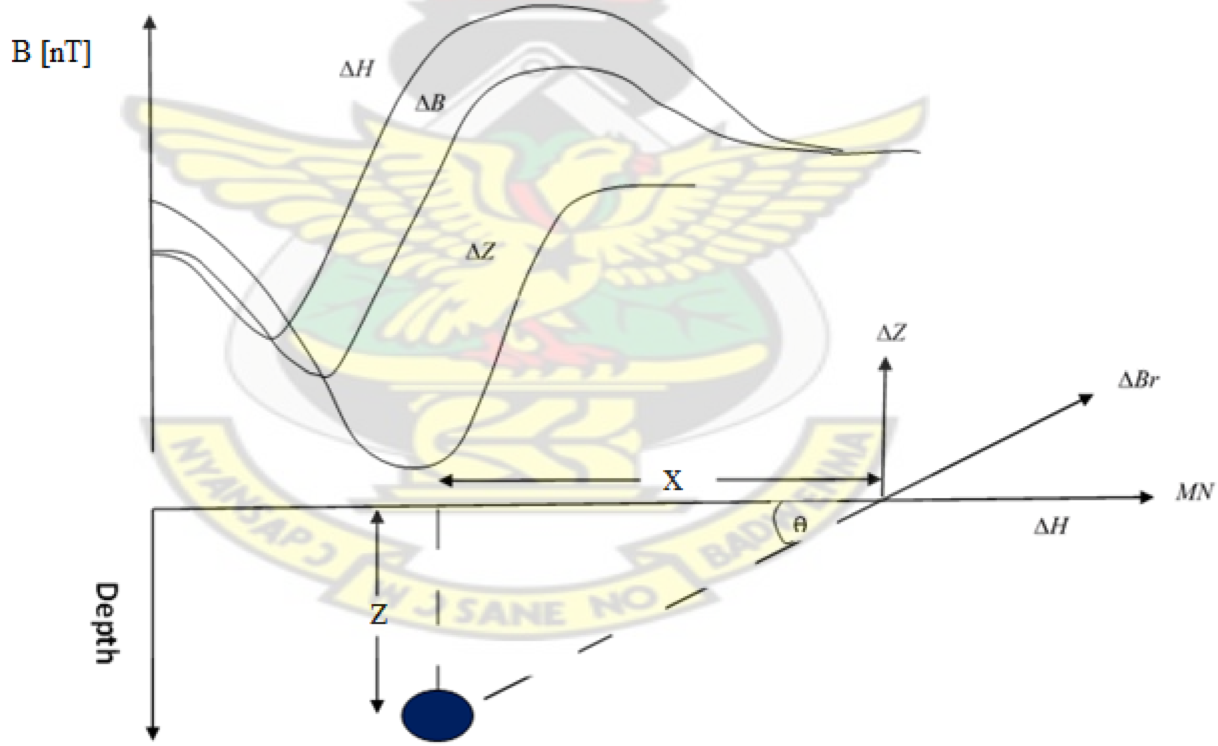

Figure 3.3 a profile of a magnetic field produce by a small magnetic body (Keary et al., 2002)

The field produced by this small body is given by

$$\Delta B = \frac{Cm}{r^2} \tag{15}$$

Where

$$C = \frac{\mu_O}{4\pi} \tag{16}$$

m is magnetic moment, r is radial distance and μ_R is the relative permeability of the media and has a value of one (1). In this case the horizontal component is written as

$$\Delta H = \frac{Cm}{r^2} Cos\theta = \frac{Cmx}{r^3} \tag{17}$$

and the vertical component is written as

$$\Delta Z = \frac{Cm}{r^2} Sin\theta = -\frac{Cmz}{r^3} \tag{18}$$

The equations (16), (17) and (18) are based on the assumption that the profile lies in the direction of magnetic north so that the horizontal component of the anomaly lies in this direction.

3.1.5 The Alkaline Vapour Magnetometer

The Alkali-Vapour magnetometer specifically cesium vapor magnetometer (optically pumped) consists of a photon emitter, an absorption chamber, a buffer gas, and a photon detector.

3.1.5.1 Principle of Operation of the Alkaline Magnetometer

The photon emitter emits light to excite atoms of Cs in the absorption chamber to higher energy levels (polarization), the electrons in the higher level fall back to level one and two. Level one then becomes over populated with electrons more than level two (optical pumping). The absorption chamber then becomes transparent and does not absorb electrons again. The energy difference between level one and two is proportional to the ambient magnetic field at that place. A radio frequency power is then used to depolarize the excited atoms; the frequency of the depolarizing wave is a measure of the magnetic field at that location.

A frequency of 0.004 Hz gives a field of ± 0.1 nT. A frequency of 2 kHz gives an accurate field reading.

3.1.5.2 Survey Procedure

With a gamma ray spectrometer and a magnetometer mounted on the aircraft, a typical flight path in airborne magnetic and radiometric survey is shown in figure 3.4.

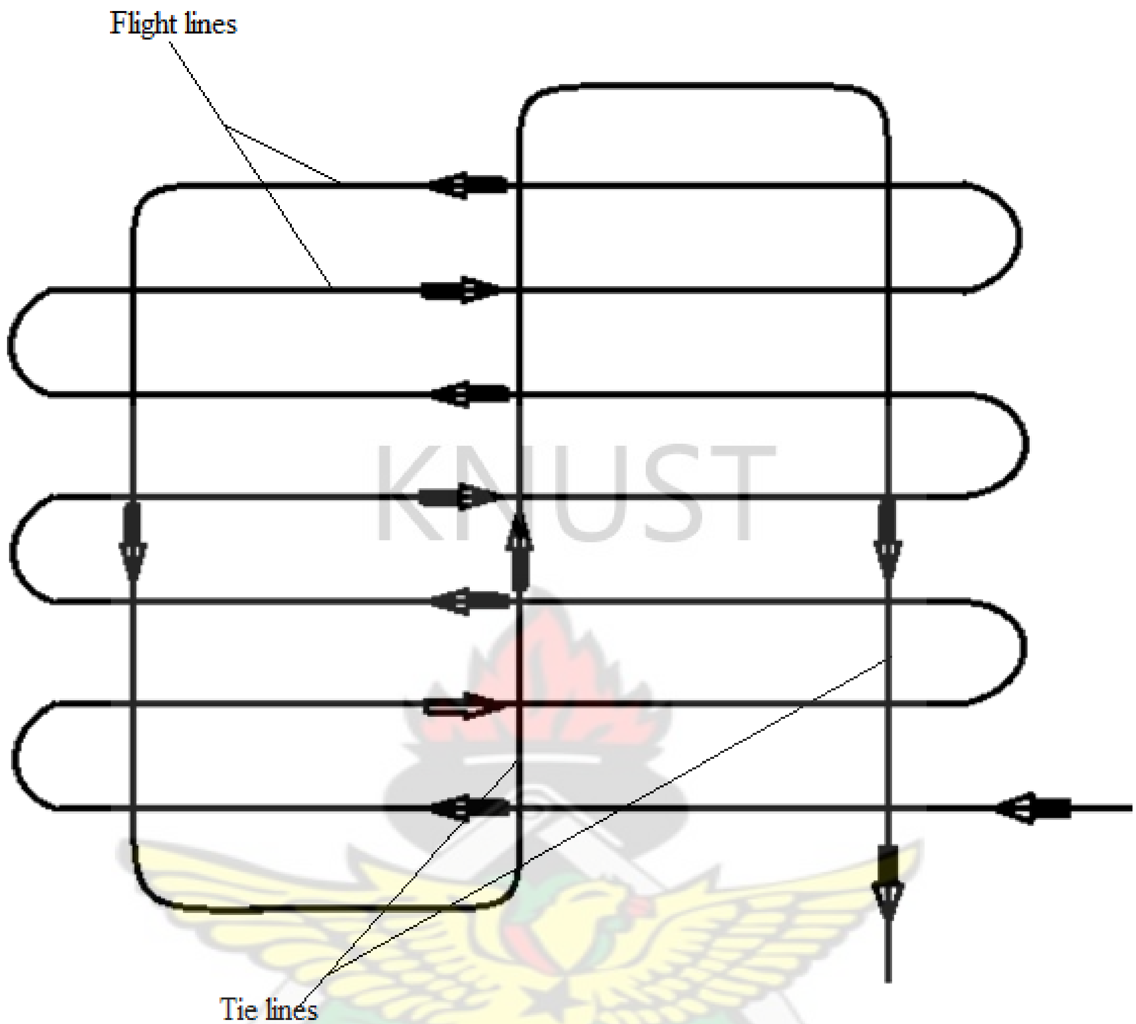

Figure 3.4 a typical flight path in airborne magnetic and radiometric survey

3.1.6 Data Reduction

This is the removal of all other causes of magnetic variations from the recorded values other than that cause by the magnetic effect of the subsurface. Three kinds of corrections are normally carried out in a magnetic data. These corrections are diurnal variation correction, geomagnetic correction, elevation and terrain correction.

3.1.7 Data Presentation

The corrected data is presented in the form of profile lines, contour map, grids or 3D map. In profiles and 3D maps, magnetic anomalies are indicated by peaks, and in the case of the contour maps, close and high contour values indicate magnetic minerals (Keary et al., 2002).

3.1.8 Data Interpretation

In data interpretation, smooth contours usually reflect sediments covered areas with relatively deep basement. Igneous and metamorphic terrains are identified by their more complex magnetic anomalies. In areas that have magnetic minerals, the contours are close with successive contours decreasing or increasing anomaly values toward a centre. Strike directions are determined with the direction of closed elongated curves. Places that have high horizontal $\frac{dB}{dx}$ anomaly gradient are often indicative of rocks with different susceptibility values. Shallow contact lying have steeper gradient, circular contours indicate circular features, and elongated dikes may be indicated by long narrow anomaly. Faults are indicated when one part of a magnetic signature is displaced with respect to others (Keary et al., 2002).

3.1.9 Quantitative Direct Method

Limiting depth; anomalies caused by shallow bodies have more short wave length than deeper bodies. Spectral analysis of the wavelength gives rapid depth estimates from regularly spaced digital data; their log power spectrum has a linear correlation.

For spherical and half-cylindrical ore bodies, the depth to centre of body is estimated to be equal to width of anomaly peak at half its maximum value. And for dipping sheets or prism, the depth to centre of body is roughly the width of linear segment of anomaly.

The Euler's deconvolution shown in equation (19) can also be used to determine the depth of the magnetic source.

$$(x - x_o)\frac{dT}{dx} + (y - y_o)\frac{dT}{dy} + (z - z_o)\frac{dT}{dz} = N(B - T) \tag{19}$$

3.2 Airborne Radiometric Survey

Radiometric also known as Gamma-Ray Spectrometry is a passive geophysical method that is used to investigate the subsurface of the Earth and it deals with the measurement of the spatial distribution of three radioactive elements (potassium-K, thorium-Th and uranium-U) in the top 30 - 40 cm of the earth's crust by detecting and measuring the intensities of the gamma rays produced by these elements in a radioactive decay (IAEA, 2003). Even though there are many natural occurring radioactive elements that decay and emit gamma rays, it is only the decay of potassium, and the decay series of daughters of thorium and uranium that are able to produce gamma rays with enough energies and intensities that can be measured with a gamma ray spectrometer. This is because the three radioactive elements are relatively abundant compared to other radioactive elements.

The average abundance of these radioactive elements in the Earth is about 2 - 2.5 %, 2 - 3 ppm, and 8 - 12 ppm for potassium, uranium and thorium respectively. ^{40}K is the radioactive isotope of potassium, and it is 0.012 % of natural occurring potassium (IAEA, 2003). This isotope decays to ^{40}Ar with the emission of gamma rays that has energies of 1.46 MeV. The decay process is shown below

$$ {}^{40}_{19}K \longrightarrow {}^{40}_{20}Ar + {}^{0}_{-1}e + \gamma $$

Thorium (^{232}Th) and Uranium (^{238}U) do not emit gamma ray when they decay, however some of their daughters do emit gamma rays when they decay. It is therefore the gamma rays emitted by daughters of Thorium (^{232}Th) and Uranium (^{238}U) as seen in figure 3.5, that are used to estimate the concentration of Thorium (^{232}Th) and Uranium (^{238}U) in the subsurface with the assumption that, the activities of the parents and daughters are in equilibrium. The diagram below shows the decay series of Thorium (^{232}Th) and Uranium (^{238}U).

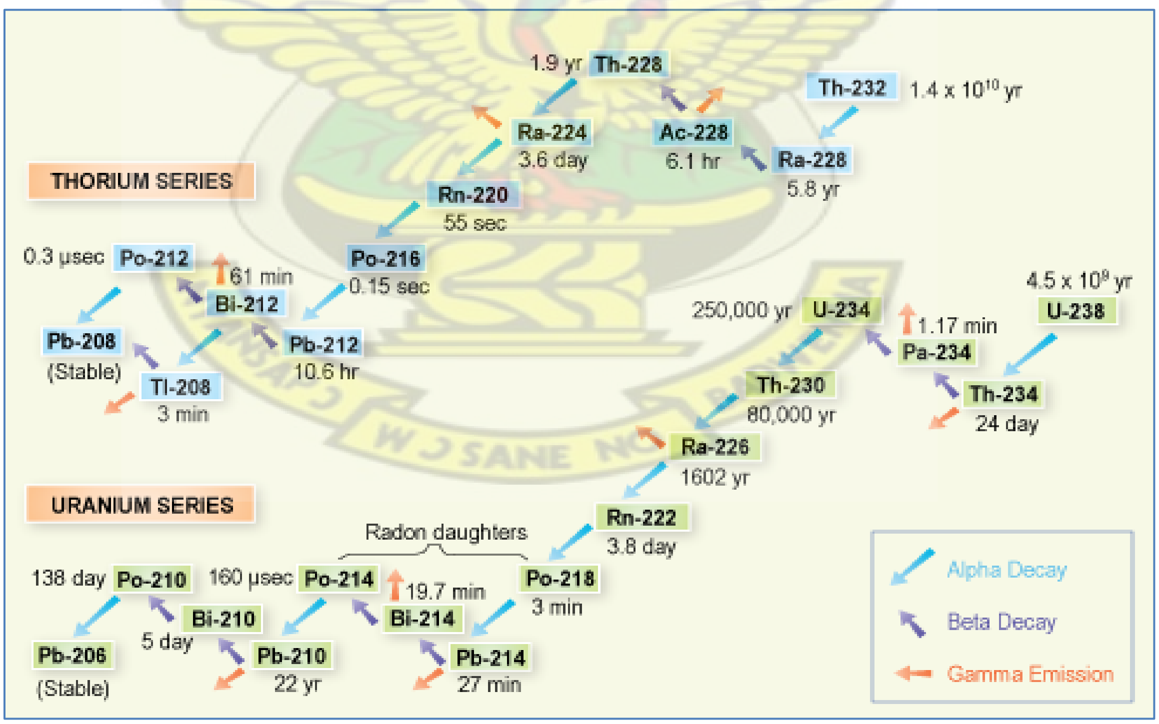

Figure 3.5 Decay series of Thorium and Uranium.

3.2.1 Principle of Radiometric Survey

The radiometric method operates on the assumption that radioactive elements occur naturally in the crystals of particular minerals, the abundance of these minerals varies across the Earth's surface with changes in rock and soil type, and because the energy of gamma rays is characteristic of the radioactive element, it can be used to measure the abundance of these radioactive elements in an area. So by measuring the energies of gamma rays being emitted in an area, the particular mineral present in the Earth crust can be deduced (IAEA, 2003).

Natural gamma-ray spectra range from cosmic radiations with energies above 3 Mev down to x-rays. Typical gamma-ray spectra are characterized by individual peaks corresponding to specific decay events due to Potassium (K), Thorium (Th), and Uranium (U) as shown in figure 3.6 below.

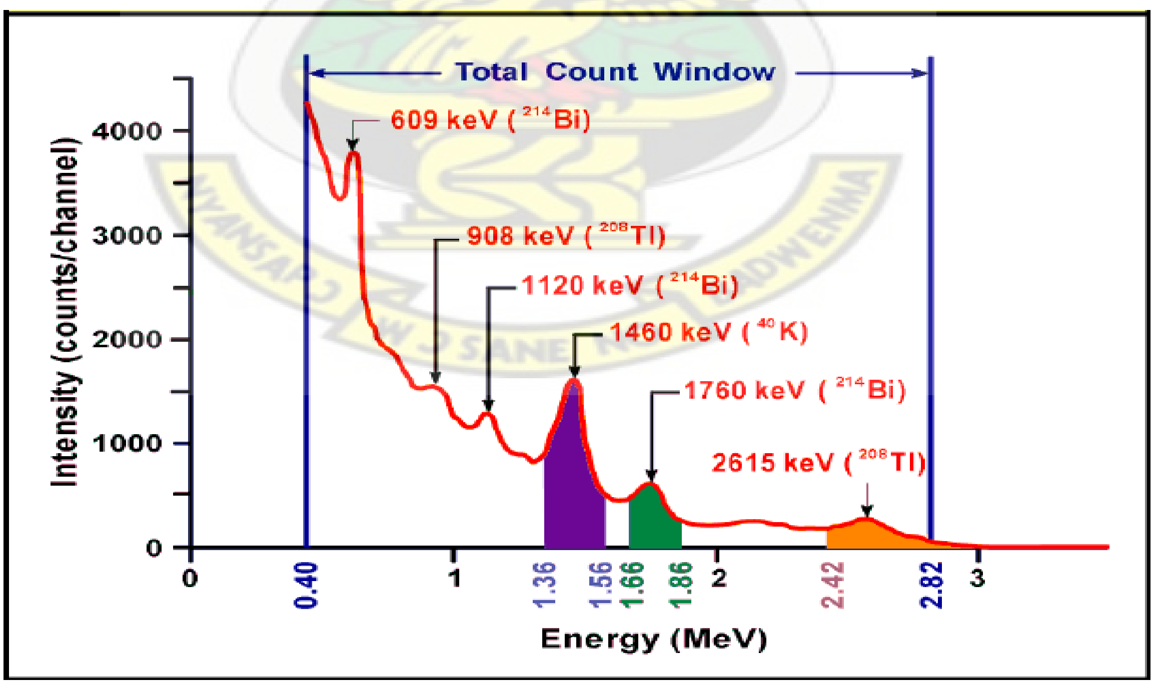

Figure 3.6 a typical gamma ray spectra (Modified after IAEA, 2003)

The peak of each element gives the energy of each photon falling somewhere within the small range determined by the nuclear kinetic energy at the time of the decay and by errors of measurement.

3.2.2 Radioactive Minerals

Radioactive elements occur naturally in the crystals of certain minerals and by virtue of the presence of the radioactive element in these minerals, the minerals become radioactive. The abundance of these minerals changes across the Earth's surface with variations in rock and soil type. Table 3.3 below shows some common radioactive minerals with radioactive elements in their crystal lattice and the environment in which these radioactive minerals occur.

Table 3.3 Radioactive Elements and the Minerals in which they occur and their Depositional environment (Telford et al. *1990).*

RADIOACTIVE ELEMENT	RADIOACTIVE MINERAL	ENVIRONMENT OF DEPOSITION
K	1.Orthoclase and microcline feldspars ($KAlSi_3O_8$)	1.Main constituent in acid igneous rocks and pegmatite
	2.Muscovite[$H_2KAl(SiO_4)_3$]	2. Main constituent in acid igneous rocks and pegmatite
	3. Alunite [$K_2Al_6(OH)_{12}SiO$]	3. Alteration in acid volcanics
	4.Sylvite,Carnallite[$KCl,MgCl_2,6H_2O$]	4. Saline deposits in sediments
Th	1.Monazite[ThO_2+Rare earth phosphate]	1..Granite, pegmatites, gneiss
	2. Thorianite[$(Th, U)O_2$]	2. Granite, pegmatites, placers
	3.Thorite, Uranothorite[$ThSiO_4$+U]	3. Granite, pegmatites, placers

U	1.Uraninite[Oxide of U, Pb, Re + Th, Rare Earth]	1.Granites, pegmatites and with vein deposits of Ag, Pb,Cu etc
	2.Carbonite[$K_2O.2UO_3.V_2O_5.2H_2O$]	2.Sandstones
	3.Gummite[Uraninite alteration]	3.Associated with uraninite

3.2.3 Nuclear Decay or Disintegration

The nuclei of some isotopes are heavy and unstable, therefore they undergo spontaneous disintegration to form stable nuclei and in the process emit particles and energy in the form of radiations. Nuclides which exhibit this phenomenon are termed radioactive nuclides and the process by which they become stable is termed nuclear decay or disintegration. The decay of radioactive isotopes is governed by the decay laws.

Law I states that in all radioactive transformation either an alpha or a beta particle is emitted but the two particles cannot be emitted together, however, any one of the particles can be emitted together with a gamma radiation (IAEA, 2003).

Law II states that the rate of decay or activity of radioactive isotopes at any time is directly proportional to the number of radioactive isotopes present at the time.

Mathematically law II is expressed as (IAEA, 2003).

$$\frac{dN}{dt} = -\lambda N \tag{20}$$

Where

λ is the constant of proportionality and λN is called the activity (Bq)

Grouping like terms and integrating left side of the equation above with respect to N and the right side with respect to time (*t*), the number of nuclei that remains after time t can be express as follows

$$\int_{N_O}^{N} \frac{dN}{N} = -\int_{O}^{t} \lambda dt \tag{21}$$

$$ln[N - N_o] = -\lambda t \tag{22}$$

$$ln\left(\frac{N}{N_O}\right) = -\lambda t \tag{23}$$

$$\frac{N}{N_O} = e^{-\lambda t} \tag{24}$$

$$N = N_O e^{-\lambda t} \tag{25}$$

where

N= the number of atoms present after time t (s);

N_O= the number of atoms present at time t = 0;

λ= the decay constant of a radionuclide(s^{-1})

3.2.4 Half Life

The time taken for a radioactive material to decrease to half of the original amount is the half-life of that radioactive element and is related to the decay constant in the equation above. Half-life is donated by the symbol $T_{1/2}$. If $N_{O,}$ radioactive material is present at time $T_{O,}$ then after the half-life ($T_{1/2}$) of the radioactive element, the amount of the element remaining would be $N_{O,}/2$. From this statement equation (25) can be written as

$$ln\left(\frac{N_O/_2}{N_O}\right) = -\lambda T_{1/2} \quad (26)$$

$$ln\left(\frac{1}{2}\right) = -\lambda T_{1/2} \quad (27)$$

$$-0.693 = -\lambda T_{1/2} \quad (28)$$

$$T_{1/2} = \frac{0.693}{\lambda} \quad (29)$$

Equation (29) shows the relationship between the half-life of a radioactive element and the decay constant of that element (IAEA, 2003).

3.2.5 Interaction of Gamma Rays with Matter

Gamma rays are electromagnetic wave with high frequencies and energies above 40 keV. An electromagnetic radiation with energy below 40 keV is known as X-rays. The energy of gamma rays is related to its frequency and wavelength by the equation below.

$$E = hf = hc/\lambda \quad (30)$$

Where *h* = Planck's constant 6.6261×10^{-34} Js; and *c* = velocity of light.

Gamma rays interact with matter in three different ways, these are Photoelectric effect, Compton scattering and pair production (ICRU, 1994). When a low energy gamma ray photon collides with an electron, all the energy of the photon is absorbed by the electron, this is known as photoelectric effect. On the other hand if the energy of the incident photon is moderate and it collides with an electron, the electron absorb part of the energy of the gamma ray photon, this causes the photon to be scattered at an angle to its original path, this phenomenon is known as Campton Scattering. And lastly when an incident photon with energy greater than 1.02 MeV collides with an electron, it is completely absorbed by the electron leading to the creation of an electron-positron pair in the electrostatic field of the nucleus.

The composition of matter and the energy of the incident photon determine the chance of the photon interacting with the matter; this is expressed as cross-section σ (m^2). Figure 3.7 shows the relationship between the scattering and absorption processes, the energy of the incident photon and the atomic number of the absorbing medium.

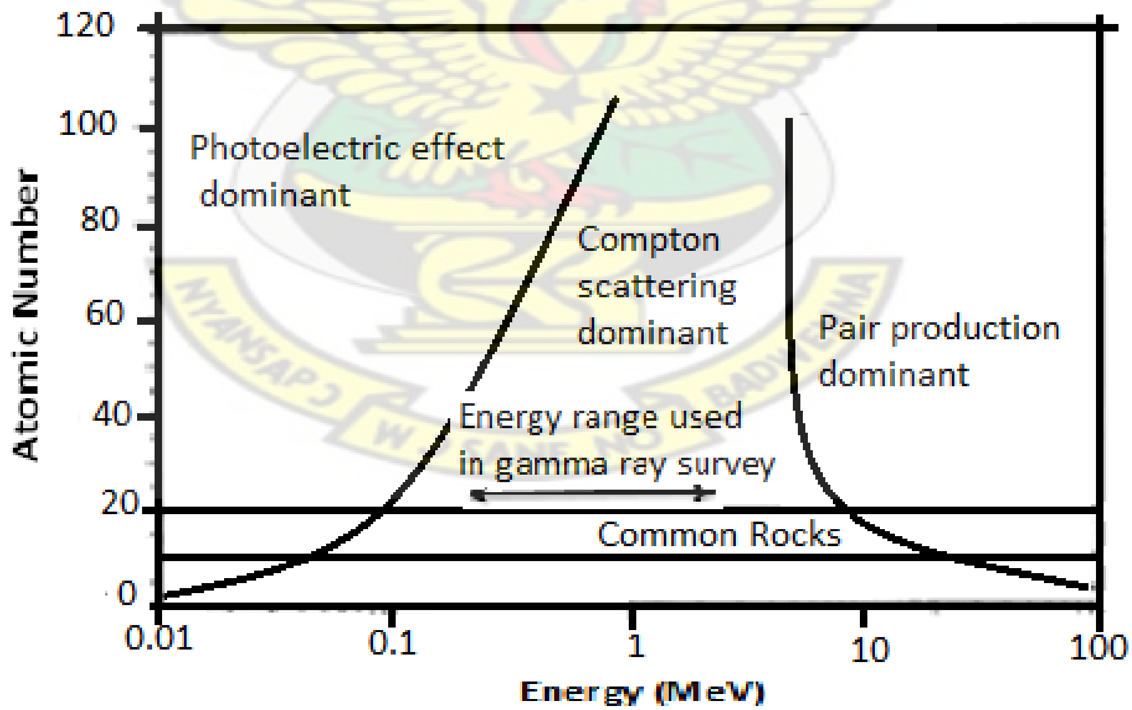

Figure 3.7 a diagram of the different ways by which gamma rays interaction with matter (IAEA, 2003)

For gamma rays of natural terrestrial origin (energies up to 2.615 MeV) and matter comprising rocks, water, and air; Compton scattering is the dominant interaction process. The gamma ray lose energy in each Compton scattering it under goes until its energy is low enough for the energy to get absorbed in an electron by the process of photo electric effect. Therefore the absorption of the photon of a particular energy in matter is described with a linear attenuation coefficient μ (m^{-1}) or mass attenuation coefficient μ/ρ (m^2/kg). The attenuation of narrow beam of gamma ray is model with an exponential function. The range of gamma rays of natural radionuclides is about 700 m in air, up to 0.5 m in rocks and a few centimeters in lead. Gamma rays have a discrete energy that is specific for a particular radionuclide. Since gamma rays are the most penetrating component of natural and man-made radiation, they are widely used in the study of the radiation environment.

3.2.6 Exploranium GR-820 Spectrometer

Exploranium GR-820 modern spectrometer system is used to measure radiations that emanates from radioactive materials. The GR-820 gamma-ray spectrometer consists of a detector pack of 33 litres of thallium-doped sodium-iodide (NaI(TI)) crystals in a thermally-insulated container, an "upward-looking" detector, a pulse amplifier, an analog to digital converter, a spectral analyser and an energy spectrum display or window display. In addition to the spectrometer are ancillary equipment such as GPS navigation (real-time differential), a radar altimeter, a barometer, a thermometer and a computer. The spectrometer is installed in the fixed wing of the aircraft and records 256 channels of summed data from either one or two crystal packs. The spectrometer employs automatic gain control to ensure stable peak positioning and therefore eliminate spectral drift.

3.2.6.1 Operation of Exploranium GR-820 Modern Spectrometer

When the aircraft with the NaI(TI) detector flies over a radioactive source, gamma rays from the source travels upward and interact with the detectors in the aircraft in three different ways. These are the pair production, Compton scattering and photoelectric effect. It is the photoelectric effect which is of paramount interest in measuring the radiations from gamma rays.

As a photon of gamma ray of sufficiently low energy interacts with the NaI(TI) crystal detector, the energy of the gamma ray photon is absorbed by orbital electrons in the crystal (IAEA, 2010). These electrons then becomes delocalized, with the application of a bias voltage, they are swept away, the movement of the electrons constitute an electric current that forms a signal pulse (photopeak) in the photomultiplier spectrum. The energy of the photopeak is equal to the energy of the incoming photon. Figure 3.8 shows the operational stages of the gamma ray spectrometer.

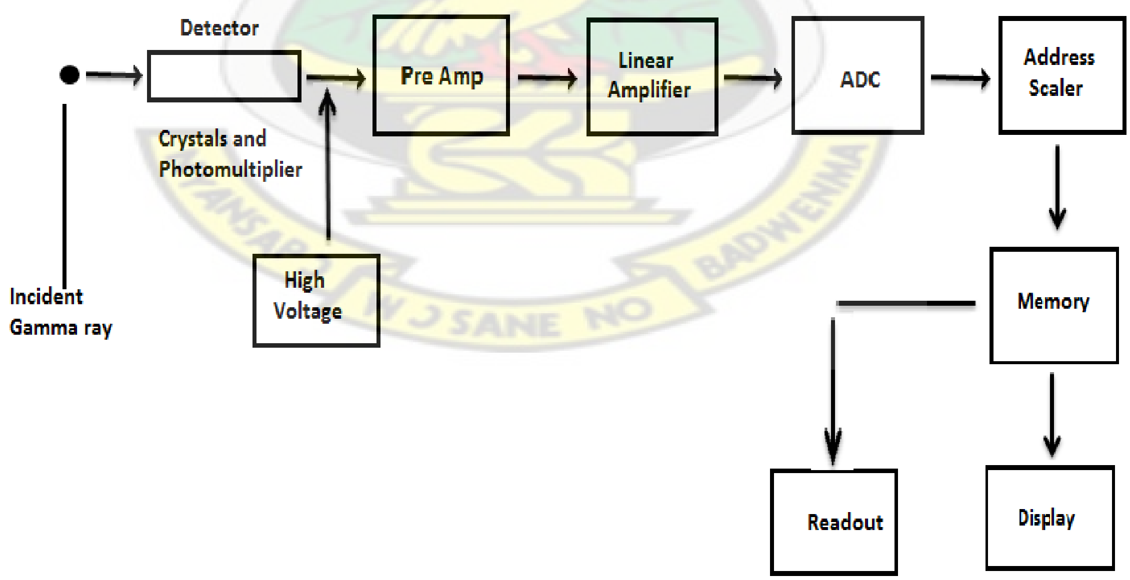

Figure 3.8 an operational diagram of a gamma ray spectrometer (IAEA, 2003)

The size of the pulse is then increase with a preamplifier, further amplification is carried out and signal shaped. The analogue signal is then converted into a digital signal with the Analogue to Digital converter (ADC). The digital data is then stored and displayed on a screen of a computer.

3.2.7 Survey Procedure

The spectrometer is mounted beneath the wings of an aircraft that is flown at an altitude of about 80 m from the ground and at a speed of 70 m/s on profile line or flight lines. The flight lines are usually in the direction of east west as shown in figure 3.4, and are spaced about 400 m apart for a detailed survey.

As the aircraft flies over radioactive minerals, the detectors in the spectrometer detect the gamma radiations from these minerals and their energies and count rates are recorded.

3.2.8 Data Procession

This involves all the corrections that have to be applied to the data to remove any anomaly that is non-related to geology and concentration of radioactive elements in the subsurface. The following corrections are carried out in data processing; pre-procession, spectral smoothening, 'dead time' correction, energy calibration, air craft and cosmic background correction, stripping, height correction, reduction to elemental concentration, and leveling of data.

3.2.8.1 Pre-processing

This is a quality control procedure that has to do with the merging of data that comes from different sources, checking of data to see that the recorded values are reasonable, checking for spurious and missing values. Data from the ancillary equipment are also filtered and corrected.

3.2.8.2 Spectral Smoothening

This is carried out to reduce noise and improve the signal to noise ratio of multichannel spectra. Two kinds of spectral smoothening exist. These are noise adjusted singular value decomposition (NASVD) and maximum noise fraction (MNF). In both cases it is the dominant spectral shape in the raw data spectra that is extracted and reconstructed to have dominant original signal with less noise.

3.2.8.3 Dead Time Correction

Dead time is the time it takes for the equipment to process the detected radiation, during this time the equipment does not detect incoming radiation. This has to be factored in the readings so that radiations that hit the detector during its dead time can be added to the observed counts. The effect of dead time is corrected by applying the formula below so that the actual count can be obtained (IAEA, 2003).

$$N = \frac{n}{1 - ct} \qquad (31)$$

where N = corrected count rate (counts/sec);

n = observed count rate (counts/sec);

c = total count rate over all channels (counts/sec);

t = the equipment dead time per pulse.

3.2.8.4 Energy Calibration

The energy of the measured spectra drifts from time to time as a result of changes in the high voltage supply and temperature which leads to changes in the gains of the photomultiplier tube. Drift introduces error into the measured spectra, and is corrected by calibrating the individual spectra to the peak positions. This is done by determining the energies of at least two pronounce photopeaks as the maximum value of a quadratic fitted within each photopeak. A linear function is then fitted to the photopeak positions (channel numbers versus energy) to estimate the energy at each channel (keV per channel) and the gain. These parameters are then used to correct each one second spectrum within the sample accumulation period by re-sampling each channel to its correct energy range using linear interpolation.

3.2.8.5 Aircraft and Cosmic Background Correction

Spectra produce by radiations from the aircraft and the background are subtracted from each of the observed spectra as shown in the equation below

$$n_i = a_i + b_i n_{cos} \tag{32}$$

$$c_i = o_i - n_i \tag{33}$$

where

c_i= corrected count rate of the ith channel

o_i=observed count rate of the ith channel

n_i = aircraft + cosmic background count rate in the i^{th} channel;

n_{cos}= cosmic window count rate;

a_i= aircraft background in the i^{th} channel;

b_i= cosmic background in the i^{th} channel normalized to unit counts in the cosmic window.

3.2.8.6 Radon Background Correction

The upward detector measures atmospheric radon concentration, unfortunately these radiations from the atmospheric radon are also detected by the downward detectors and are registered in the channels. These unwanted radiations that contribute to the observed spectra would have to be remove from the observed spectra.

The uranium window or channel has a radon contribution given by the equation below (IAEA, 1991). This factor would therefore be subtracted from the observed uranium window.

$$U_r = \frac{u - a_1 U - a_2 T - a_2 b_t - b_u}{a_u - a_1 - a_2 a_t} \tag{34}$$

Where

U_r= radon background count

u= count rate in the upward detector

U= count rate of uranium

T= count rate of thorium

a_1, a_2, a_u, a_t,b_u and b_t are constants derived by suitable calibration.

The radon background count in the uranium channel is linearly related to the radon background count in the total count window and the potassium count window (Grasty et al., 1984). So by calibration, radon background count in the uranium channel is used to calculate the radon background count in the total and potassium channels. The radon background in the thorium channel is also calculated from the radon background in the uranium channel by the equation below

$$T_r = a_t U_r + b_t \tag{35}$$

All these background readings from radon are subtracted from their respective windows or channels.

3.2.8.7 Stripping Correction

This is the removal from a channel gamma rays that have Compton scattered into the channel.

The equations below show how uranium, potassium and thorium channel are corrected for gamma rays that Compton scattered from each channel into another.

$$n_{th(corr)} = \frac{n_{th} - a n_u}{1 - a \propto} \tag{36}$$

$$n_{u(corr)} = \frac{n_u - a n_{th}}{1 - a \propto} \tag{37}$$

$$n_{k(corr)} = n_k - \beta n_{th(corr)} - \gamma n_{u(corr)} \quad (38)$$

where

$n_{th(corr)}$, $n_{u(corr)}$ and $n_{k(corr)}$ are the corrected count rate of thorium, uranium and potassium,

n_{th}, n_u and n_k are the observed count rates of thorium, uranium, and potassium

$\propto, \beta, \gamma$ and a are the stripping ratios. $\propto$ are the counts in the U window per unit count in the Th window for a pure Th source. β are the counts in the K window per unit count in the Th window for a pure Th source. γ are the counts in the K window per unit count in the U window for a pure U source, and a are the counts in the Th window per unit count in the U window for a pure U source.

3.2.8.8 Height Correction

In a height range of 50 m to 300 m the detector response to radiations decreases exponentially with an increase in heights of the detector from the source. The observed count rates in an airborne survey are therefore less than the actual count. The deficient in count rate is corrected for by applying the equation below

$$n = n_o e^{-\mu(H-h)} \quad (39)$$

where

μ= the channel attenuation coefficient per meter

n_o= the observed count at the standard temperature and pressure at the height h

n= the corrected or supposed count rate for the nominal survey terrain clearance H

3.2.8.9 Reduction to Elemental Concentration

This is the conversion of corrected count rates of each window to the abundance of that window radioactive element concentration in the ground. The conversion is done using the sensitivity constants and with the assumption that the activities of uranium and thorium are in equilibrium with the activities of their daughters nuclei. The equivalent abundance of thorium and uranium are in parts per million, and the abundance of potassium in percentages. The equations for calculating the abundance of each of these elements are shown below.

$$eTh = C_{Th}N_{Th(corr)}e^{-mTh(h-ho)} \quad (40)$$

$$eU = C_{U}N_{U(corr)}e^{-mU(h-ho)} \quad (41)$$

$$K = C_{K}N_{K(corr)}e^{-mK(h-ho)} \quad (42)$$

where

eTh and eU are the equivalent amount of thorium and uranium respectively in the ground and K the amount of potassium in the ground

C_{Th} , C_U and C_K are the sensitivity constant of thorium, uranium and potassium respectively

N_{Th} , N_U and N_K are the corrected count rates of thorium, uranium and potassium respectively

$m_{Th,}$ m_U and m_K are the attenuation coefficient of thorium, uranium and potassium respectively.

3.3 Georefrence and Data Presentation

Geo-referencing is carried out to ensure that corrected data is well positioned and its location on the ground is well defined without any ambiguities. This is done by geo-referencing and projecting or transforming the coordinate in which the data was collected into common coordinate system or map datum for all data. This is to ensure integration of different sources of data.

3.3.1 Leveling

This is the removal of systematic noise within the data due to drags, direction or slight variation in the altitude. The gridded data is leveled with filters. Filtered grids are used to correct the line data (Minty, 1991).

3.3.2 Scattered Plots

Scattered plots are able to analyze the relationships that exit between the radioactive elements, their trends and area in which they are concentrated. The scattered plots are used to analyze the association of radioactive elements with mineralization (Shives et al., 1995).

3.3.3 Profile Lines

The data is presented as single, multiple or stacked profiles. Profile presentation enables data to be displayed at full spatial resolution, and the application of a one dimensional filter to the spectra improves the signal to noise ratio. When profile are stacked they provide vital information for the interpretation of the interrelationships among the channels, the stacked profile are also integrated with a lithological profile for easy inference of areas with possible mineralization.

3.3.4 Contour Maps

Contours are lines joining areas with equal values, they enable the extraction of data amplitude and the presentation of undistorted anomaly shapes (Gunn et al., 1997). Contour maps do not also require large digital space for their storage.

3.3.5 Gridding

The minimum curvature gridding utilizes two dimensional splines to interpolate the corrected data onto a mesh with regular spaced interval values, using the minimum curvature iterative algorithm that adapts weights such that the curved nature of the surface is reduced according to Briggs conditions (Briggs, 1974). In gridding, a specified radius is defined around the grid node (intersect) within which flight line sample is included in the interpolation and for the surrounding nodes an inverse distance function is used in calculating distance weighted average from the surrounding grid node. The curvature of the interpolated surface is compared with the curvature of the interpolated surface in the previous step, resulting in an adaptation of the weight function. The interpolation is complete after a specified number of iterations have been reached, or when the flight line samples are within a specified tolerance from the surface. For airborne surveys, the search distance should be larger than the flight line spacing to include two adjacent flight lines in the computation of the distance weighted average. Each of the grid cells is then assign a colour based on its value and then presented as high quality images on a display device such a screen of a computer as shown below in figure 3.9.

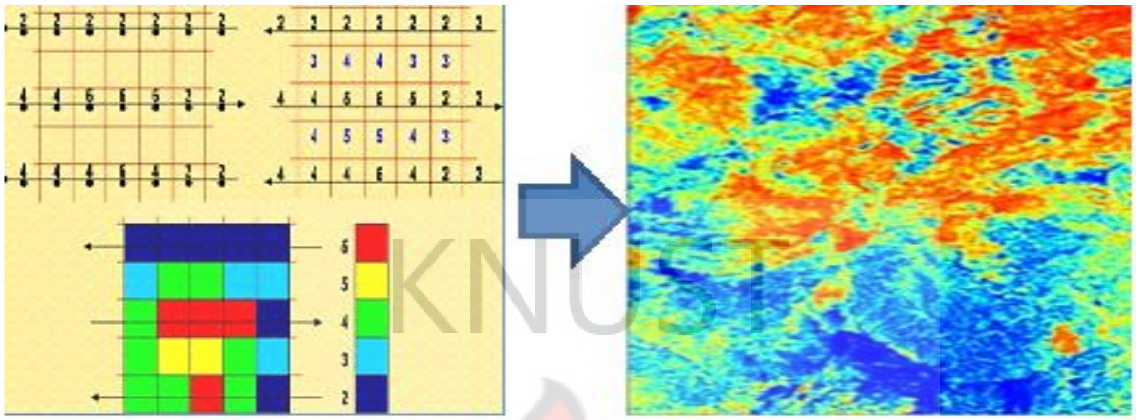

Figure 3.9 example of a gridded image.

3.3.6 Data Analysis and Interpretation

Analysis of the grids is done with the identification and mapping of similar features from the grids. The interpretation of the features identified is done with knowledge of the geology of the area, the style of mineralization, and the deposit type found in the area.

CHAPTER FOUR: MATERIALS AND METHODS

4.1 Materials

The materials used in the field for data collection include

- A light aircraft with fixed wings Cessna Titan 404 (C-FYAU)
- Scintrex Cesium SC-2
- Exploranium GR 820, 256 channels with 2048 in^3 NaI downward looking crystal and 256 in^3 upward looking crystal

4.1.1 Data processing software

The under listed software were used in data processing and enhancement

- Oasis Montaj, version 6.4.2
- Global mapper version 13
- Arc GIS version 10.0

4.2 Research Methodology

The methods employed in the research include pre-survey calibration, data collection, data enhancement and interpretation. Each of these processes is outlined below, and has contributed significantly to the interpretation of the data.

4.2.1 Pre-Survey Calibrations

- Determination of flight speed, flight altitude, flight path and the establishment of a base station were carried out.

- Radiometric calibration tests were carried out in order to calculate the attenuation coefficient, sensitivity, stripping ratio, aircraft and cosmic backgrounds radiation. These calibrations are based on the International Atomic Energy Agency standards.

4.2.2 Metadata

The data was collected in most parts of the Birimian in the Eastern region of Ghana by the Geological Survey of Finland (GKT) in collaboration with the Geological Survey of Ghana between 1997-1998 using a light aircraft that was flown in NW-SE direction with a nominal terrain clearance of 70 m and at a speed of 70-80 m/s, and covering an area of 561.69 km^2 with a flight line spacing of 400 m apart (GSD, 1998). The aircraft had a gamma ray spectrometer mounted on its wings and a magnetometer that is housed in a cage and towed behind the aircraft. The radiometric data and magnetic data were sampled at a rate of 1 sec and 0.1 sec respectively, using the Exploranium GR-820 modern spectrometer system and the cesium vapor magnetometer. All the preprocessing corrections and corrections such as diurnal, spectral drift, dead time, energy calibration, aircraft and cosmic radiations, radon background radiations, stripping, height correction, reduction to elemental concentration and leveling of the data were all carried out by the Geological Survey of Finland.

4.2.3 Data Enhancement

The corrected data was obtained from the Ghana Geological Survey department through the Physics Department of Kwame Nkrumah University of Science and Technology. The data was further processed, enhanced and interpreted with Geosoft (Oasis Montaj), Arc GIS, and Global mapper.

Firstly, on a Geosoft platform the two datasets were projected to Universal Transverse Mercator (UTM) coordinate system Zone 30 N using World Geodetic System (WGS) 84 as the datum. The data was then gridded with the minimum curvature method of gridding.

4.2.3.1 Magnetic Data Enhancement Techniques

MAGMAP filtering utilities were then applied to the magnetic grids to enhance the data for easy interpretation. The filters in MAGMAP are a range of linear and nonlinear mathematical algorithm which selectively enhances the anomalies due to one group of geological source relative to anomalies due to other group of geological source (Milligan and Gunn, 1997). The mathematical enhancement techniques are complemented by a range of imaging routines such as the step by step procedure in MAGMAP which can be specified to visually enhance the effects of selected geological sources. The two dimensional Fast Fourier Transform (2D-FFT) in MAGMAP is particularly useful in the transformation from the frequency domain to the wave number domain and also for the calculation of derivatives (Telford et al.,1990).

In this project the MAGMAP filters that were used in enhancing the magnetic data include reduction to the pole, upward continuation, downward continuation, first vertical derivative, and analytical signal.

4.2.3.1.1 Reduction to the Pole

At low magnetic latitude the magnetic anomalies are asymmetrical to their source; this is regarded as a directional noise. RTP uses azimuthal filter in frequency domain to convert the field at the low latitude to the field at the pole where the inducing field is vertical. In order to minimize the directional noise that is observed in the low magnetic latitudes, the angle of declination and inclination were calculated using the central longitude and latitude coordinates of the area. The angle of declination and inclination were then specified in the MAGMAP step by step filter and data then reduced to the pole.

4.2.3.1.2 Downward and Upward Continuation Filter

The downward continuation filter simulates data acquisition closer to the ground, this simulation sharpens the effect of high frequency anomalies that originates from shallow geological source.

The upward continuation filter smoothed out high frequency anomalies that originated from shallow source, and enhanced anomalies that originated from deeper structures.

4.2.3.1.3 First Vertical Derivative

This was used to enhance high frequencies relative to low frequencies, it peaks over tops of sources and indicates the outline of source by steep gradients and inflections.

4.2.3.1.4 Analytic Signal

The analytic signal is a type of reduction to the pole, the signal is without a negative componet and it is related to magnetic field. The analytic signal is independent of the magnetized field direction and the Earth's magnetic field direction. Therefore bodies that have the same geometry have the same analytic signal. The analytic signal is not affected by the instabilities that are associated with transformations of magnetic fields from low magnetic latitude (MacLeod et al., 1993). The source position is defined by them regardless of remanence in the source. The analytical signal was applied to the data to place anomalies over their source.

4.2.3.2 Enhancement of Radiometric Data

The data were levelled and micro-levelled for the removal of residual errors and noise. Ratio maps were also created for the enhancement of subtle structures. Ternary image of the three radioactive elements were also created for easy mapping of geology.

4.2.3.2.1 Gridded Channels of Tc, K, U, Th, Ratio Maps and Ternary Map

The airborne radiometric data were gridded with the minimum curvature gridding technique. The gridded images were then used to interpret and map the geology of the area by making inferences from literature what high or low radioactive material implies in relation to geology at a particular region of the study area.

Ratio and ternary image were produced to help in the identification and mapping of zones that are hydrothermally altered. A decrease in Th and an increase in K is indicative of alteration environments in an ore deposit (Ostrovskiy, 1975). A low uranium concentration with a high potassium concentration would lead to a low values U/K ratio which is indicative of granitoid rocks. The depletion of uranium leaves negative aureoles which is the results of pervasive hydrothermal alteration (Boyle, 1979). Even though, thorium is generally immobile, an enrichment of thorium and potassium is indicative of hydrothermal alteration in some gold deposits (Silva et al., 2003). A ternary map was created with the grid display in Geosoft by assigning potassium with red, thorium with green and uranium with blue. The ternary map showed the concentration of the elements relative to each other.

CHAPTER FIVE: RESULTS AND DISCUSSIONS

The results from the processed and enhanced radiometric and magnetic data were developed into different maps which are shown below in this chapter. These maps are interpreted below and hydrothermal alteration zones, structures and geology are then mapped from these maps. The interpreted alteration zones, structures and geology are path finders of gold mineralization zones in the Birimian and the Tarkwaian formation. The zones that have the potential of hosting gold mineralization are mapped in this chapter.

5.1 Digital Elevation Map

Figure 5.1 is the Digital Elevation Map (DEM) of the study area, it shows that the elevation of the study area range from 148 m to 593 m above mean sea level. The study area has low land in the western part and high land in the eastern part. The highlands trend north east with an average height of about 350 m above mean sea level. The highlands occupy about two thirds of the study area as shown by the digital elevation map (figure 5.1). A notable high land is the famous Atiwa range. The lowland areas depicted by blue colour range from 148 m to 177 m above mean sea level, these lowland areas are found in the north western part of the study area and are noted to be the valleys of the Atiwa range.

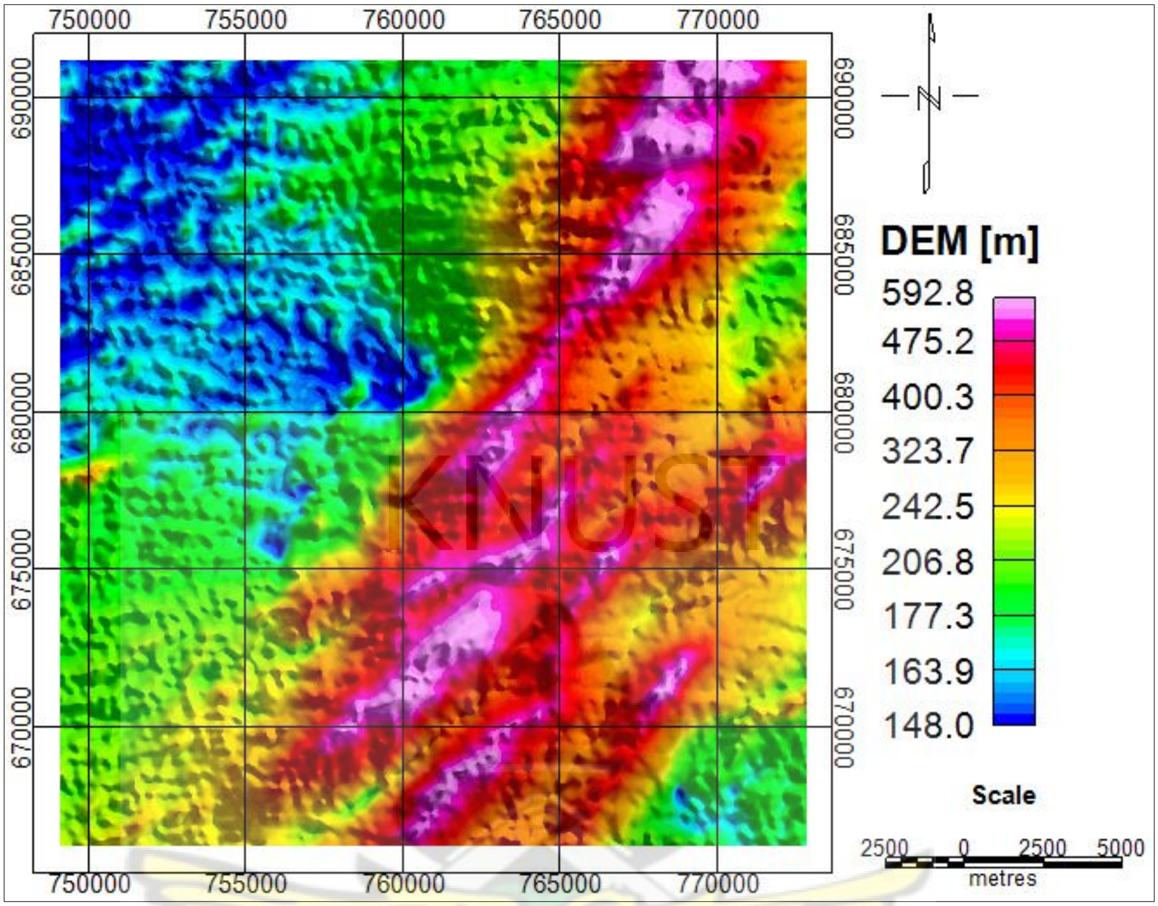

Figure 5.1 digital elevation map (DEM) of the study area.

5.2 Maps From The Airborne Maganetic Surveys

Airborne magnetics maps depict in different colours the amount of magnetic minerals (magnetite, pyrrhotite) in different rock formations. The red colour is used to indicate areas with high content of magnetic minerals and the deep blue colour indicates areas with low content of magnetic minerals. Airborne magnetic maps also highlight structures such as folds, faults or shear zones, lithological boundaries between different rock types, and crosscutting features such as dykes, and borders of intrusions. In interpretation of airborne magnetic maps, the magnetic minerals content and the features (faults, dykes, and folds shear zones) present in the survey area are very useful in identifying possible zones of gold mineralization.

5.2.1 Total Magnetic Intensity Map

The total magnetic intensity is the magnetic field that is observed in a particular location, it is a combination of the Earth's magnetic field and the field produced by magnetic bodies that are in the subsurface. Figure 5.2 is the Total Magnetic Intensity (TMI) map of the surveyed area. From the map, the high magnetic intensity regions are actually areas with low magnetic intensities which represent the metasedimentary formation (MS) and the intruded granites, and the low magnetic intensity regions are actually areas with high magnetic intensities which represents the metavolcanic formations and the mafic dykes . This misrepresentation is called directional noise that is observed in low magnetic latitude areas due to the inclination of the Earth's magnetic field at these low latitude, this problem is corrected by reducing the total magnetic intensity to the pole where the Earth's magnetic field is vertical. This directional noise problem if not corrected can cause data misinterpretation, hence there was the need for reducing to the pole for easy interpretation of the results.

In addition to the high and low magnetic anomalies observed in the TMI map, a number of features such as lineaments indicated by F1, F2, F3, F4, F5, F6, and F7 are also identified in the TMI map.

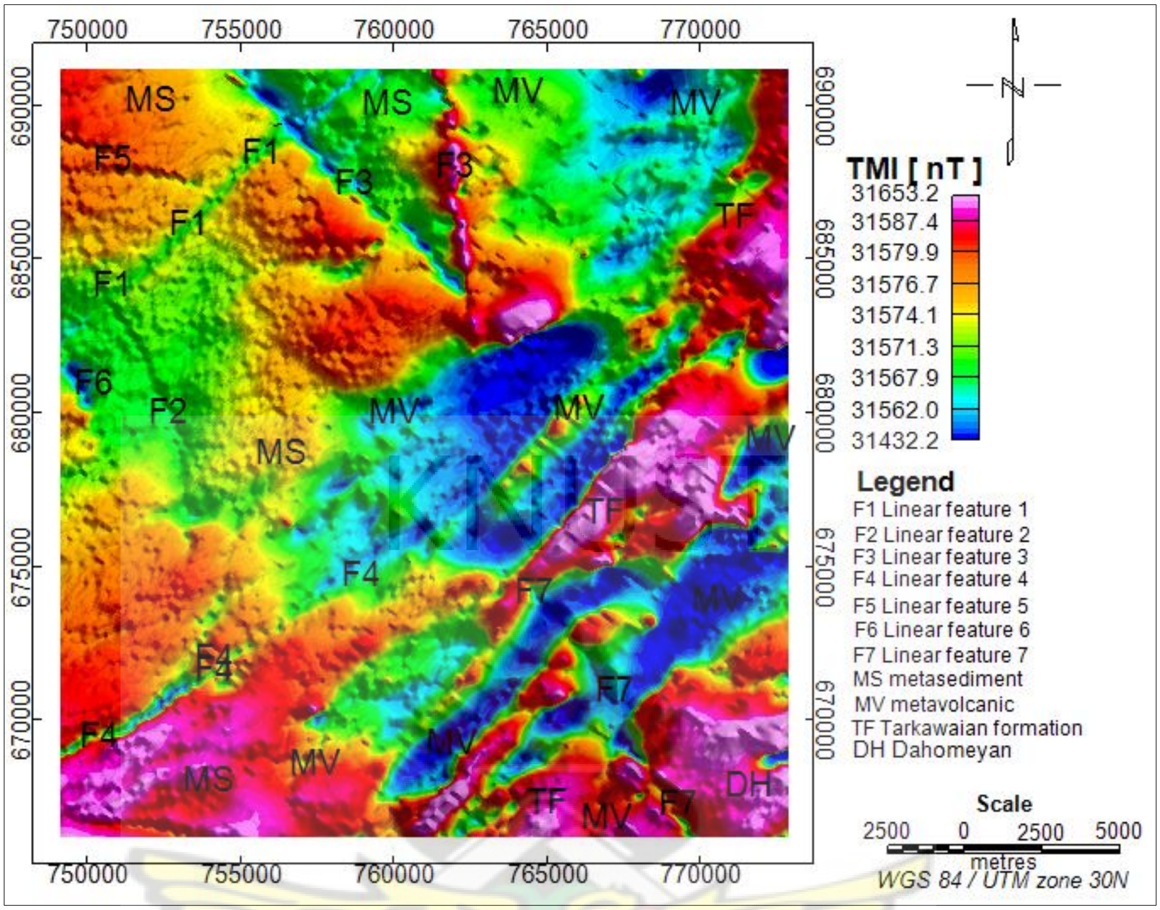

Figure 5.2 Total Magnetic Intensity (TMI) map.

5.2.2 Reduction To The Pole

Reduction to the pole is the process of converting the magnetic field developed by magnetic bodies from the magnetic latitude where the Earth's field is inclined, to the field at the Earth's magnetic pole, where the inducing field is vertical. When the Earth's field is inclined, magnetic anomalies due to induction have forms that are asymmetrically related to their sources as this is noticed in figure 5.2 where high magnetic intensity regions were seen as low magnetic intensity region and the reverse, but when the inducing field is vertical, the induced anomalies are directly over their sources. This is seen between the TMI (figure 5.2) and the RTP map (figure 5.3) that regions with high magnetic intensities in the TMI map are recording low magnetic intensities in the RTP map and vice versa. Reduction-to-the-pole (RTP) is a useful and effective operation designed to transform a total magnetic intensity (TMI) anomaly caused by an arbitrary source into the anomaly that this same source would produce if it were located at the pole and magnetized by induction only (Li, 2008).

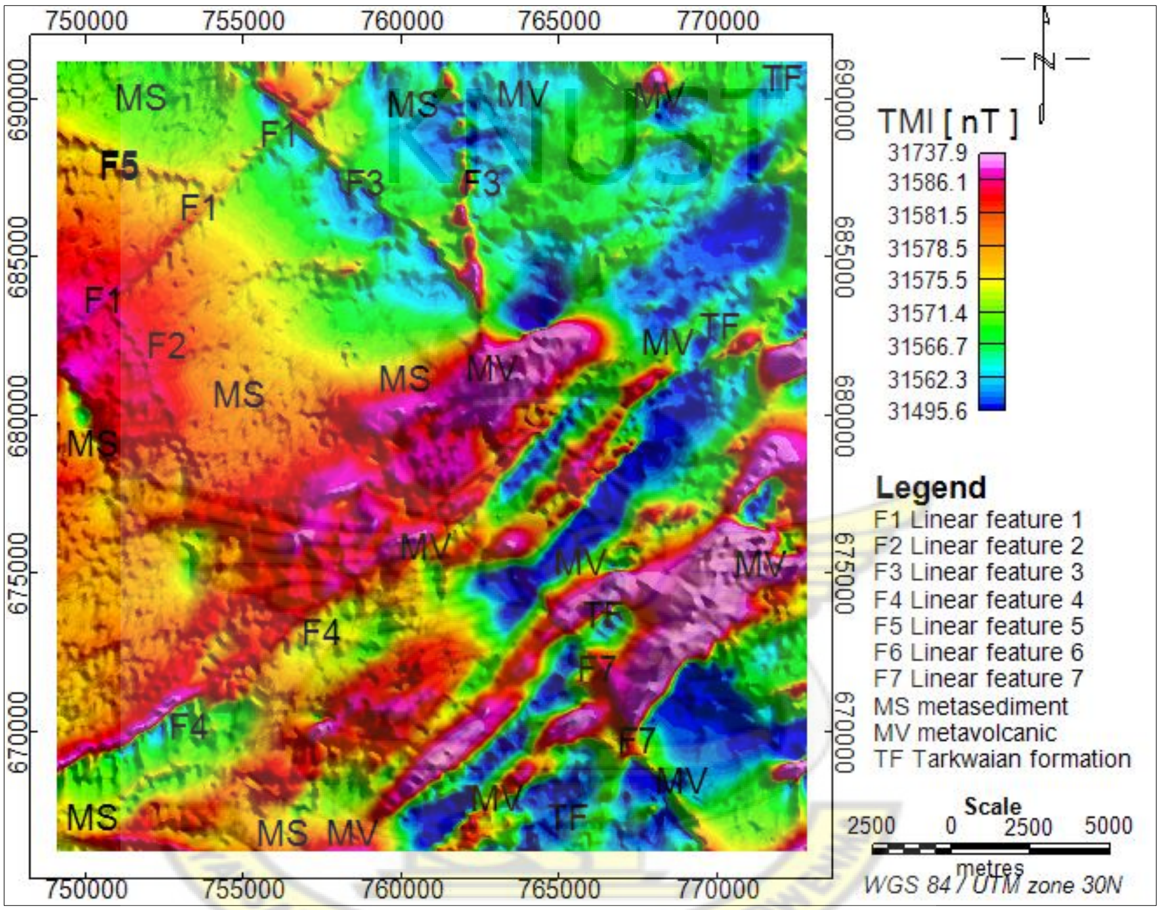

Figure 5.3 Total magnetic intensity map reduced to the pole (RTP)

The same process can be used to convert magnetic fields between any two magnetic latitudes. A basic assumption of the reduction to the pole process is that all bodies are magnetised by induction.

From the RTP Map the formation labelled MS are metasediment, those labelled MV are the metatvolcanic, those labelled TF are the Tarkwaian formation and most of the linear features seen in the TMI map are also seen in the RTP map.

5.2.3 Analytical Signal of the TMI and First Vertical Intergral

The vector nature of magnetic field at low magnetic latitudes places like Ghana makes the magnetic field (anomalies) developed by magnetised rocks complex and difficult to interpret (Macleod et al., 1993). This has resulted in the use of data processing techniques reduction to the pole which produces anomalies vertically over the bodies. But reduction to the pole suffers instability during the transformation and also produces artifacts that are not acceptable in the results. A better alternative for positioning anomalies vertically over the bodies is to apply analytical signal to the total magnetic field and the vertical integral of the magnetic field. With this method a maximum anomaly is always produced over the magnetic body regardless of the direction of magnetization of the body (Macleod et al., 1993).

Analytic signal transformation is a kind of reduction to the pole from low magnetic latitude. It has an advantage over reduction to the pole and reduction to the equator in that; it is completely independent of the direction of magnetization and the direction of the Earth's field (Milligan and Gun, 1997). This implies that all bodies with the same geometry have the same analytic signal. In addition to this, analytical signal transformations are not subjected to the instability that occurs in reduction to the pole from low magnetic latitudes. The analytic signal maps also define source positions regardless of any remanence in the sources (Macleod et al., 1993).

Figure 5.4 is a map of the analytical signal of the TMI, it is seen from this figure that the high magnetic intensity regions and the low magnetic intensity regions are clearly outlined compared to that seen in the TMI map (figure 5.2) and the RTP map (figure 5.3).

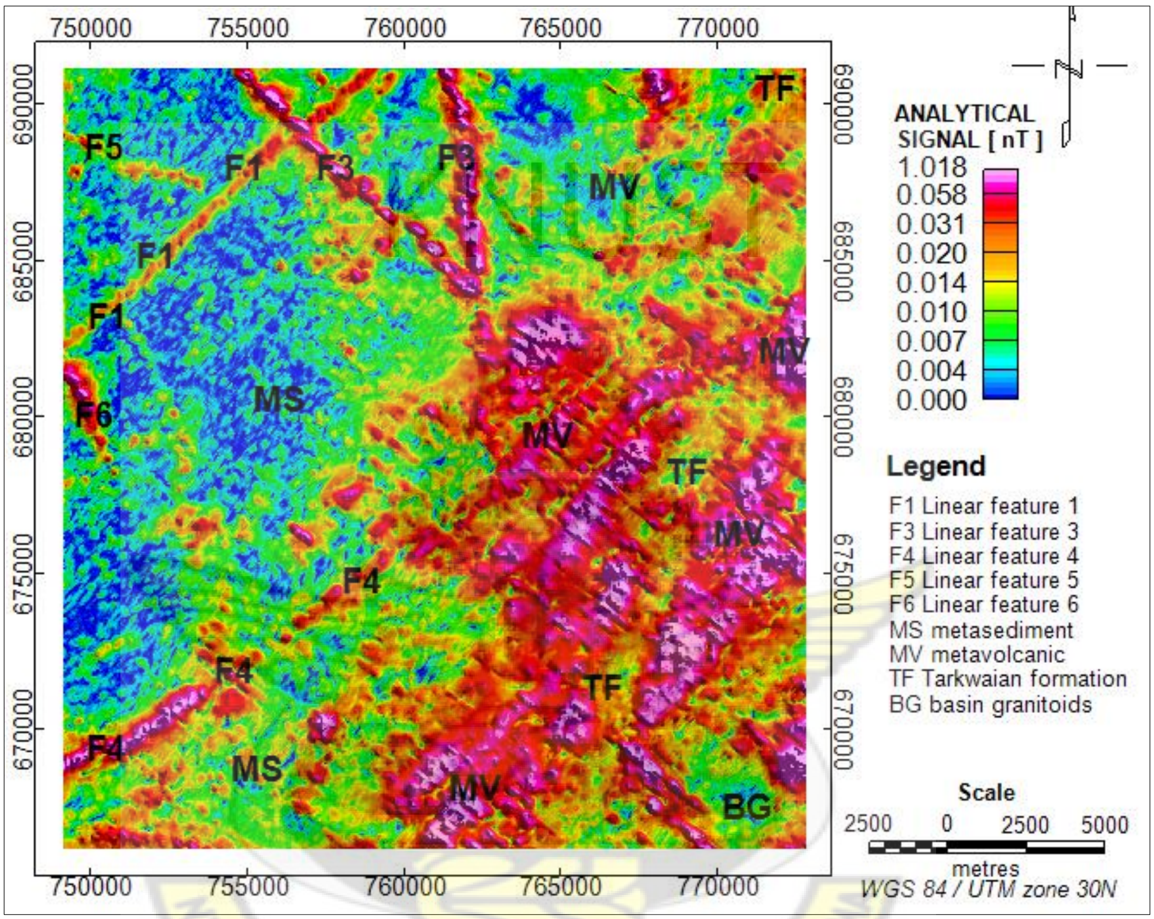

Figure 5.4 Analytical signal applied to TMI

Also high magnetic intensity regions in the TMI are seen as actually having low magnetic intensity in the analytical signal map (figure 5.4) and vice versa. The analytical signal map has been able to position the anomalies correctly over their causative bodies because the source positions of the anomalies are defined vertically over the source regardless of any remanence in magnetization. In addition, maximum anomaly has been produced over the magnetic body regardless of the direction of magnetization. So in totality the boundaries that exist for the different geological formations in the study area are well demarcated by the application of the analytical signal; the blue area depicts the metasediments, the green area depicts the mafic volcanic and the reddish area depicts igneous formation.

Figure 5.5 is a map of the analytical signal of the vertical integral, from this map regions of low magnetic intensity in the TMI are observed as regions with high magnetic intensity in the analytical signal of the vertical integral and vice versa.

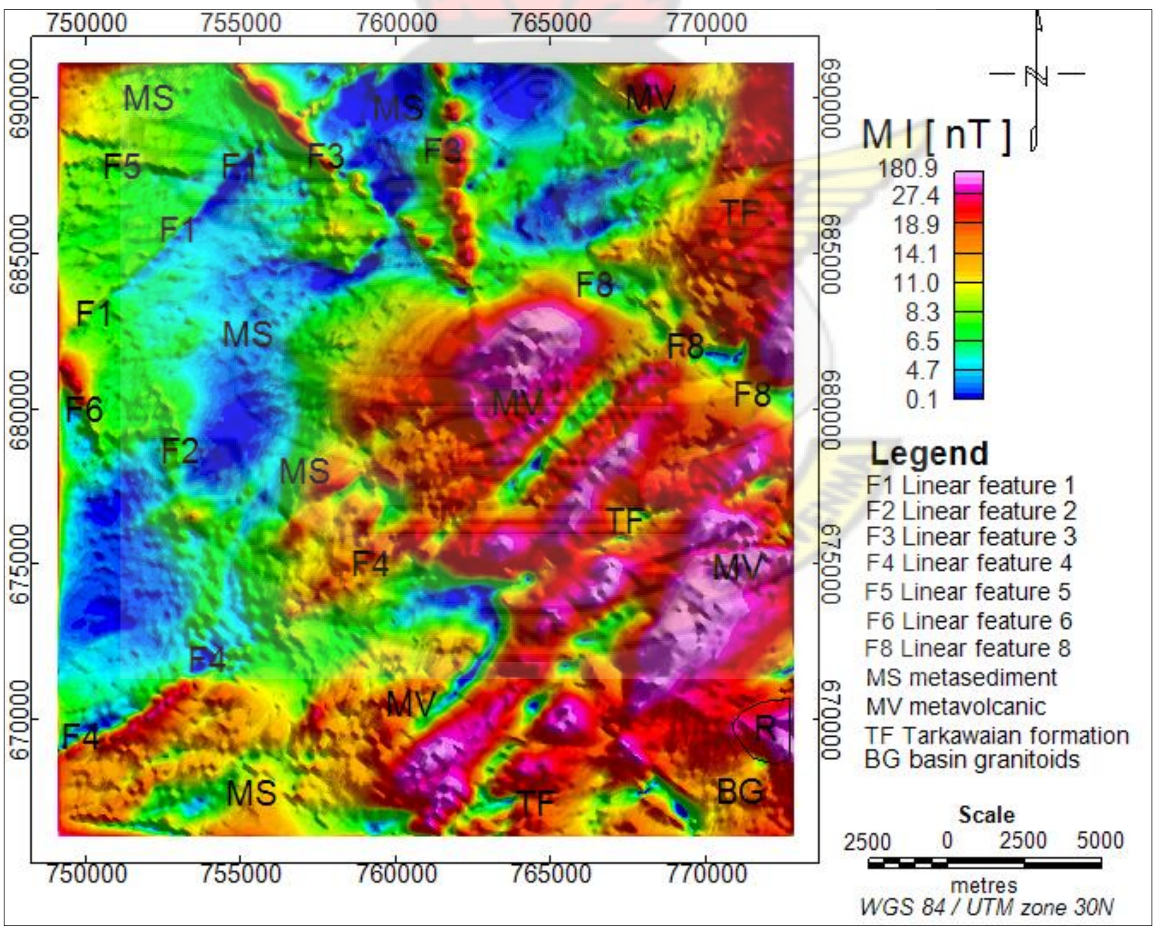

Figure 5.5 a map of analytical signal applied to Vertical Integral

It is also seen that the high magnetic intensity regions and the low magnetic intensity regions are clearly outlined in the analytical signal map of the vertical integral (figure 5.5) than that in the TMI map and the RTP map. Moreover, a feature such as F7 is clearly seen in figure 5.5 than in the TMI and RTP map. Features are seen clearer in the analytical signal maps (figure 5.4 and figure 5.5) than the TMI and RTP map because the source positions of the anomalies are defined vertically over the source regardless of any remanence in magnetization. In addition, maximum anomaly has been produced over the magnetic body regardless of the direction of magnetization with regards to analytical signal.

From the analytic signal maps shown in figure 5.4 and figure 5.5 it is seen that the formation MS recorded the lowest magnetic intensity, low magnetic intensity is generally associated with sediments. This suggests that the formation labelled MS which is indicated by deep blue is made of metasediments. This correlates with the airborne radiometric interpretation that suggest that the MS is metasediment. The average magnetic signatures registered at some parts of the MV suggest that, these formations are composed of green schist facies of mafic to ultra-mafic rocks in the greenstone belt, this again correlates with the interpretations from the radiometric data that interpreted this area to be the mafic to ultra-mafic volcanic unit. The high magnetic intensity observed in the mafic-ultra mafic volcanic regions are granulite facies of mafic formation, since it is very magnetic and is located within the greenstone belt, its strong magnetism arise because of the great production of secondary magnetite related to amphibole and pyroxene growth during prograde reactions.

In general the high magnetic intensities values of 31587 nT upwards observed within the Birimian volcanic units of figure 5.2 and 5.3 suggest that, the formations are made of igneous rocks rich in iron. The analytic signal maps (figure 5.4 and figure 5.5) have also revealed a number of features such as dykes which are indicated by F3 and F4 and other features such as F1 and F8 which are identified as major faults. A number of minor faults are also seen to be trending in the north – east direction in areas with high magnetic intensities.

5.2.4 Downward Continuation Filter

Downward continuation simulates data acquisition closer to the ground, this simulation sharpens the effect of high frequency anomalies that originates from shallow geological source. In this case, noise may also be amplified. Figure 5.6 below is a 0.4 m downward continuation of the analytical signal of the TMI map.

From the downward continuation map, it is seen that the boundaries of the different formations are well demacarted and the features that are present are well enhanced and the entire map is well smoothened compared to the previous maps. From this the metavolcanic (MV), metasediments (MS) and the Tarkwaian formation (TF) are clearly seen. In addition a number of dykes, major faults, and minor faults are identified. A features such as F7 is seen to be trending N-W and F4 and F1 are also seen trending N-E.

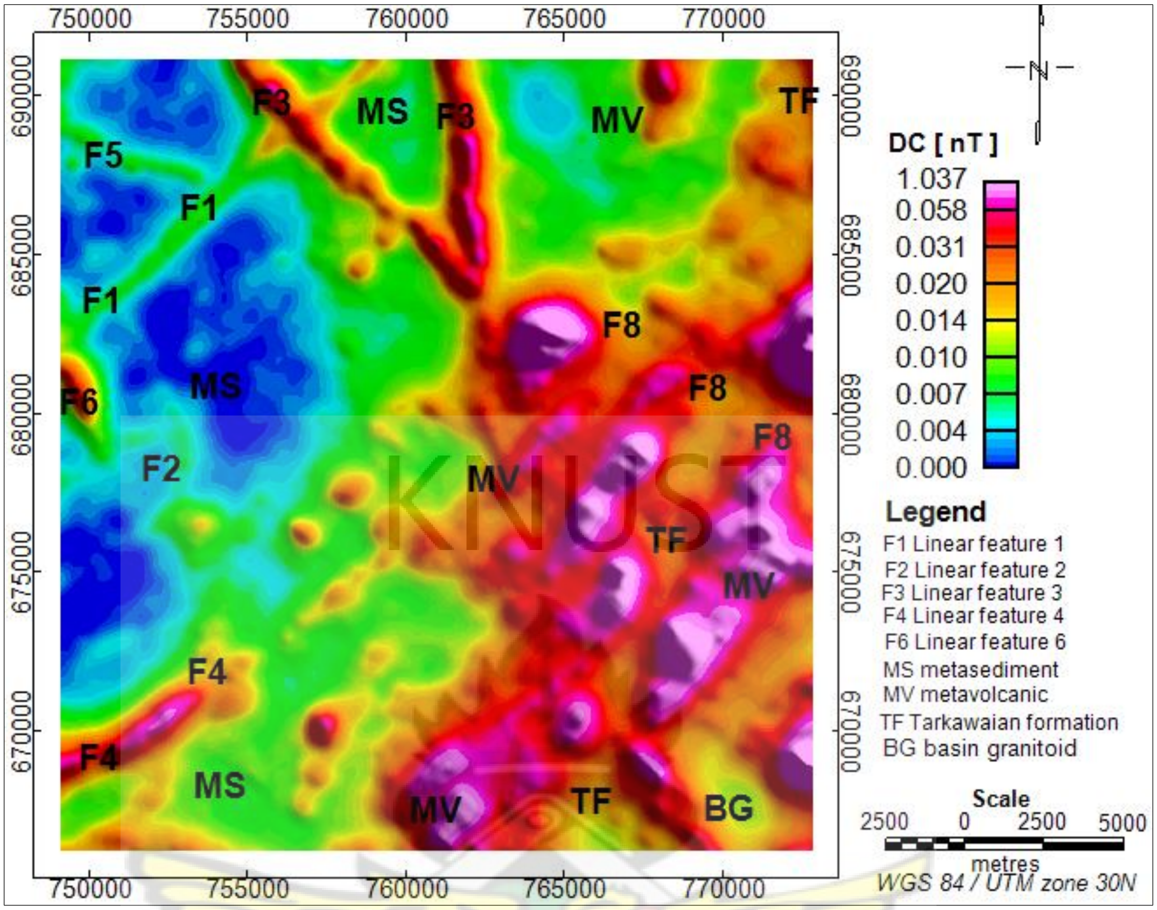

Figure 5.6 a 0.4 m downward continuation of the analytical signal

5.2.5 Contour Map

Figure 5.7 is a contour map superimposed on the upward continuation map. From the map, the smooth contour seen at the areas labeled MS with the deep blue colour reflects areas covered with sediments with relatively deep basement. The complex contours lines observed in the remaining area with high magnetic intensities are indicative of igneous and metamorphic terrains. The areas with the closed contours with successive contours values decreasing or increasing towards the centre, and those areas with circular and oval magnetic anomalies indicated by arrows in figure 5.7 may be due to accumulations of magnetite and or pyrrhotite. The accumulation of magnetite and pyrrhotite may be associated with economic grade of gold, silver, zinc, lead or copper (Boddiington and Hughes, 1990).

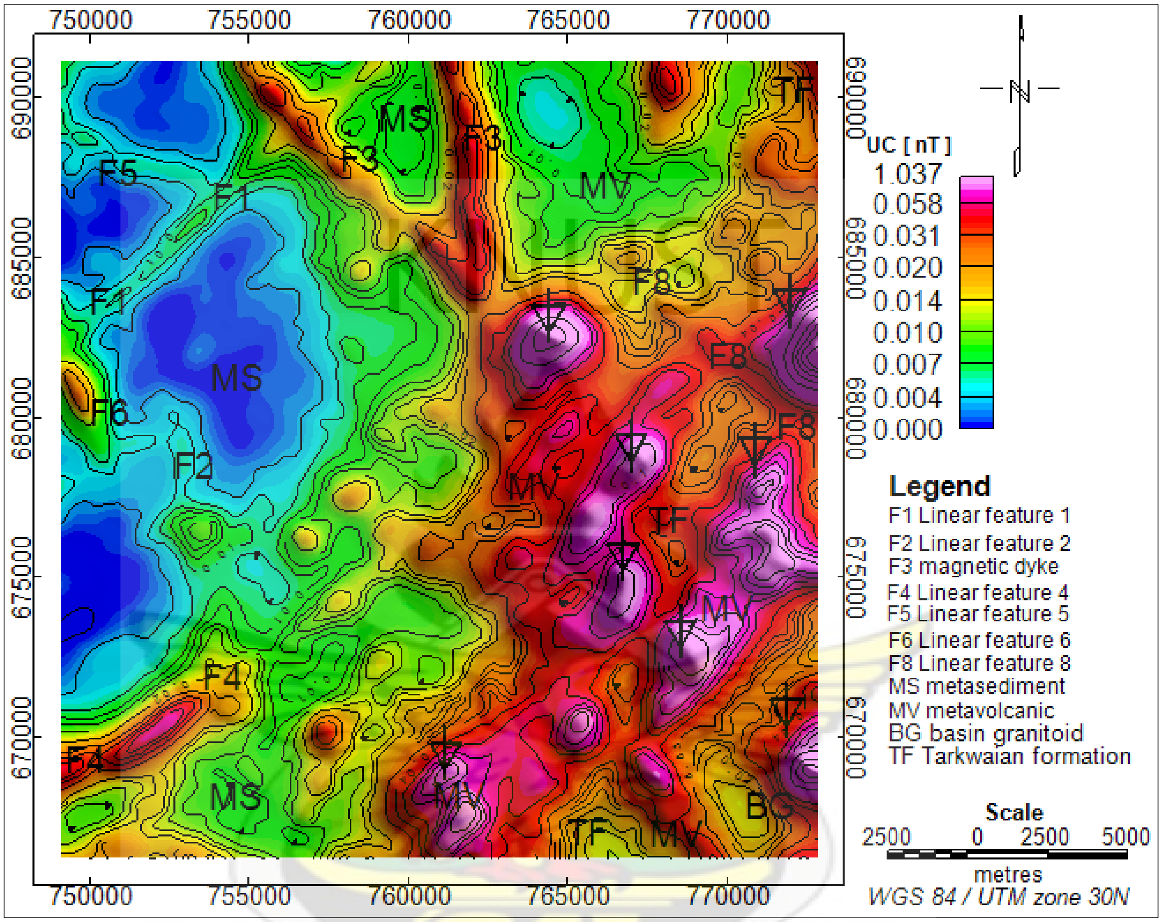

Figure 5.7 a contour map superimposed on an upward continuation map

The high horizontal anomaly gradient seen between the deep blue and the pink areas are indicative of rocks with different susceptibility values. The circular contours are indicative of circular features such as cone or sphere. The long narrow anomalies like, F3 and F4 indicate elongated dikes. The areas with very high magnetic intensities could be due to magnetite and remanently magnetised massive pyrrhotite, the average magnetic intensities indicated by green colour adjacent to the high magnetic intensities could be due the destruction of the pyrrhotite by alteration processes. The sharp contrast in the colours are indicative of lithological boundaries or faults, the weak narrow linear magnetic features seen in F1 and F5 in the contour map (figure 5.7) may be due to accumulations of magnetic minerals in fault planes or differences in magnetic properties.

5.2.6 Vertical Derivative

Computation of the first vertical derivative in an aeromagnetic survey is equivalent to observing the vertical gradient directly with a magnetic gradiometer and has the same advantages, namely enhancing shallow sources, suppressing deeper ones, and giving better resolution of closely-spaced sources. A gray scale is applied to the first vertical derivative of the TMI and the first and second vertical derivatives of the analytical signal. This helped in the identification of features such as *f1*, *f2*, *f3*, *f4* and *f5* as folds in the derivatives maps.

Figure 5.8 is the first vertical derivative of the analytical signal, from this map two folds named as *f3* and *f4* are identified and markded with red, other derivative maps such as the second vertical derivative maps were also produced that led to the mapping of more structures as it is seen in figure 5.9 .

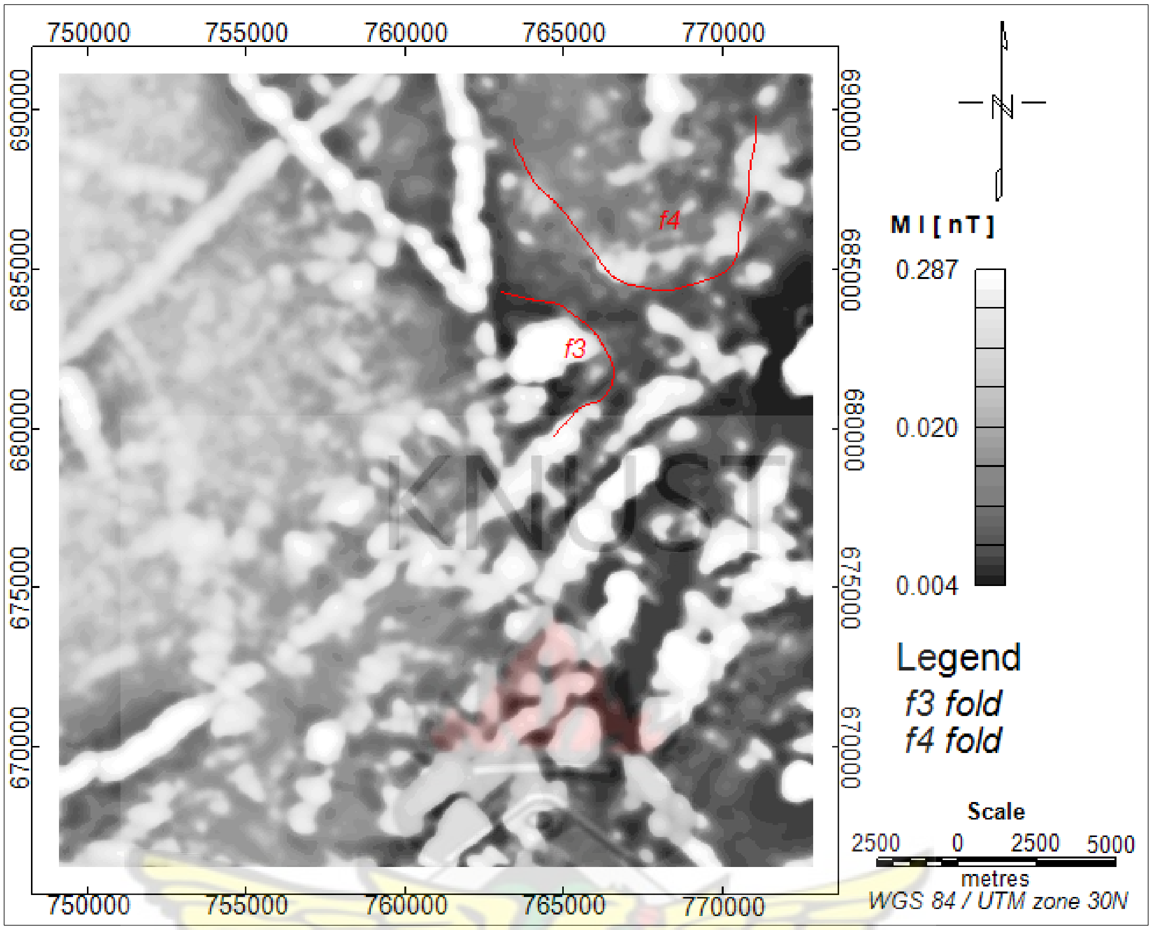

Figure 5.8 First vertical derivative of analytic signal

Figure 5.8 has not been able to show most of the features clearly but it can be seen in the first vertical derivative of the analytical signal (figure 5.9) that features such as *f1* and *f2* that were not seen in figure 5.8 are now made clearer and even *f3* is more clearer in this first vertical derivative of the analytical signal (figure 5.9).

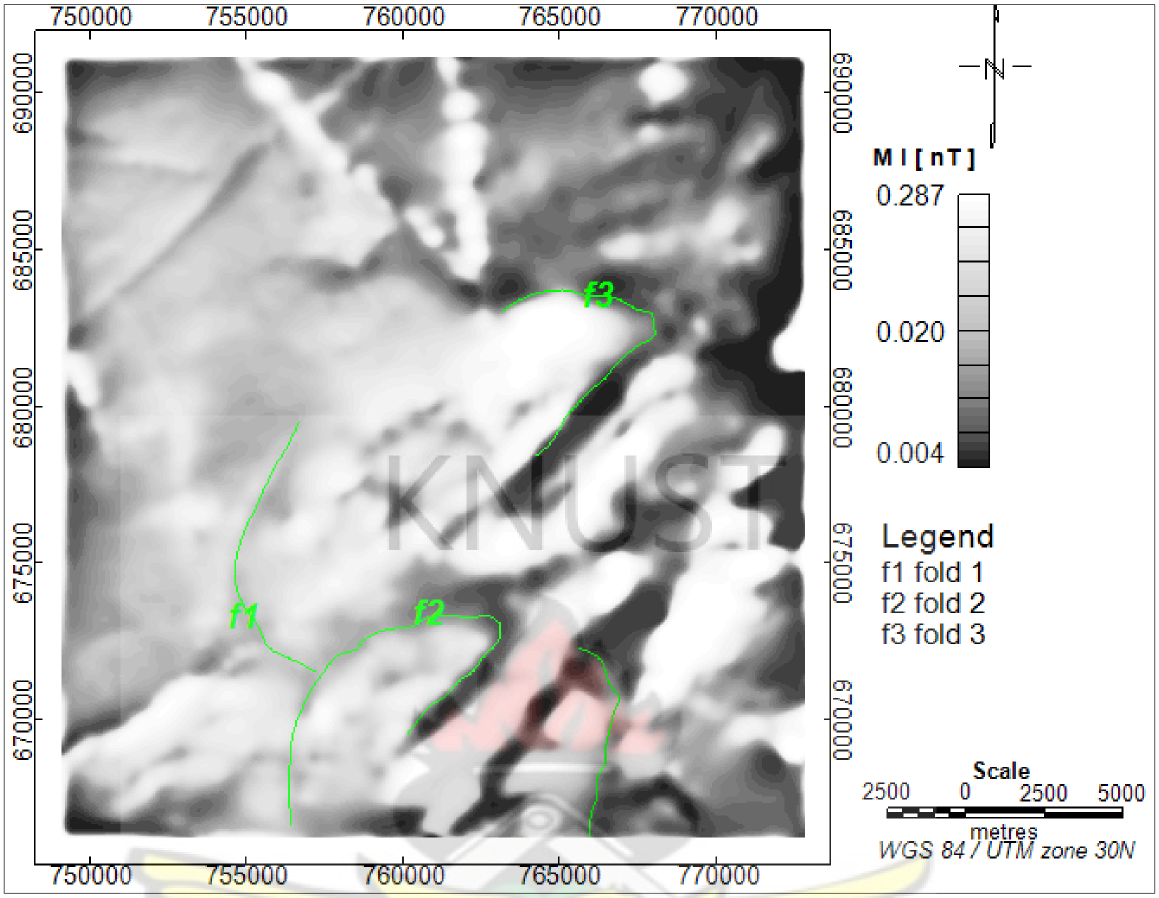

Figure 5.9 First vertical derivative of the analytical signal

The second vertical derivative of the analytical signal is presented in figure 5.10. In this map all the features seen in figure 5.8 and 5.9 are enhanced, additionally some features such as *f6*, upto *f9* which could not be seen in figure 5.8 and 5.9 are seen in this map (figure 5.10). Also most of the other features such as F1 to F8 that were seen in the analytical maps are also enhanced in this second vertical derivative of the analytical signal map.

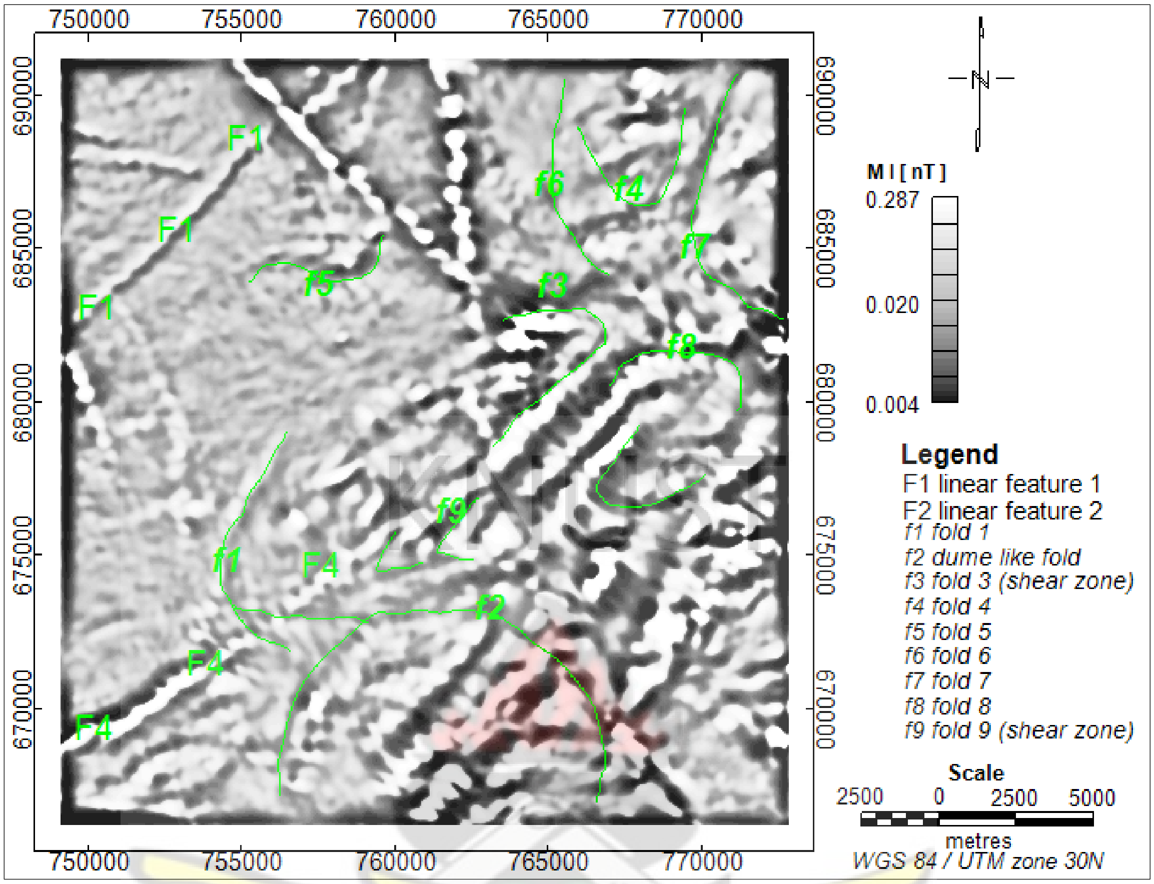

Figure 5.10 Second vertical derivative of the analytical signal of the vertical integral.

The features labelled *f1,f2, f3, f4, f5, f6, f7, f8* and *f9* are all features that correspond to deformational stages in the Eburnean Orogeny and its associated magmatism. These are prominent in the metavolcanic and Tarkwaian formation, and gold mineralization and its associated sulphide deposits are associated with these deformational stages (Allen, 2011).

5.2.7 Interpreted Structural Map

From the magnetic maps shown above, the interpreted structural map of the study area is deduced as shown below in figure 5.11, it is seen that the study area has a lot of structurally complex features such as dykes, major faults that trend northeast and northwest, minor faults, shear zones, fractures and folds. Areas that have complex structures are known to correlate with gold deposits; therefore areas with higher structural complexity are likely zones of mineralization (Zlotnikov, 2012).

These structures were formed during the deformational stages of the Eburnean orogeny and have served as conduits for rising hydrothermal fluid which contains dissolved minerals.

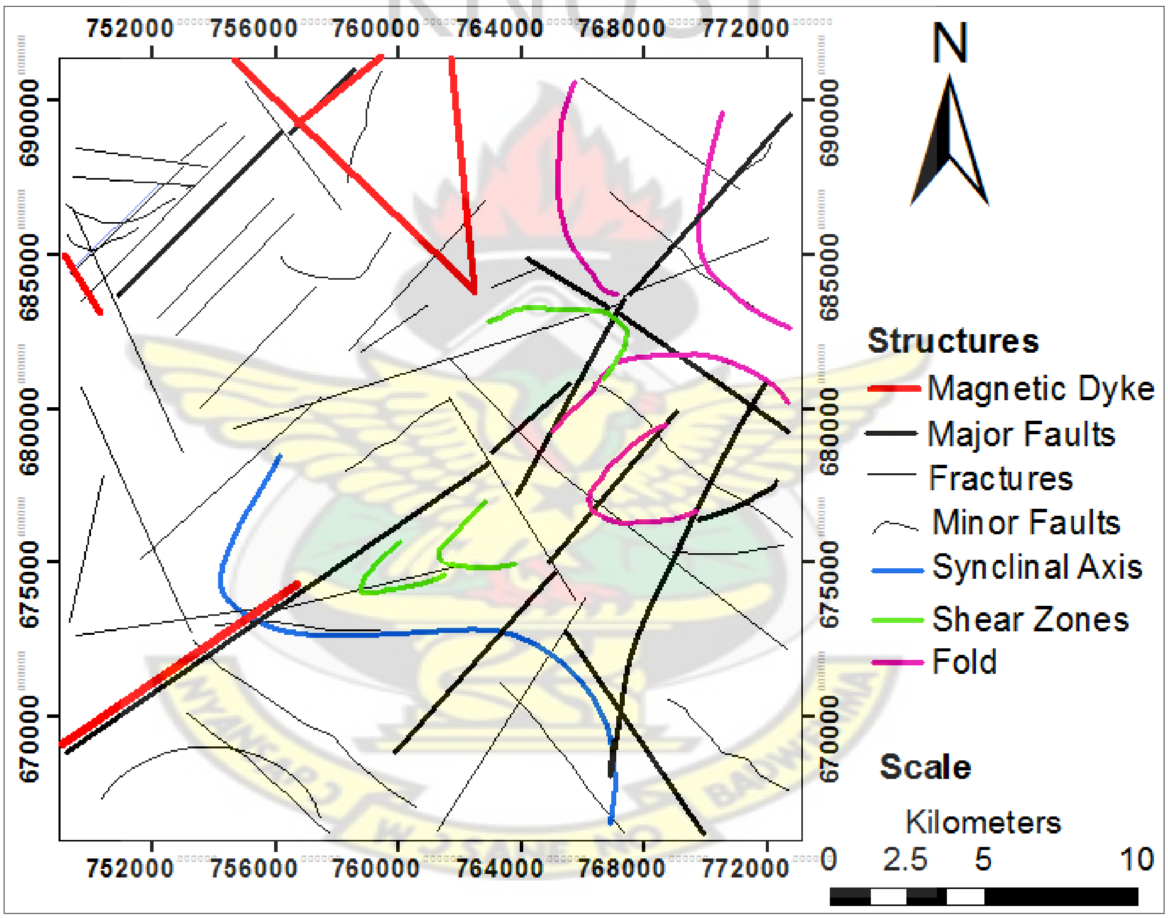

Figure 5.11 Interpreted structural map of the study area.

5.2.8 Interpreted Geological Map of Magnetic Data

The interpreted geological map (figure 5.12) of the surveyed area from the airborne magnetic data showed that three main geological formations namely the metasediments, metavolcanic and the Tarkwaian formation are present in the study area. The areas with high magnetic intensity within the metasediments are most likely to be sediments dominated by shale, since in sedimentary environment it is pyrrhotite within shale formation that cause magnetic anomaly to be observed.

The low magnetic values recorded within the metavolcanic are likely to be as a result of the intrusion of mafic volcanic units and the high magnetic intensity areas within the metavolcanic formation could be as a result of the presence of magnetic minerals such as magnetite and pyrrhotite. From the map a V-shape magnetic dyke is also seen at the upper part of the surveyed area.

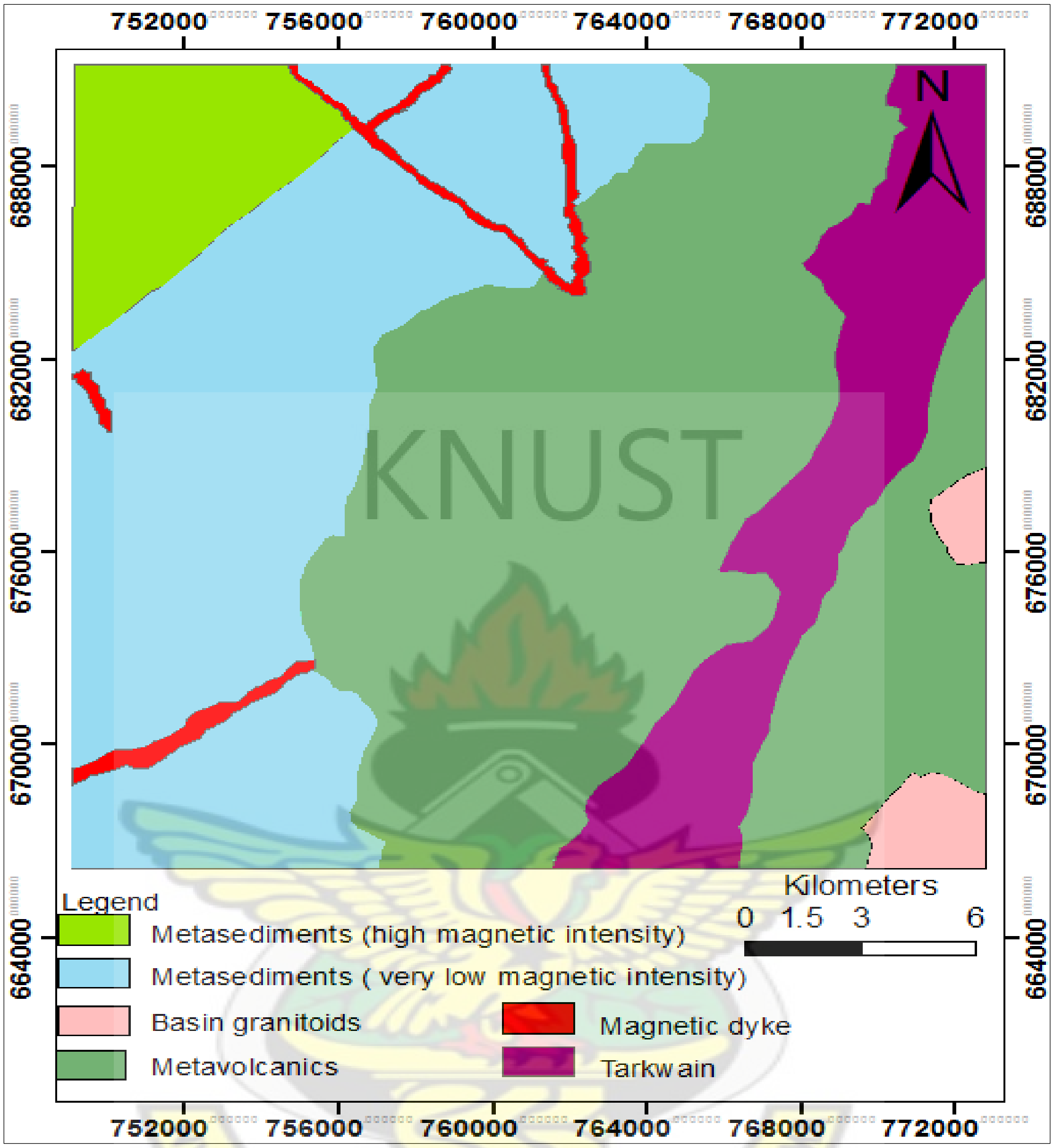

Figure 5.12 Interpreted geological map from the magnetic data.

5.3 Results of Radiometric Survey

Although, radiometric surveys measures the spatial distribution of radioactive elements from the top 30 cm to 40 cm of the regolith, it is capable of mapping the geology of the subsurface because the radioactive element content of the bedrock is reflected in the composition of the superficial material (Urquhart, 1995). Moreover, the distribution of radioactive elements relates to the differences of lithology of common rocks and alteration or metamophism processes. (Urquhart, 1995).

5.3.1 Potassium Concentration

Potassium is normally added to host rocks by mineralizing hydrothermal solutions, K therefore is the most reliable pathfinder in airborne gamma ray surveys in locating hydrothermal ore deposits, especially gold deposits (Hoover and Pierce, 1990). Minerals such as K-feldspar or muscovite are normally the source of K in rocks that are hydrothermally altered, and these minerals can be detected by a rise in K counts or activity. Rocks that are free of these minerals have very low K-activity. Thus, K-activity is very low in all mafic and ultramafic rocks. Hydrothermal alteration of host rock can give measurable haloes even in cases when gold is found in quartz veins (Hoover and Pierce, 1990).

The potassium content of sedimentary rocks is highly variable but tends to be higher in shale than in carbonates or sandstones. In general, the potassium content of rocks increases with acidity. The concentration of potassium is a key factor in the identification of geologic units that are affected by hydrothermal systems favourable to the development of gold mineralization.

From the potassium concentration map (figure 5.13), a high potassium region one (Hp1) has high potassium activity. This high potasium counts at Hp1, suggest that Hp1 could be made of sediments with a lot of shale, since shale normally contains high potassium activity (ICRU, 1994). Moderate potassium region one (Mp1) is also found in a Birimian sediment zone and is having a moderate amount of potassium, and this could be as a result of carbonates and sandstones with occasional shales in minute amount (ICRU, 1994).

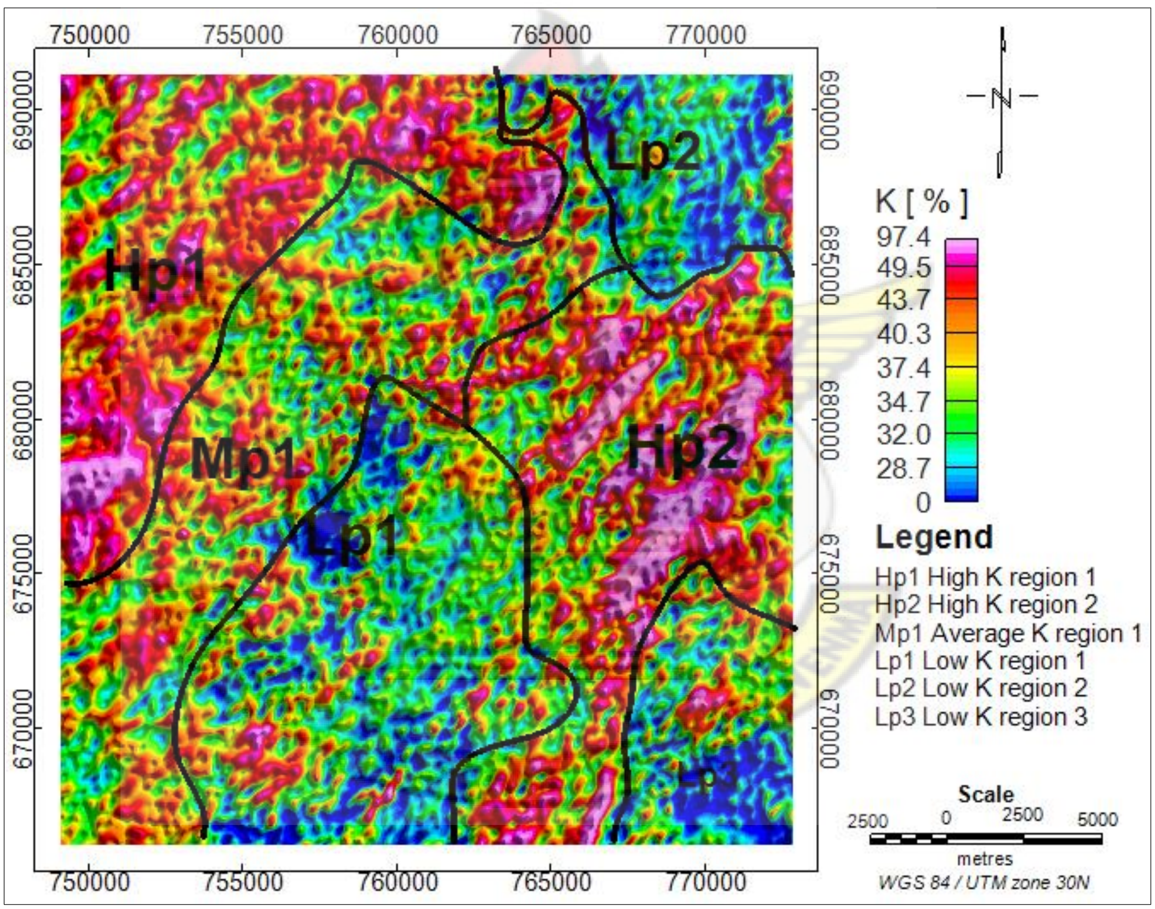

Figure 5.13 a map of potassium concentration in percentage

Lp1, Lp2 and Lp3 are regions with low potassium activity, these regions have the lowest potassium count rates in the study area and these are found in the Birimian volcanics.

Low potassium count or activity in the Birimian volcanic formation is associated with mafic and ultra mafic volcanic rock unit such as diorite (andesitic) and gabbro (basaltic). High potassium region two (Hp2) lies in the Tarkwaian which is composed of distinctive volcaniclastic sediments, and this suggests that the formation of Hp2 is made of sediments of felsic igneous rock formation such as granite, rhyolitic (quartz, felspar, and muscovite) and syenite.

5.3.2 Thorium Concentration

Figure 5.14 is the thorium concentration grid and it shows Hp1 to have a high concentration of thorium that coincides with high concentration of potassium in figure 5.13. The high concentration of thorium at Hp1 coupled with the high concentration of potassium in this same Hp1 is further suggesting that Hp1 could be sediments with shale because shale normally has high felsic intrusion which is characterized by a relatively high potassium and thorium content.

It is also observed that Mp1 has moderate amount of potassium in figure 5.13. It also recorded moderate amount of thorium in figure 5.14 and this could be as a result of sediments with sandstone and carbonates.

The boundaries of Lp1 and Lp3 are well defined in the thorium map and it is seen to have a north eastern trend with very low or no thorium count. This region lies in the Birimian volcanics and also recorded no potassium or very low potassium counts in figure 5.13. These characteristics of Lp1 and Lp3 suggest that, the region Lp1 and Lp3 are made of mafic to ultra-mafic metavolcanic rock units, since mafic volcanic rocks generally lack thorium and potassium activities.

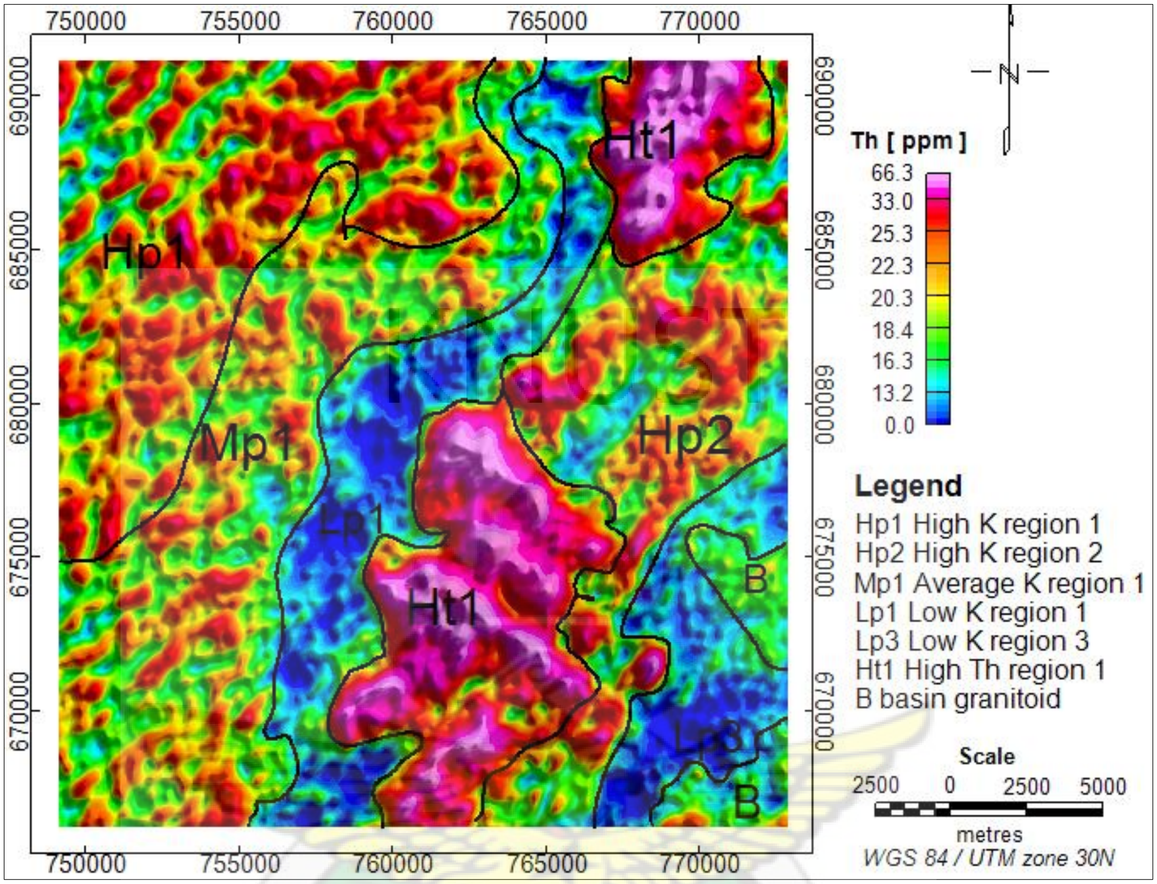

Figure 5.14 a map of thorium concentration in part per million

Ht1 are regions with the highest thorium concentration in figure 5.14, these regions also lie in the Birimian volcanic formation. High thorium count rates are associated with minerals such as pegmatites, zircon, monazite, allanite, sphene apatite and xenotime, and these minerals are concentrated in igneous rocks (Keary et al., 2002). It then suggests that, Ht1 are igneous formations and contain the above mentioned minerals. It is also suggestive that Ht1 are batholiths with high thorium content. Hp2 has a moderate amount of thorium and it is found in the Tarkwaian, suggesting that the formations of Hp2 are vocaniclastic sediment that lies on the Birimian volcanics. The formation marked

B has some amount of thorium activity and is found in the basin, this low amount of thorium is suggestive of granitoids intrusions.

5.3.3 Uranium Concentration

In the uranium concentration map (figure 5.15), Hp1 has high amount of uranium, thorium and potassium which is an indication of felsic intrusions in the metasediment. The high uranium, thorium and potassium activities in Hp1 in figure 5.15 still further suggest that Hp1 is sediments with shale, because shale contains high amount of potassium and tends to absorb uranium and thorium as part of their clay content. The very high uranium count rates at Ht1 in figure 5.15 are suggestive of later stage of magmatic differentiation of igneous formation.

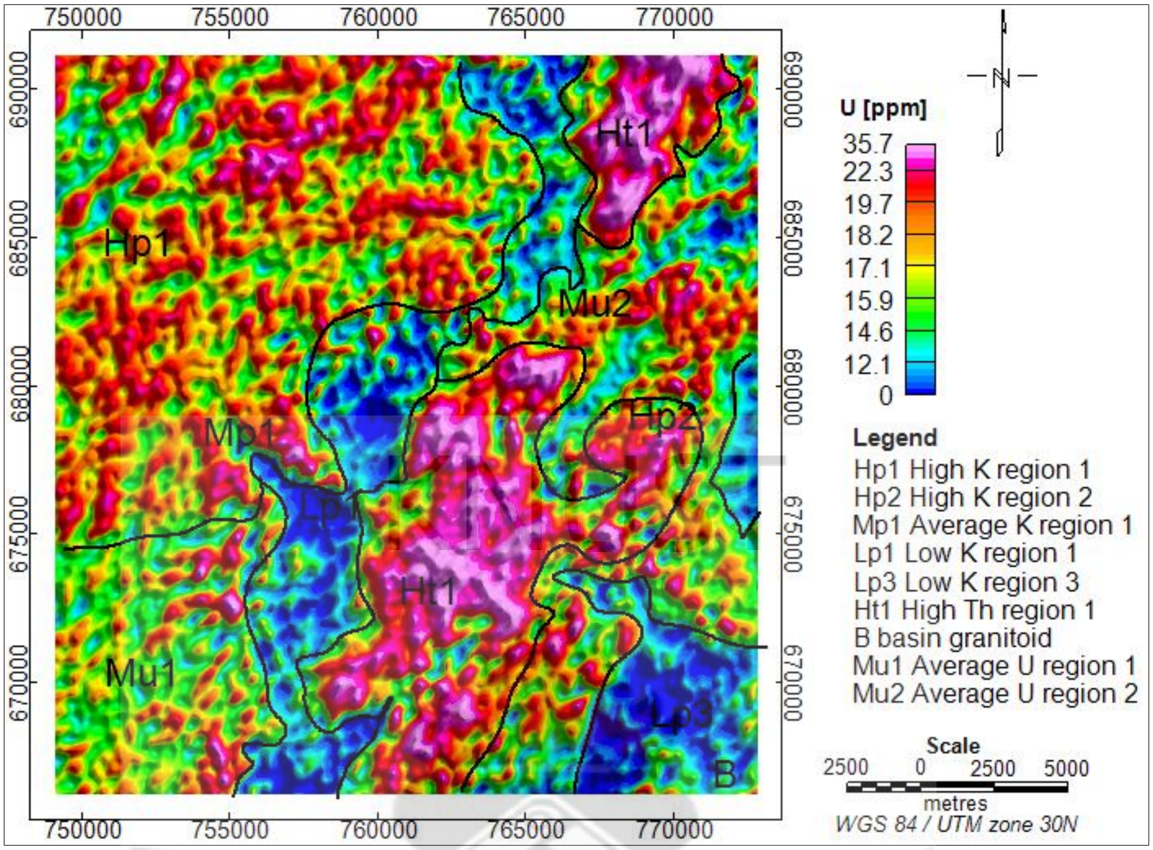

Figure 5.15 a map of uranium concentration in part per million

Lp1 and Lp3 are seen to have the lowest uranium count rates, very low uranium count is associated with mafic to ultra-mafic volcanic units. The moderate amount of uranium at Mu1 and Mu2 is indicative of sediments with high amount of sandstone and carbonate.

The high concentration of uranium at Ht1 in figure 5.15 and the high concentration of thorium at Ht1 figure 5.14 coupled with the low concentration of potassium at Ht1 in figure 5.13 are suggestive that Ht1 could contains minerals such as pegmatite, quartz, and monzonite in an igneous formation. The high uranium concentration at Ht1 is further suggesting of the presence of batholiths at Ht1 with high concentrations of thorium and uranium. Hp2 is located within the Tarkwaian and the high potassium could be as a result of clastic sediments.

5.3.4 Ratio Maps

The abundance ratios, U/Th, U/K and Th/K, are often more diagnostic of changes in rock types, alteration, or depositional environment than the values of the radio-isotope abundances themselves, which are subject to wide variations due to soil cover, etc. The effect of environmental factors on radiometric response, such as soil moisture, vegetation, and topography, are less evident on band ratios. The ratios therefore often correlate more highly with geological units. Also, since there is usually a high correlation between bands, the ratios often show subtle features that are not apparent on the original grids.

The ratio maps used in this project are U/Th, U/K and Th/K and these maps have been used to indicate zones within the study area that are hydrothermally altered, since hydrothermal alterations normally lead to the enrichment of one radioactive element at the expense of the other (Schwarzer and Adams, 1973; Lundien, 1967).

5.3.4.1 Thorium Potassium Ratio Map

Thorium generally is not affected by alteration processes due to the fact that Th is typically immobile in mineralization processes or it can only partly be depleted in areas of intense K-alteration and silicification. The K/Th ratio is therefore a better indicator of hydrothermal alteration than any single radioelement alone. The concentration of soil clay and silt are also characterized by thorium and Th/K (Schwarzer and Adams, 1973; Lundien, 1967). In many gold deposits, Th has been mobilised and depleted with the simultaneous increase of K, although Th is generally unaffected by alteration processes (Durrance, 1986; Hoover & Pierce, 1990; Dickson & Scott, 1997).

In the Th/K ratio map (figure 5.16) it is observed that the features marked Lp1 and Lp3 have very low Th/K ratio values in the range of 0.3 - 0.4 ppm / % as seen in the legend of this map. The formations of Lp1 and Lp3 are noted to contain low potassium count rates as deduced from the potassium map (figure 5.13) which then suggested that Lp1 and Lp3 are made of mafic volcanic units. However, the very low Th/K values in the range of 0.3 -0.4 ppm / % at Lp1 and Lp3 in the Th/K map (figure 5.16) suggest an enrichment of potassium in Lp1 and Lp3 and this is a strong indication of hydrothermal alterations at Lp1 and Lp3 of the Th/K map (figure 5.16). The sediments in Hp1, Mp1 and Hp2 of the Th/K ratio map have Th/K ratio of 0.9 ppm / % this goes to say the amount of potassium is almost the same as the amount of thorium. In the K, Th and U maps shown in figure 5.13, 5.14 and 5.15 respectively Hp1, Hp2 and Mp1 have high counts rates for all the elements, this high count rates coupled with the Th/K of 0.9 ppm / % at Hp1, Hp2 and Mp1 suggest that no hydrothermal alteration took place at Hp1, Hp2 and Mp1. Ht1 have Th/K ratio of 1.6 ppm / % in the Th/K ratio map (5.16) and these Ht1 recorded high count rate of thorium and low count rates of potassium in figure 5.14 and 5.13 respectively. The high Th/K ratio of 1.6 ppm / % together with the high count rate of thorium at Ht1 in figure 5.14, and the low count rate of potassium at Ht1 in figure 5.13 is a clear indication that no alteration took place at Ht1 in the Th/ K ratio map (figure 5.16).

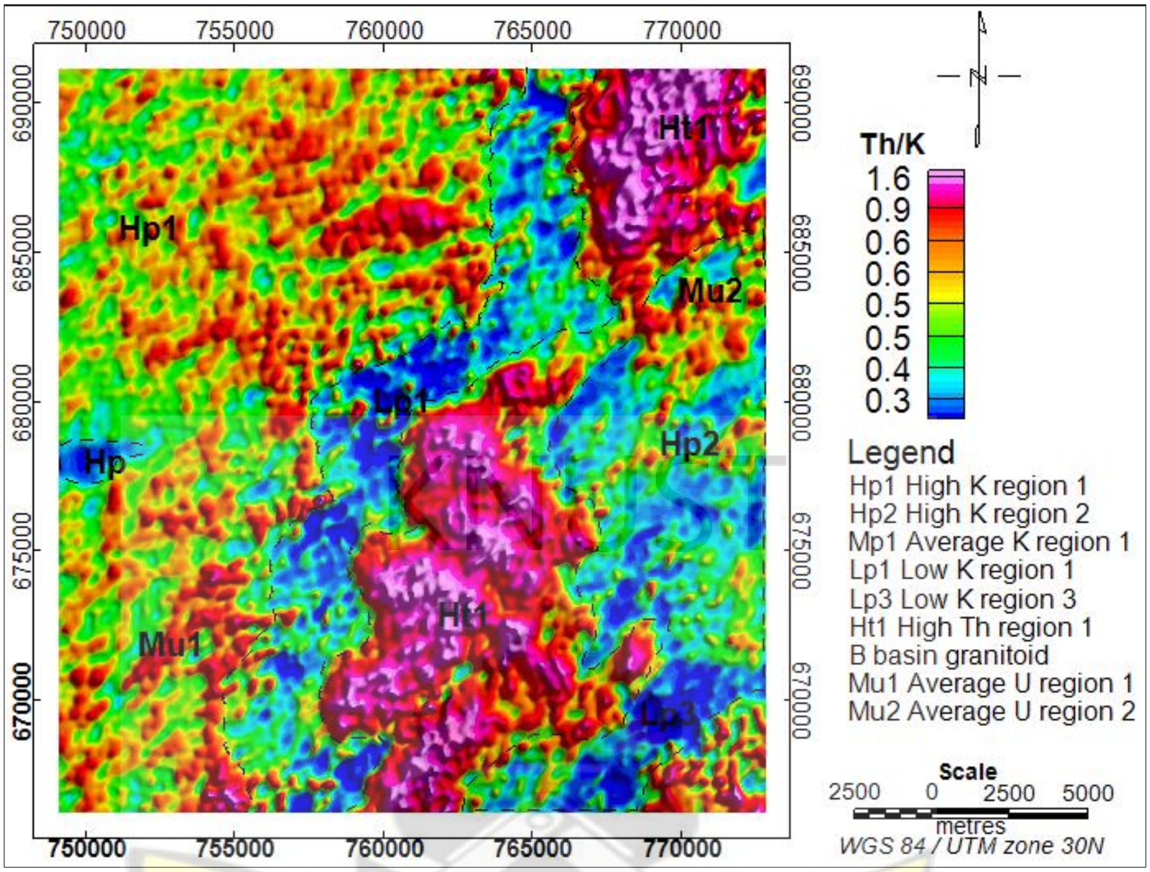

Figure 5.16 a ratio map of Th and K (Th / K)

5.3.4.2 Uranium Potassium Ratio Map

Uranium is a very mobile element in hydrothermal and other geological processes; an enrichment of uranium may or may not be accompanied with an enrichment of potassium. The U/K ratio is therefore not a good indicator in identifying mineralization. Notwithstanding, U/K ratios are indicative of sulphide deposits (Airo, 2007).

Figure 5.17 shown below is the U/K ratio map. In this figure 5.17 it is shown that Ht1 have high U/K ratios, this observation is suggestive of suphide deposit at Ht1, because sulphide deposits are characterized by an increase in U and a decrease in K and Th; which leads to enhanced ratio values of U/Th and U/K.

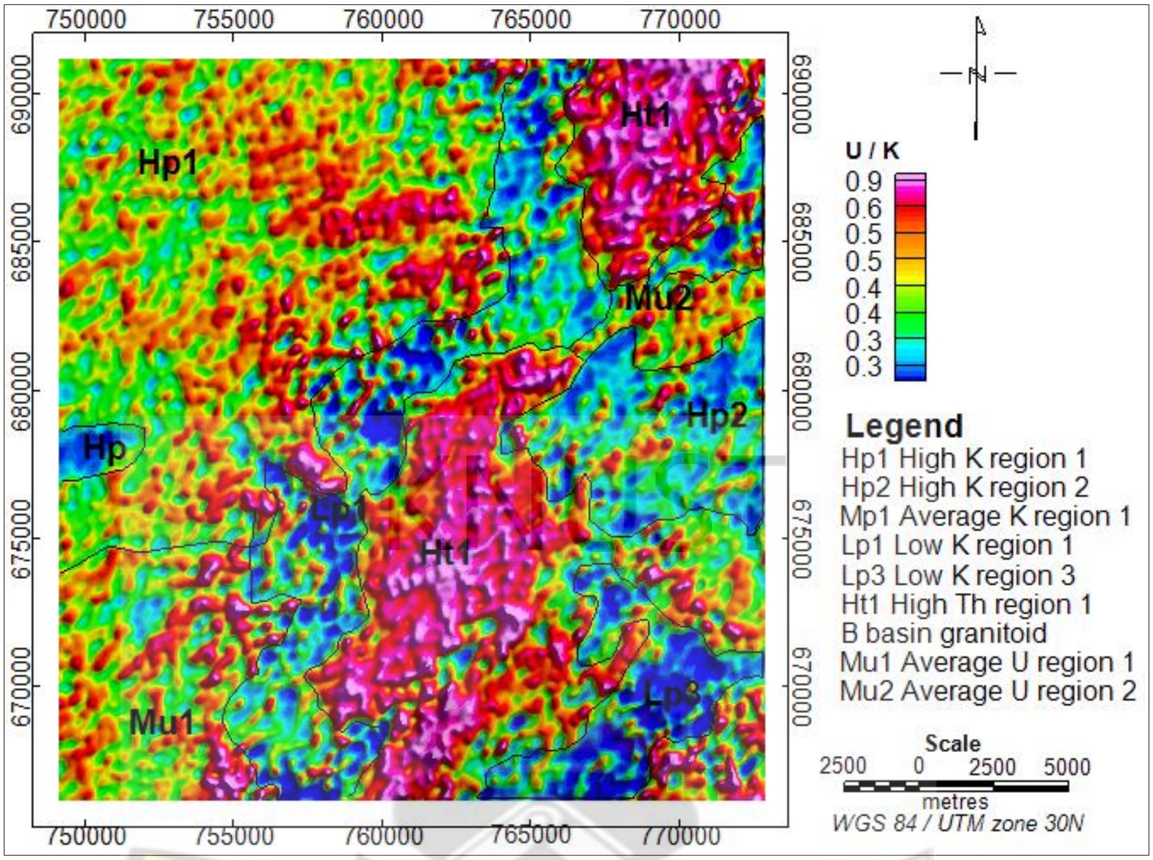

Figure 5.17 a ratio map of U and K (U/K)

Also the high U/K values of 0.9 ppm / % recorded at Ht1 of figure 5.17 indicate that Ht1 have high concentration of uranium which suggests that the formation of Ht1 could be made of minerals such as uranite, carbonite and gummite with the possible rocks being an igneous formation.

The regions Lp1 and Lp3 have also recorded low U/K ratios meaning that Lp1 and Lp3 have very low uranium count rates as compared to the count rates of potassium in these regions; this could be an indication of potassium enrichment. Hp1 and Mu1 are seen to have patches of high U/K ratios within the metasediments, this high U/K ratio could be as a result of sulphide deposition in the metasediments.

5.3.4.3 Thorium Uranium Ratio Map

Thorium concentration is decrease in sulphide mineralization while uranium concentration is enhanced, a low Th/U ratio is therefore indicative of sulphide mineralization. Variation of Th/U ratios also reflects the environmental condition during primary diagenesis or a later deformational phase.

Figure 5.18 is a Th/U ratio map. From this map it is shown that with the exception of the mafic volcanic unit that has an enrichment of uranium compared to Th, the remaining geologic formation namely the metasediments and the metavolcanic units such as the igneous formation have higher concentration of Th compared to U. This is suggestive of sulphide deposition in the mafic volcanic units at Lp1 and Lp3.

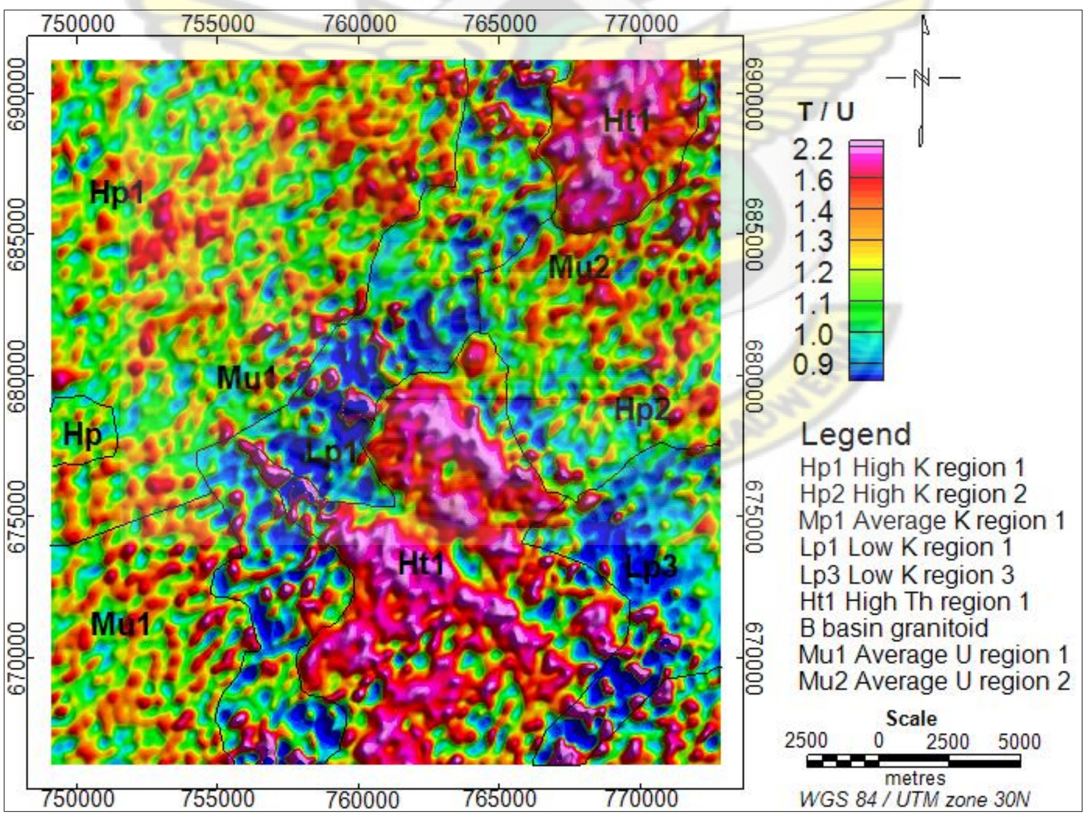

Figure 5.18 a ratio map of Th and U (Th/U)

5.3.5 Ternary Map

Figure 5.19 is a ternary map of all the three radioactive elements and the colours are interpreted as follows;

Red is high potassium with low uranium and thorium

Blue is high uranium with low potassium and thorium

Green is high thorium with low potassium and uranium

Cyan is high thorium and uranium with low potassium

Magenta is high potassium and uranium with low thorium

Yellow is high potassium and thorium with low uranium

Black is low potassium, thorium and uranium

White is high potassium, thorium and uranium.

Using the colour scheme, the following interpretations are made from the ternary map. It is seen that formation Hp1 has higher concentration of U, K and Th depicted by the white colour. High concentrations of all the three radioactive elements are linked with rholitic volcanic rocks (metasediments) that are associated with pyroclastic rocks and pumice. Since these observations are made in the metasedimentary formation of the Birimiam, Hp1 is likely to be made of sediments with high content of shale.

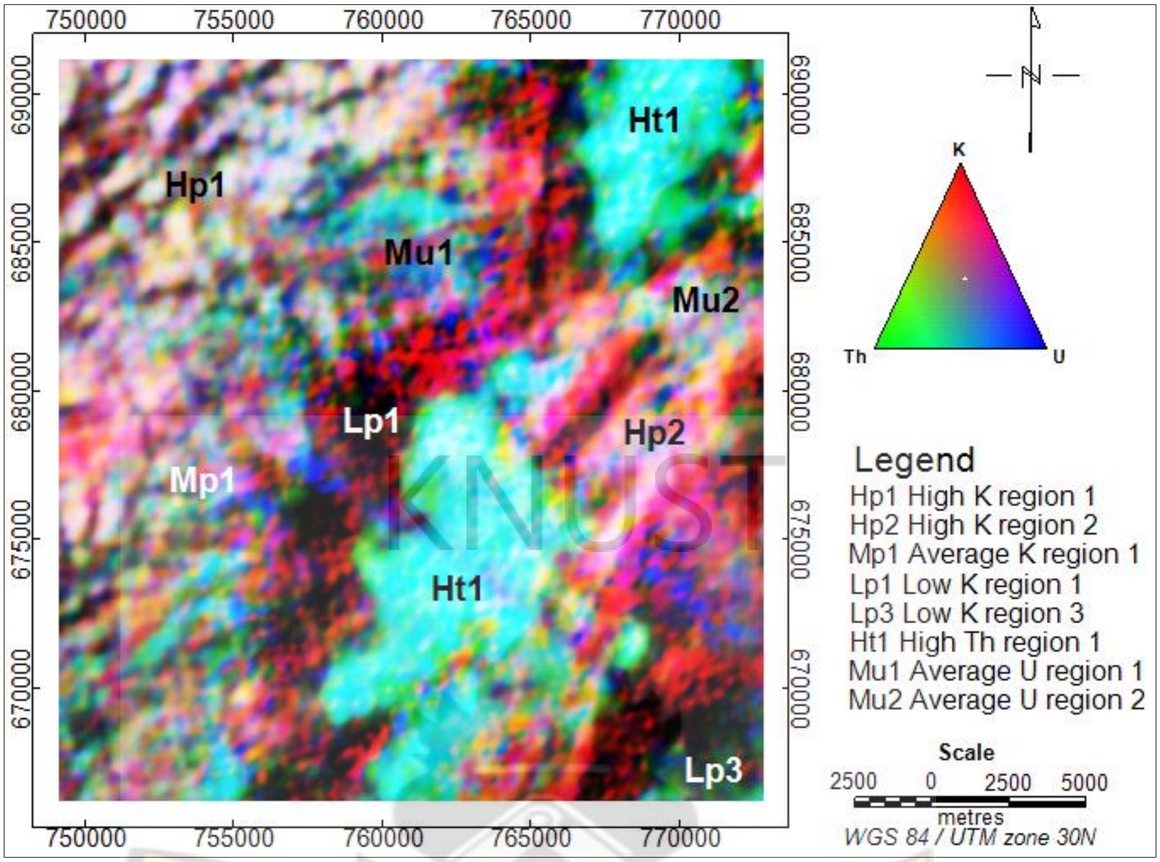

Figure 5.19 a ternary image of K, Th, and U

The formation Mp1 is dominated by thorium with occasional intrusions of uranium and potassium in the Birimian formation. This kind of observation within the Birimiam sediments could be attributed to sediments with high content of sandstone and carbonates.

Lp1 has consistently recorded very low concentration of potassium, uranium and thorium in all the three concentration maps of the radioactive elements and the ratio maps. The very low concentration of all the three radioactive elements is characteristic of mafic to ultra-mafic volcanic rocks. It is therefore suggestive that the formation Lp1 is mafic to ultramafic volcanic rocks. Besides that mafic and ultra-mafic rock units are mostly located within the contact zone between volcanic rocks and their intervening sedimentary basins, and since this Lp1 is found between the meta-volcanic and their intervening metasediments it is most likely Lp1 is mafic to ultramafic volcanic formation. From the ternary map shown in figure 5.19, it seen that the region Lp1 is observed to have patches of higher concentration of potassium compared to the other elements, meanwhile from all the concentration maps (potassium , thorium and uranium) Lp1 has consistently recorded very low activity of all these elements. It therefore suggests that the high concentration of potassium in Lp1 in the ternary map of figure 5.19 is an indication of enrichment of potassium in region Lp1 compared to the other elements. The enrichment of potassium relative to the other elements especially thorium is an indication of hydrothermal alteration. And because Lp1 has higher potassium activity compared to the other elements, it means Lp1 has been altered hydrothermally. The very black areas within the Lp1 formation are areas of lowest activity of all the three radioactive elements and it suggest that hydrothermal alterations did not take place in these black areas within the mafic volcanic units.

The formations Ht1 are seen to have very high concentration of thorium and uranium in figure 5.14 and figure 5.15 respectively, and low potassium in figure 5.13. In the ternary map in figure 5.19 it is seen that Ht1 have recorded high concentration of thorium and uranium with the thorium content being slightly above the uranium. The high concentration of thorium and uranium in these areas is an indication that Ht1 could be granitic in nature, and may be batholiths with magmatic evolution.

The formation marked Lp3 has quite high amount of thorium activity with patches of uranium and is found in the Dahomeyan, this patches of relatively high thorium and uranium are indicative of granitoids intrusions. Hp2 has high amount of thorium at the upper part, equal amount of all the three elements in the middle portion and high potassium on the lower part with thorium intrusion. The varied nature of the distribution of the three radioactive elements in this region suggests that the formation in Hp2 could be the Tarkwaian formation, since the Tarkwaian is noted to contain distinctive clastic sediments.

5.3.6 Proposed Geological Map of the Study Area from Airborne Radiometric Data

From the analysis and interpretations drawn from all the radiometric maps, the proposed geological map of the study area with respect to airborne radiometric data is presented in figure 5.20.

Six different kinds of formations are identified and delineated, these are the meta-sediments rich in shale, the meta-sediments rich in carbonates, the mafic volcanic units, the Tarkwaian, the igneous formation of the metavolcanic, and the basin granitoids. The shale rich meta-sedimentary units are seen to record high radiometric activity for all the three radioactive elements, and the interpreted carbonate and sandstone rich meta-sediments have recorded a relatively lower activity of the three radioactive elements. Notably the high uranium and thorium concentrations observed in the igneous formations are associated with the Banso batholith within the region. The Banso batholith is well foliated, often magmatic and contains high content of thorium (Kesse, 1985).

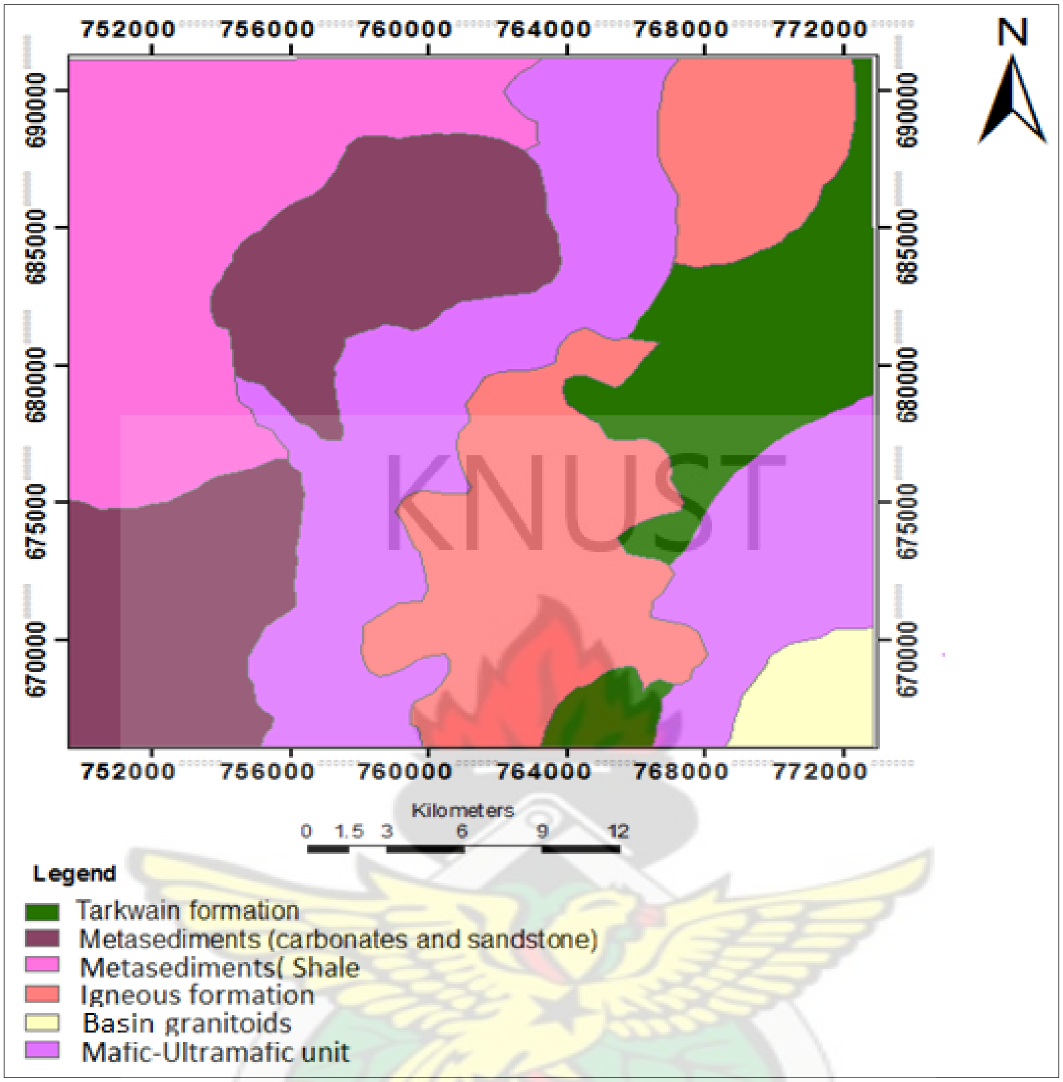

Figure 5.20 Interpreted geological map from airborne radiometric data

The very low radiometric response located between the meta-sediments and the meta-volcanic is identified as mafic to ultramafic volcanic units. This mafic to ultramafic unit has been altered hydrothermally. The Tarkwaian formation is characterized by high thorium content in the upper right corner of the ternary map with equal amount of all the three elements in the middle portion and high potassium on the lower part with thorium intrusion.

The lower right corner of the study area recorded high content of thorium at the base with the middle portion having pockets of uranium and the top consisting of high potassium; this area was identified as been part of the basin granitoids.

5.4 Relating Geophysical Datasets to Geology

Figure 5.21 is a composite map of the magnetic and radiometric data and it is a combination of the geology, structures and alteration zones delineated from the magnetic and radiometric data. From the composite map, it is seen that the study area is highly fractured and faulted with a lot of cross cutting features most of which trend in the NE and the SW direction. Large folds, shear zones and synclinal axis that appear to be associated with the D2 and D3 deformations are observed in the study area.

The metavolcanic and the Tarkwaian formation are seen to be structurally altered more than metasediments and the undiferenciated granitoids. It is also observed that a NS trending magnetic dyke intersects a SE dyke at the contact zone between the metasediment and the mafic volcanic units creating a 'V' like shape magnetic dyke.

The SE part of the 'V' shape dyke is intersected by short NE trending dyke in the sedimentary basin, these cross cutting dykes creates an inverted 'A' like feature which is conspicuous in all the magnetic maps. All the different types of geological formations identified are seen to have a NE trending, a characteristic of the paleoproterozoic granite-greenstone belts and their intervening metasedimentary basins in Ghana (Abbott and Koimtsidis, 2010). The mafic volcanics lies within the contact zone between the metavolcanics and the metasediments and have undergone intense alteration. They have also been intruded by the metasediment at the point marked *x* in figure 5.21. This led to the creation of a hanging wall of the mafic volcanic at the point marked *x*. The Tarkwaian formation is a narrow NE trending formation that divided the birimian volcanics in to two parts.

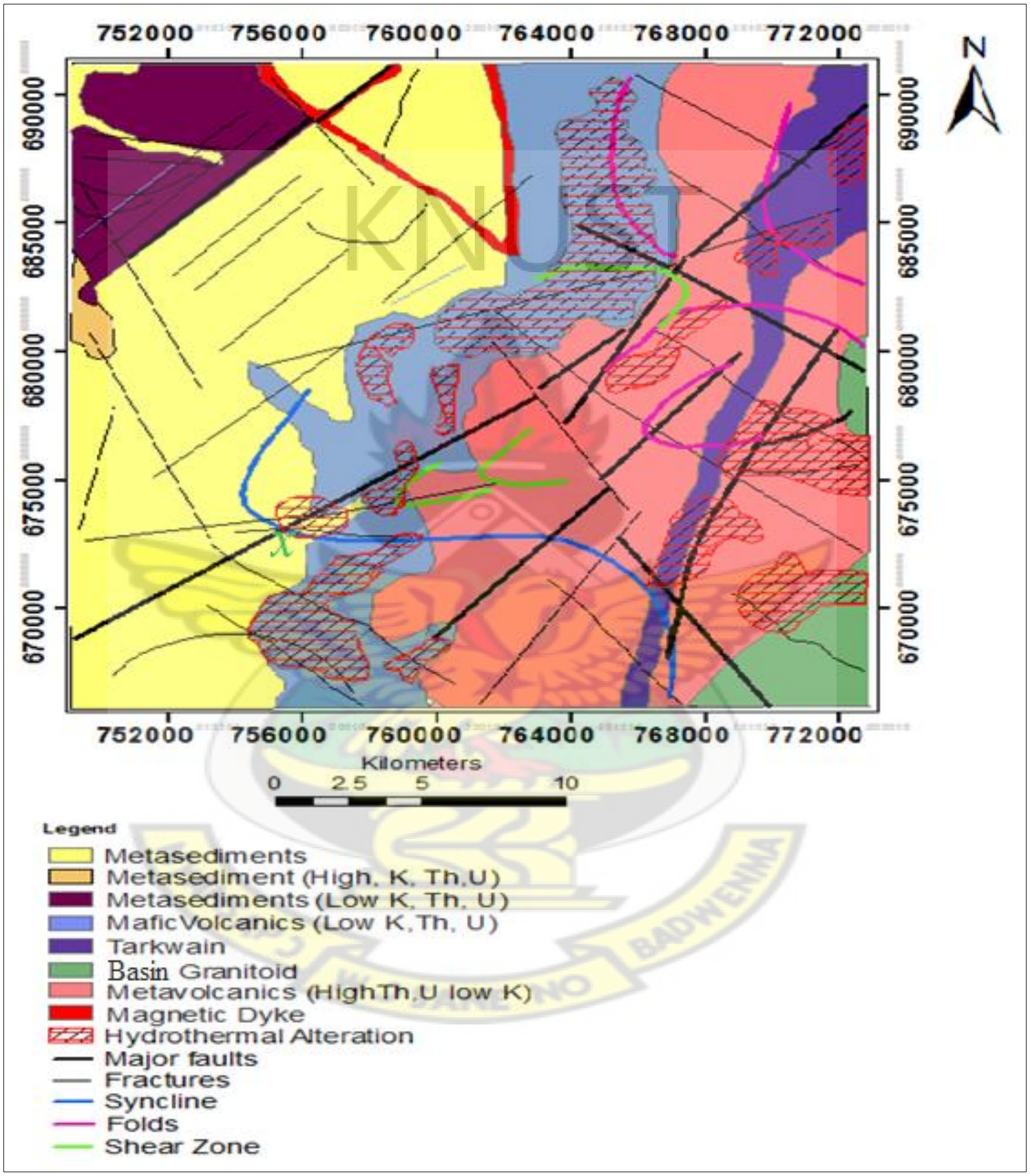

Figure 5.21 a composite map of magnetic and radiometric data.

5.4.1 Tectonics and Geological Structures

The structures mapped in the survey area from the radiometric and magnetic data are complex in nature and include folds, shear zones, fault, lithological boundaries, dykes, and fractures. These structures were found mainly in the Birimian and the Tarkwaian formation, with most of them striking NE and dipping steeply in the NW direction. A notable feature in the study area is the inverted 'A' like shape of a magnetic dyke that occurs at the upper part of the study area.

Perrouty et al. (2009) proposed the existence of five deformational stages in the Eburnean Orogeny and its associated magmatism. These are the D1 stage which occurred prior to formation of the Tarkwain system, the D2 and D3 deformation which resulted in the creation of large folds trending NE in the Birimian and the Tarkwain formation, the D4 deformation which created sub horizontal cleavage and recumbent fold and finally the D5 deformation which resulted in a NE-SW shortening. The D2 and D3 kinds of deformation are seen in the vertical derivatives maps (figure 5.8, 5.9 and 5.10) of the magnetic data, and are indicated by *f1*, up to *f9*. Gold mineralization and its associated sulphide deposits are associated with the D1, D2 and D3 deformation (Allen, 2011). From the interpreted structural and alteration map (figure. 5.11), the D2 and D3 deformation produced a NE-SW striking faults and fractures.

The NE trending shear zone (green lines in figure 5.21) is interpreted as a high angle fault that is formed in a regional NE-SW compression, this shear zone may have reached mantle-derived mafic magma (Griffis, 1998), leading to the formation of mafic formations. The high tectonic activities within the survey area made it possible for the passage of hydrothermal fluids which are capable of dissolving and transporting wide range of metals and salts and consequently played important role in ore deposition processes (Boamah, 1993; Manu, 1993). Usually hydrothermal solutions access conduits in rocks where it transports its loads and deposit them as ore whenever the physio-chemical conditions for ore deposit formation are favourable. The sources of the hydrothermal fluid could be magmatic, marine, connate metamorphic or meteoric water or combination of any of these (Evans, 1993).

It can be seen in the composite map (figure 5.21) that almost all the hydrothermally altered zones had one or more structures within them, these structures served as channels for migrating hydrothermal fluids, and rock formation that is found within these structures got altered by the chemical reaction between these fluids and the rocks.

5.4.2 Alteration

Rock alteration could be due to structural deformation, or chemical reaction (Amenyoh et al., 2009) and gold mineralization in the Birimian is associated with an event that promotes rock alteration (Leube et al., 1990; Milesi et al., 1992). From the composite map (figure 5.21), a number of hydrothermally altered zones are seen especially in the mafic volcanic unit and the Tarkwaian formation. Gold mineralization is closely connected to hydrothermally altered zones of the bedrock and commonly controlled by both large scale and local structural and tectonic features in southern Ghana (Manu, 1993). Evidence of alteration that preceded gold mineralization is best preserved in spatially associated altered mafic dykes, and alteration of country rocks occurred under rock-dominant, greenschist facies conditions (Mumin et al., 1996). The mafic and ultramafic units identified have seen an increase in their K content due to intensive potassic alteration (biotitization and sericitization), pre, syn and post gold chemical alterations characterised the gold bearing greenstones. Therefore the areas that are hydrothermally altered are potential sites for gold mineralization most importantly those areas that lie within or adjacent to major faults.

5.4.3 Potential Mineralized Zones

In determination of zones with possible gold mineralization and deposits in the study area, the structural map, the alterations and the geological maps were considered. The alteration zones marked by low magnetic intensity and high potassium content that lie within or close to a structure (fault, fold, shear zone, fracture or contact zone) that has a NE trending are identified as favourable zone for gold mineralization.

At the point marked x1 of the proposed geological map (figure 5.22), it is seen that a deformational synclinal axis intersects with a D2 and D3 NE trending fault in a hydrothermally altered zone within the mafic volcanic units. This is good indication of a zone that has been potentially mineralised.

The area x2 is located within a contact zone between the Tarkwaian and the Birmian volcanics, this zone is also characterised by hydrothermal alteration and a NW trending fault and a NE trending fault. The features present at zone x2 are favourable features for mineralization. Zones x3, x5, x6 and x7 are found within folds, sheared zones and faults that are within hydrothermally altered zones. These characteristics of x3 ,x5,x6 and x7 made them favourable for the mineralization of gold. The areas marked by x4 and x8 are also located within hydrothermal altered zones and they are lying within structures, therefore the mineralization of gold could be possible in these areas.

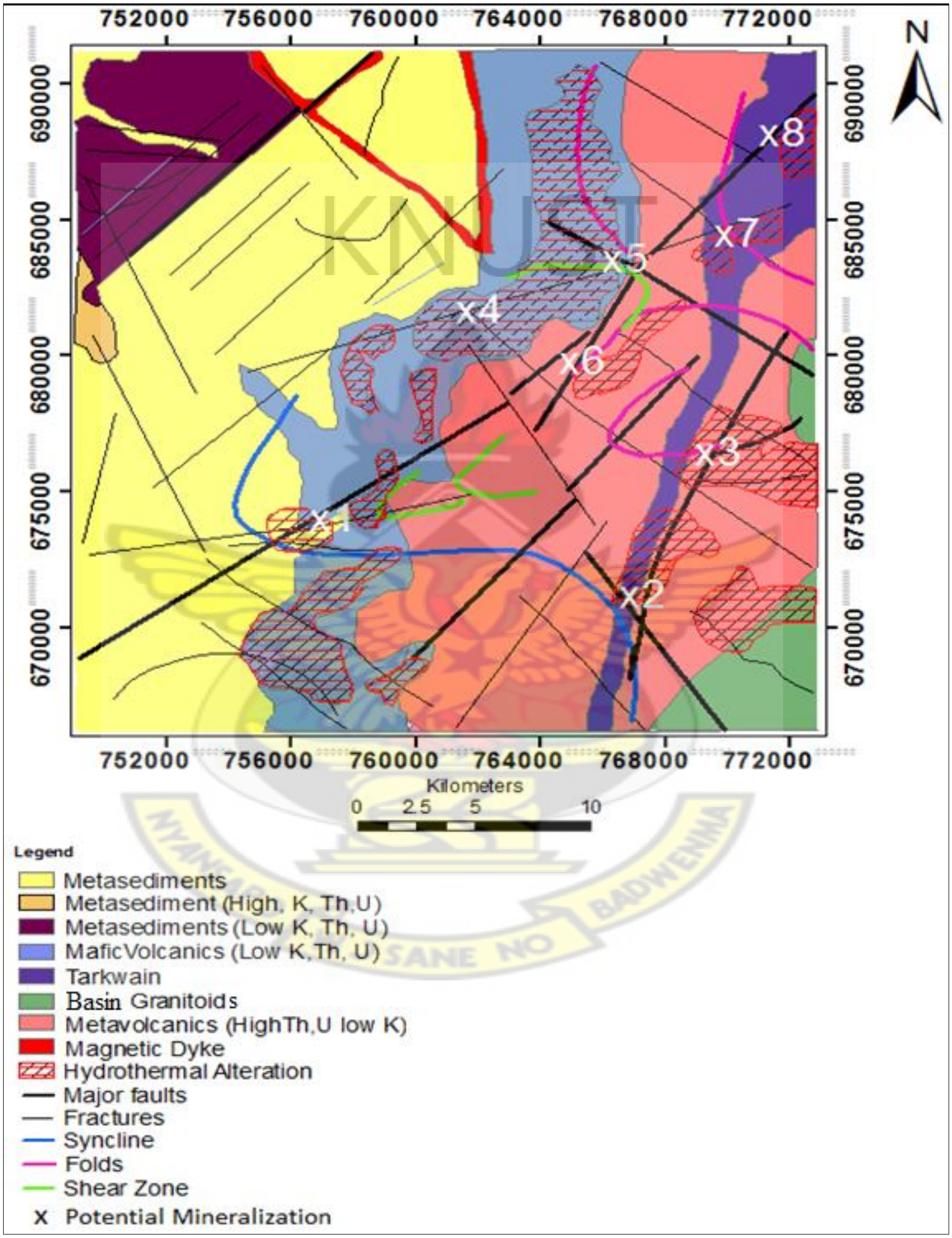

Figure 5.22 a composite geological map of the study area with potential zones of gold

CHAPTER SIX: CONCLUSION AND RECOMMENDATION

6.1 Conclusions

In conclusion the interpretation of the processed and enhanced radiometric and magnetic data led to the delineation of five geological formations namely the metamorphosed Birimian sediments, metavolcanics, mafic to ultramafic units, Tarkwaian and the basin granitoids. These geological formations were seen to trend in the NE-SW direction with a lot of structural deformation that correspond to the D1, D2, and D3 deformational stages that has been outlined by Perrouty et al. (2009) with regards to deformation of the subsurface in southern Ghana. The structures mapped include faults, folds, synclines, fractures and shear zones which favour mineralization of gold. In addition to the mapped structures, hydrothermal alteration zones were also mapped. These hydrothermal alteration zones are noted to be associated with gold mineralization in the Birimian (Manu, 1993).

The delineated geology, structures and hydrothermally altered zones led to the identification of eight zones with the potentials of gold mineralization. These potential gold mineralized zones are indicated by x1, x2, x3, x4, x5, x6, x7, and x8 in the composite geological map (figure 5.22). The zones indicated by x3, x 5, x6 and x7 are ranked higher in terms of gold mineralization because they are located within very complex structures and hydrothermal altered zones.

6.2 Recommendations

It is recommended that ground base magnetic and radiometric survey be carried out to validate the findings of the airborne data. Geochemical sampling and test drill should also be conducted after the ground radiometric and magnetic survey. Additionally, zones that are within or close to a structure and are having an intense hydrothermal alterations need further investigations.

The survey areas need to be extended in the NE-SW direction to cover larger area since it is seen from the geological map that, the metavolcanics, and the Tarkwaian formation which host the mineralization zones are trending in the NE-SW direction beyond the area surveyed.

REFERENCES

Abbott and Koimtsidis. (2010). *A Review of Three Permits in the Bolgatanga area, Upper East Region Ghana.*

Airo, M. L. (2002). Aeromagnetic and aeroradiometric response to hydrothermal alteration. . *Surveys in Geophysics 23, 273–302*.

Airo, M.-L. (2007). Application of Aerogeophysical Data for Gold Exploration: implications for the Central Lapland greenstone belt. *Geological Survey of Finland, Special Paper 44*,, 189.

Allen, D. G. (2011). The Fahiakoba gold project Ghana, West Africa. Technical report, Asante Gold Corporation. .

Amenyoh, T., Wemegah, D. D., Menyeh, A., and Danuor, S. K. (2009). The use of landsat and aeromagnetic data in the interpretation of geological structures in the Nangodi Belt. Master's thesis, University of Cape Coast.

Atiwa District Assembly. (2012). *Atiwa District Composite Budget.*

Betts, P., Williams, H., Stewart, J., Ailleres, L.,. (2007). Kinematic Analysis of Aeromagnetic Data: Looking at Geophysical Data in a Structural Context. Gondwana Res 11, 582–583.

Billings, S. D. (1998). Geophysical aspects of soil mapping using airborne Gamma-Ray.

Boadi, B., Wemegah, D.D., Preko, K. (2013). Geological and Structural Interpretation of the Konongo Area of the Ashanti Gold Belt using Airborne Magnetic and Radiometric data.

Boamah, D. (1993). Application of soil geochemistry to gold exploration in the Birimian rocks of Ghana. pages 1–6. Case study from Demoni/ Dankyira area (Unpublished).

Boddiington, T.D. and Hughes F.E. (1990). Abra leas-silver-copper-gold deposit In: Geology and mineral resources of Australia and Papua New Guinea. Australia and Papua New Guinea. Australasian Institude of Mining and Metallurgy, Monograph 14,659-664.

Boyce, J.I. and Morris, W.A.,. (2002). Basement-controlled faulting of Paleozoic strata in southern Ontario, Canada: new evidence from geophysical lineament mapping. *Tectonophysics 353, 151–171.*

Boyle, R. (1979). The geochemistry of gold and its deposits (together with a chapter on geochemical prospecting for the element). Geological Survey of Canada.

Briggs, I. C. (1974). Machine contouring using minimum curvature: Geophysics, 39, 39-48.

Bullock and Isles. (1994). Magnetic Susceptibility of common rocks.

Dickson, B. L. and Scott, K. M. (1997). *Interpretation of aerial gamma ray surveys-adding the geochemical factors. AGSO Journal of Australian Geology and Geophysics, 17(2):187–200.*

Durrance, E. (1986). *Radioactivity in geology: principles and applications. Chichester: Ellis Horwood, 441 p.*

Eisenlohr, B. N.; Hirdes, W. (1992). The structural development of early Proterozoic Birimian and Tarkwaian rocks in southwest Ghana,West Africa. Journal of African Earth Science, 14(3):313–325.

El-awady, M. M., El-etr, H., Bakrah, A. (1984). Aeromagnetic geophysical investigation in El-Faiyum district, western desert, Egypt. Qatar Univ. Sci. Bull, 5:335–356.

Evans, M. E. (1993). An archaeointensity investigation of a Kiln at Pompeii. Journal of Geomagnetism and Geoelectricity., 43:357–361.

Fallon, and Backo. (1994). Magnetic Minerals and their magnetic susceptibility. *World Geosciences*.

FS. (2011). *Filling Service Canada; Potential of the Western Contact Zone* . World Geoscience.

Goldfarb, R.J., Phillips, G.N., Nokleberg, W.J. (1998). Tectonic setting of synorogenic gold deposits of the Pacific Rim. Ore Geol. Rev. 13, 185–218 Žthis issue..

Grasty, R.L., Carson, J.M., Charbonneau, B.W., Holman, P.B. (1984). *Natural Background Radiation in Canada, Geological Survey of Canada Bulletin 360.*

Griffis, R. J. (1998). Explanatory Notes - Geological interpretation of geophysical data from Southwestern Ghana. Minerals Commission, Accra, page 51.

GSD. (1988). *Geology of Ghana.* Accra: Geological Survey Department, Ghana.

Gunn, P. J., Minty, B. R. S., and Milligan, P. (1997). *The Airborne Gamma-ray spectrometric response over Arid Australian terranes. Exploration, 97:733–740.*

Hirdes, W.; Nunoo, B. (1994). *The Proterozoic paleoplacers at the Tarkwa gold mine,SW - Ghana -sedimentology, mineralogy, and precise age dating of the main reef and* *west reef, and bearing of the investigations on source area aspects. In Oberthür, T. (ed.), Metallogenesis of Select.*

Hoover, D. B. and Pierce, H. A. (1990). Annotated bibliography of gamma-ray methods applied to gold exploration. U.S. Geological Survey Open-file Report 90-203, page 23.

IAEA. (2010). *Nuclear Energy Series.* International Atomic Energy Agency.

IAEA. . (1991). *Nuclear Energy Series; Radioelement Mapping.*

IAEA. (2003). *Nuclear energy series.* International Atomic Energy Agency.

ICRU. (1994). *Gamma ray Spectrometry in the Environment, ICRU Report 53. International Commission On Radiation Units And Measurements, Bethesda, USA.*

Junner, N. (1940). The geology of the Gold Coast and western Togoland. , 1940. 40 p. *Bull. Geol.Surv. Gold Coast, vol. 10*, 40.

Keary Philip, Michael Brooks, Ian Hill. (2002). *An Introduction to Geophysical Exploration Third Edition.* Osney Mead, Oxford OX2 0EL: Blackwell Science Ltd.

Kerswill, J. (1996). Iron Formation-hosted strata-bound gold, in Geology of Canadian Mineral Deposit Types, DNAG Geology of Canada 8, 367-382. .

Kesse, G. O. (1985). *The Mineral and Rock Resources of Ghana.*

Leube, A., Hirdes,W., Mauer, R., and Kesse, G. (1990). The early proterozoic Birimian supergroup of Ghana and some aspects of its associated gold mineralisation. *Precambrian Research,*, 46, 139–165.

Li, X. (2008). *Magnetic reduction-to-the-pole at low latitudes.* Fugro Gravity and Magnetic Services. Houston, USA.: Fugro .

Lowrie, W. (1997). *Fundamentals of Geophysics.* London.

Lowrie, W. (2007). *Fundamentals of Geophysics, second edition.*

Lundien, J. R. (1967). *Terrain analysis by electromagnetic means: Laboratory investigations in the 0- to 2.82 –MeV gamma-ray spectral region. U.S. Army Engineers Waterways Experiment Station, Vicksburg, Mississippi, Technical report 3–693. 41 p.*

MacLeod, I.N., Jones K., and Dai,T.F. (1993). 3-D analytic signal in the interpretation of total magnetic field data at low magnetic latitudes. Exploration Geophysics, 24(4), 679–688.

Manu, J. l. (1993). Gold deposits of Birimian greenstone belts in Ghana: Hydrothermal alteration and thermodynamics. Verlag Mainz, Wissenchaftsverlag, Aachen Herstellung: Fotodruck Mainz GmbH Susterfeldstr. 83. 52072 Aachen.

McElhinny, M. W. (1973). *Paleomagnetism and Plate Tectonics.* Cambridge: Cambridge University Press.

MCG. (2010). *Gold Deposits in Ghana.*

Metelka, V. (2011). Geophysical and remote sensing methodologies applied to the analysis of regolith and geology in Burkina Faso, West Africa.

Milesi, J. P., Ledru, P., Feybesse, J. L., Dommanget, A., and Marcoux, E. (1992). Early proterozoic ore deposits and tectonics of the Birimian orogenic belt, West Africa. Prec. Res., 58:305–344.

Milligan, P. R.; Gunn, P. J. (1997). Enhancement and presentation of airborne geophysical data. *AGSO Journal of Australian Geology & Geophysics, 17*(2), 63-75.

Minty, B. (1991). Simple Micro Levelling for Aeromagnetic Data., Exploration Geophysics 22, p591-592.

Moxham, R. M. (1963). *Gamma-ray spectrometer studies of hydrothermally altered rocks. Economic Geology, 6:653–71.*

Mumin, A. H., Fleet, M. E., and Longstaffe, F. J. (1996). Evolution of hydrothermal fluids in the ashanti gold belt, ghana; stable isotope geochemistry of carbonates, graphite, and quartz. Economic Geology, 91(1):135–148.

Ostrovskiy, E. A. (1975). Antagonism of radioactive elements in wellrock alteration fields and its use in aerogamma spectrometric prospecting. International Geological Review, 17:461–8. .

Perrouty, S., Jessell, M., Aillères, L., Baratoux, L., and Bourassa, Y. (2009). Structural analysis of the southern Ashanti belt, Ghana, using airborne geophysical data. ASEG Extended Abstracts, 2010(1):1–4.

RGC. (2008). *The Lily Gold Project.*

Robert F., Poulsen K.H., Cassidy K.F., and Hodgson C.J. (2005). Gold Metallogeny of the Superior and Yilgarn Cratons, in Economic Geology 100th Anniversary Volume, 1001-1034.

Robert, F. (2004b). Characteristics of lode gold deposits in greenstone belts, in 24ct Au Workshop, Hobart, CODES Special Publication 5, 1-12.

Robert, F., Sheahan, P.A., Green, S.B. (1991). Greenstone Gold and Crustal Evolution.Geol. Assoc. Can., Mineral Deposits Div. Publ. 252.

Roux, A. (1967). *The Application of Geophysics to Gold Exploration in South Africa. 425-438 In Morley, L.W (Ed.), Mining and Groundwater Geophysics. Proc. Can. Cen. Con. Mining & Groundwater, Queen's Printer, Ottawa, 722pp. .*

Sawyer, L. M.; Gunn, P. (2008). *Bulman Project EL 23814, MLN 726, MLN 727, Airborne Geophysics Data Interpretation. Geos Mining project 2141 -1.*

Schwarzer, T. F. & Adams J.A.S. (1973). *Rock and soil discrimination by low altitude airborne gamma-ray spectrometry in Payne County, Oklahoma. Economic Geology 68, 1297–1312.*

SGC. (2012). *State-of-the-art geophysics confirms Frasers Find' large gold system potential.*

Shives, R.B.K., Ford, K.L., and Charbonneau, B.W. (1995). Applications of Gamma-ray spectrometric/Magnetic/ VLF-EM surveys–Workshop Manual: Geological Survey of Canada, Open File 3061. 82.

Sibson, R.H., Robert, F., Poulsen, K.H. (1988). High-angle reverse faults, fluid pressure cycling, and mesothermal gold–quartz deposits. Geology16, 551–555.

Sillitoe, R. (2000b). Enigmatic Origin of Giant Gold Deposits, in Geology and Ore Deposits 2000: The Great Basin and Beyond, in Geological Society of Nevada Symposium Proceedings, 1-18.

Sillitoe, R.H., and Thompson, J.F.H. (2006). Changes in mineral exploration practice: consequences for discovery, in Society of Economic Geologists special Publication 12, 193-219.

Silva, A. M., Pires, A. C. B., McCafferty, A., Moraes, R. A. V., and Xia, H. (2003). Application of airborne geophysical data to mineral exploration in the uneven exposed terrains of the Rio Das Velhas greenstone belt. Revista Brasileira de Geociências, 33(2):17–28.

Simon, S. M., Amanor, M., Nimoh, A. (2010). *National Instrument 43-101 Technical Report.* Accra: SEMS Exploration Services Ltd.

Telford, W. M., Geldart, L. P., and Sheriff, R. E. (1990). *Applied Geophysics.* Cambridge.

Urquhart, W. (1995). Geophysical Airborne Survey: Radiometrics -- Gamma-Ray Spectrometry. *GeoExplo Ltda*.

Wilford, J. R., Bierwirth, P. N., Craig, M. A. (1997). Application of airborne gamma-ray spectrometry in soil/regolith mapping and applied geomorphology. AGSO Journal of Australian Geology and Geophysics, 17(2):201–216.

Wright, J., Hastings, D., Jones, W., and Williams, H. (1985). Geology and Mineral Resources of West Africa. 187.

Zlotnikov. (2012). Automated Image Analysis Targets Ground Selection; Application of Aeromagnetic Structural Analysis Techniques for Greenfields Gold Exploration.

APPENDIX

Appendix A

Table A. 1: A Sample of Airborne Magnetic Data

Line	X [m]	Y [m]	TMI [nT]	DEM [m]	Lev_TMI [nT]
L1	749100	666200	31593.30	228.16	31,593.30
L1	749150	666200	31593.40	227.40	31,593.40
L1	749200	666200	31593.45	226.22	31,593.45
L1	749250	666200	31593.50	224.94	31,593.50
L1	749300	666200	31593.55	223.80	31,593.54
L1	749350	666200	31593.50	223.02	31,593.50
L1	749400	666200	31593.50	222.66	31,593.50
L1	749450	666200	31593.45	222.74	31,593.44
L1	749500	666200	31593.30	223.24	31,593.30
L1	749550	666200	31593.20	224.14	31,593.20
L1	749600	666200	31593.15	225.30	31,593.14
L1	749650	666200	31592.95	226.52	31,592.95
L1	749700	666200	31592.80	227.56	31,592.80
L1	749750	666200	31592.65	228.20	31,592.65
L1	749800	666200	31592.45	228.32	31,592.45
L1	749850	666200	31592.25	228.04	31,592.25
L1	749900	666200	31592.10	227.48	31,592.10
L1	749950	666200	31591.90	227.02	31,591.91

Table A.2 A sample of Airborne Radiometric Data

Line	X [m]	Y [m]	K [%]	TH[ppm]	U[ppm]
L1	749100	666200	43.72	18.36	16.73
L1	749150	666200	42.16	17.75	16.41
L1	749200	666200	40.38	17.15	16.09
L1	749250	666200	38.51	16.65	15.81
L1	749300	666200	36.83	16.36	15.60
L1	749350	666200	35.58	16.32	15.45
L1	749400	666200	34.83	16.52	15.37
L1	749450	666200	34.43	16.91	15.38
L1	749500	666200	34.22	17.39	15.48
L1	749550	666200	34.11	17.89	15.66
L1	749600	666200	34.21	18.40	15.90
L1	749650	666200	34.67	18.95	16.19
L1	749700	666200	35.55	19.62	16.58
L1	749750	666200	36.63	20.44	17.08
L1	749800	666200	37.50	21.38	17.70
L1	749850	666200	37.92	22.36	18.39
L1	749900	666200	37.93	23.21	19.05
L1	749950	666200	37.81	23.79	19.57
L1	750000	666200	37.88	23.96	19.84

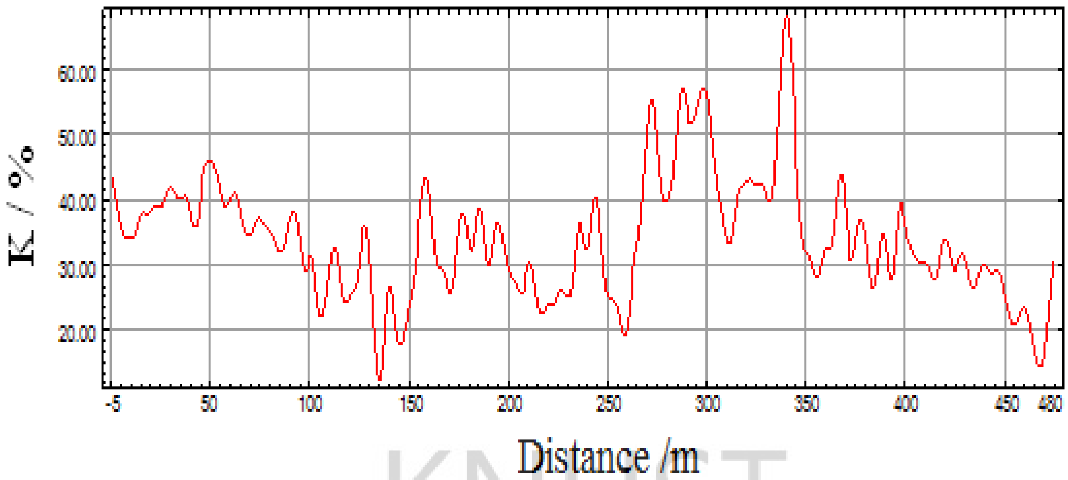

Figure A. 1 : A sample of K abundance along a profile line

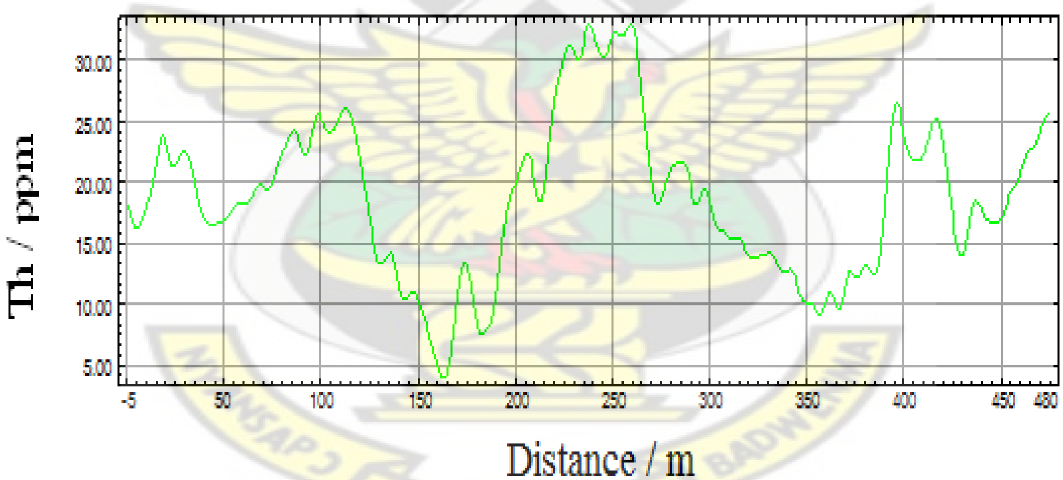

Figure A. 2: A sample of Th abundance along a profile line

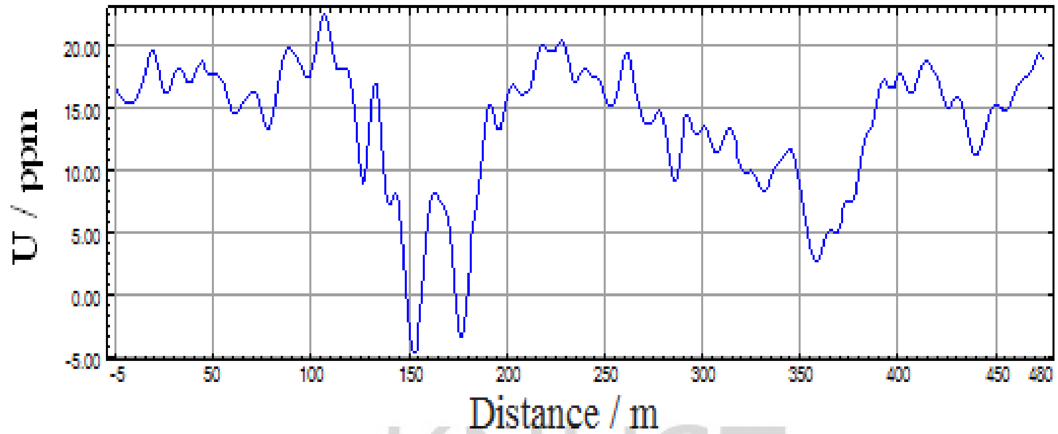

Figure A. 3 A sample of U abundance along a profile line

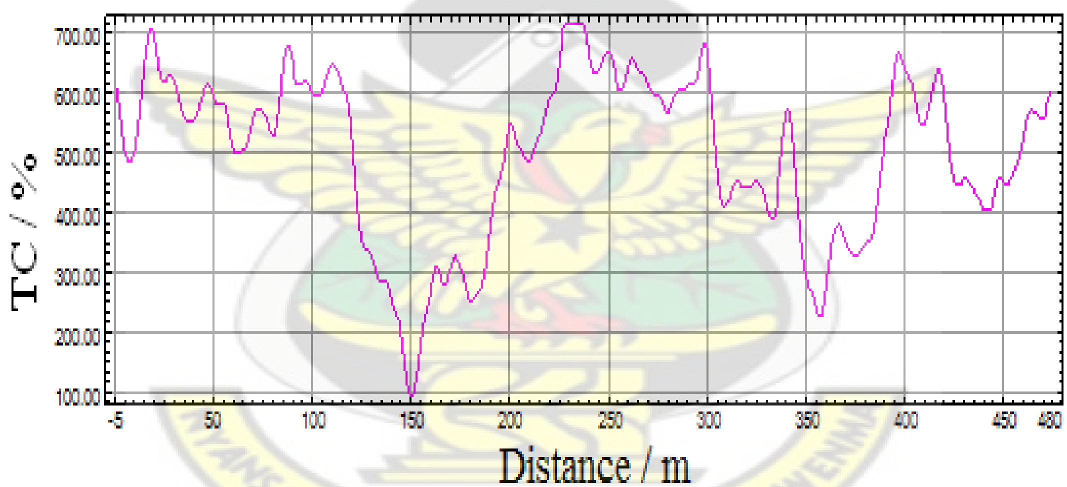

Figure A. 4: A sample of the total count (TC) of the radioactive elements abundance along a profile line

Appendix B

B.1 Used Software

I. Oasis Montaj (Geosoft): data processing and enhancing tools

II. ARC GIS

III. Global mapper

IV. Microsoft word

V. Microsoft paint

VI. Golden Surfer 9